UNIVERSITY OF CALIFORNIA, SAN DIEGO

Electric Field Directed Self Assembly of Nanoparticle Structures

A dissertation submitted in partial satisfaction of the requirements for the degree

Doctor of Philosophy

in

Electrical and Computer Engineering (Applied Physics)

by

Dietrich Alexander Dehlinger

Committee in charge:

Professor Sadik Esener, Chair
Professor Michael Heller, Co-Chair
Professor Xiaohua Huang
Professor Yu-Hwa Lo
Professor Kenneth Vecchio

2008

The dissertation of Dietrich Alexander Dehlinger is approved, and it is acceptable in quality and form for publication on microfilm and electronically:

_____

_____

_____

_____

_____

University of California, San Diego

2008

Dedication

To Cephalopods everywhere

Table of Contents

List of Symbols

DNA –Deoxyribonucleic Acid

DEP – Dielectrophoresis

MEMS-Micro Electrical Mechanical Systems

CMOS- Complementary metal–oxide–semiconductor

SEM-Scanning Electron Microscope

EPD – Electrophoretic Deposition

PDMS-Polydimethylsiloxane

List of Figures

Acknowledgements

I would like to acknowledge the mentorship of Professor Michael Heller, for all the assistance and discussions we've had over the years. Without your guidance and support, none of this would be possible.

In addition I would like to thank Dr Esener for both his support, and for the enthusiasm he's brought to me over the years.

To my family, Tom, Carole, Marlene, Carmen, and Eva, I want to thank you for being there. Here is your chance to see read I've been up to all this time.

My friends have helped keep me sane all this time. Riah, I especially thank you for helping me with all of this. Paul, Nikki, Aaron, Ed, and the goons have all provided the time away from this work I needed to get back to it.

I would like to thank Nanogen for all the material assistance they have provided to this dissertation, as well as the assistance of Paul Swanson and Dalibor Hodko. Without their knowledge and expertise, we could not have brought this work to fruition.

To the fellow students I've worked with over the years, Benjamin Sullivan thank you for providing someone to knock ideas around with as well as being a friend. Jennifer Marciniak has provided assistance with the creation of this

dissertation as well as with the bad movie lifestyle. In addition Sanja Zlatanovic, Alex Hsiao, Raj Krishnan, Robert Mifflin, Juhi Saha, Avery Sonnenberg, and Michael Benchimol have all provided invaluable assistance.

Chapter 2, in part is a reprint of the material as found in Small: Dehlinger, D.A., Sullivan, B.D., Esener, S. and Heller, M.J. (2007) Electric-field-directed assembly of biomolecular-derivatized nanoparticles into higher-order structures. *Small*, **3**, 1237-1244. The dissertation author was the primary investigator and author of this paper.

Chapter 3, in part is a reprint of the material as found in Nano Letters: Dehlinger, D.A., Sullivan, B.D., Esener, S. and Heller, M.J. (2008) Directed Hybridization of DNA Derivatized Nanoparticles into Higher Order Structures. *Nano Lett*. The dissertation author was the primary investigator and author of this paper.

VITA

2001	Bachelor of Arts Physics, Reed College
2001-2002	Device Development Engineer, Reflectivity
2005	Master of Science, University of California, San Diego
2008	Doctor of Philosophy, University of California, San Diego

PUBLICATIONS

Dehlinger, D.A., Sullivan, B.D., Esener, S. and Heller, M.J. (2008) Directed Hybridization of DNA Derivatized Nanoparticles into Higher Order Structures. Nano Lett.

Sullivan, B.D., Dehlinger, D.A., Zlatanovic, S., Esener, S.A. and Heller, M.J. (2007) Low-frequency electrophoretic actuation of nanoscale optoentropic transduction mechanisms. Nano Letters, 7, 950-955.

Dehlinger, D.A., Sullivan, B.D., Esener, S. and Heller, M.J. (2007) Electric-field-directed assembly of biomolecular-derivatized nanoparticles into higher-order structures. Small, 3, 1237-1244.

Dehlinger, D., Sullivan, B., Esener, S., Hodko, D., Swanson, P. and Heller, M.J. (2007) Automated Combinatorial Process for Nanofabrication of Structures Using Bioderivatized Nanoparticles. Journal of the Association for Laboratory Automation, 12, 267-276.

Dehlinger, D. and Mitchell, M.W. (2002) Entangled photons, nonlocality, and Bell inequalities in the undergraduate laboratory. American Journal of Physics, 70, 903-910.

Dehlinger, D. and Mitchell, M.W. (2002) Entangled photon apparatus for the undergraduate laboratory. American Journal of Physics, 70, 898-902.

BOOK CHAPTERS

Hodko, D., Swanson, P., Dehlinger, D., Sullivan, B.D. and Heller, M.J. (2007) In Lee, H., Ham, D. and Westervelt, R. M. (eds.), CMOS Biotechnology. Springer, New York, pp. 179-206.

Dehlinger, D., Sullivan, B.D., Esener, S., Swanson, P., Hodko, D. and Heller, M.J. (2007) In Busnaina, A. A. (ed.), Nanomanufacturing handbook. CRC Press/Taylor & Francis, Boca Raton, FL, pp. 107-126.

Dehlinger, D., Sullivan, B.D., Esener, S. and Heller, M.J. (2006), NSTI-Nanotech 2006, Vol. 1, pp. 389-392.

Heller, M.J., Sullivan, B.D. and Dehlinger, D. (2005), NSTI-Nanotech 2005, Vol. 1, pp. 769-772.

ABSTRACTS

Heller, M.J., Dehlinger, D., Sullivan, B.D. and Esener, S. (2007), NSTI-Nanotech 2007, Vol. 1, pp. 269-271.

Heller, M.J., Dehlinger, D., Esener, S. and Sullivan, B.D. (2007), ASME Proceedings of BioMed 2007, Vol. Next Generation Devices-38093.

Sullivan, B.D., Dehlinger, D., Zlatanovic, S., Esener, S. and Heller, M.J. (2006), NSTI Nanotech 2006, Vol. 2, pp. 209-212.

Heller, M.J., Dehlinger, D. and Sullivan, B.D. (2006) In Fritzsche, W. (ed.), DNABased Nanoscale Integration Symposium. American Institute of Physics.

ABSTRACT OF THE DISSERTATION

Electric Field Directed Self Assembly of Nanoparticle Structures

by

Dietrich Alexander Dehlinger

Doctor of Philosophy in Electrical and Computer Engineering (Applied Physics)

University of California, San Diego, 2008

Professor Sadik Esener, Chair

Professor Michael Heller Co-Chair

It is traditionally difficult to integrate a wide range of nanocomponents into macroscopic or mesoscopic scale systems. Traditional methods of nanofabrication use large scale patterning of homogenous layers, or make use of the intrinsic properties of the particles in to bind them together in an uncontrolled fashion.

In this dissertation, a method for the rapid, highly controlled deposition of water soluble nanoparticles is demonstrated. Through the use of direct current controlled electrodes in a buffered solution, nanoparticles are pulled from a dilute solution to a complementary binding surface in a few seconds where they form a single layer. By repeated processing steps we are able to rapidly fabricate

multilayered structures using different nanoparticles, making use of both overall directed assembly and the local self assembly of the particles themselves. Because we are able to control the particle concentration, we can effectively control the particle binding rate at the deposition surface. Described in detail is a method for characterizing the deposition process to determine both the optimal parameters (in terms of deposition time and current) for a given particle type, and methods to determine the level of interparticle self binding. Optical fluorescent imaging and electron microscopy were used extensively to characterize the rate of particle accumulation both as a function of current and time for a single deposition, and for the overall process through subsequent layers. The electric field assisted self assembly work was carried out for 40nm and 200nm biotin/streptavidin coated particles, as well as particles covered in various DNA sequences, quantum dots, and gold particles.

Particle deposition profiles across the electrode are also discussed, with the root causes for the observed pattern explained using various electric field deposition from this work, as well as some supporting experiments from tangentially related experiments. These experimental results are compared to various simulated systems.

Finally some preliminary work on long range, high voltage, high conductivity dielectrophoresis systems is discussed with an eye towards fully integrated sample analysis systems.

Chapter 1: Introduction

1.1. Introduction

Manufacturing processes depend both on the ability to construct functional components and then to assemble those components into a useful whole. In recent years, nanotechnology has made great strides in assembling an array of interesting and novel building blocks. Nanotubes, nanowires, and nanoparticles of many sizes, shapes, surface chemistries and inner compositions have been fabricated. Less progress has been made however, on methods of assembling these constructs into systems.

The motivation of the research in this dissertation is the development of an electrophoretic manufacturing platform that will allow for the highly controllable, scalable, and rapid assembly of a wide range of nanoparticles into complex, higher order structures. Current methods are either limiting in the nature of the particles they can accept, the throughput of the particles, are slow, or only produce nanoscale sized structures. The methods described in this dissertation are meant to help bridge the gap between these problems. We believe, that in conjunction with other techniques, electrophoretic assisted assembly of nanoparticles will allow for the fabrication of novel, heterogeneous nanostructures.

Two broad process categories have been developed for the assembly of nanoscale systems. The first of these categories (colloquially known as “top down”) is

the directed patterning and positioning of components(1). The key feature is that the design, fabrication, and assembly of all the pieces are controlled directly and externally from the production process. Parts are fabricated separately then assembled in place according to an external design. This is how objects are made on the normal scale of everyday objects. This type of method works well when the individual pieces are relatively small in number and can be easily handled, or when they can be assembled in parallel. Photolithographic construction of microchips us an example of top down assembly, where the system is built using sequential fabrication steps comprised of externally defined mask, and chemical etching steps. The fabrication steps being controlled external to the process makes it top down. The limitation of this methodology when applied to nanoparticles is that when the number of particles is large, and the size grows small, individual handling or patterning becomes difficult.

The other end of the fabrication spectrum is called “bottom up”. This type of methodology uses objects that have some intrinsic form of self recognition and binding to build a larger object. When mixed together, two or more such objects will come together and bind in a specific manner to form a larger composite object. This is how biological systems operate on their lowest levels. Proteins have specific binding sites for various other molecules which allow them to bind or modify those molecules. Cells recognize their position relative to other cells and develop and behave in a certain manner, and so on. Here the intrinsic properties of the molecules

and systems allow them to build into larger structures or to perform specific activities. Bottom up methodologies are useful when the particles of interest are too small and too numerous to individually control (2-5). When you have a *mole* of individual molecules, you will spend forever attempting to position them if you do it individually. The parallel nature of bottom up methods helps to get around this problem. In some sense, strict self assembly is too parallel. The scope at which it works is so narrow that to build up larger structures either requires a vast array of specific high precision components or the combination of various fabrication methods.(6)

Of course most fabrication processes lie on the continuum between top down and bottom up methods. Things like industrial chemical production and cellular growth contain aspects of both overall control and the individual self assembly of the base level components. A cell, for example, contains a plethora of high fidelity recognition molecules, but generally those molecules are held in discrete, localized pockets. It is the subject of **Directed Self Assembly** (7,8) that concerns the bulk of this dissertation. By spatially and temporally controlling the concentrations of various reactants, it is possible to use the high precision local effects of self assembly to place together smaller particles, but to do it in an overall controlled manner. The local assembly of component particles is controlled by their inherent binding properties, but the localization and concentration of these various constituents is controlled by external forces. This allows for the combination of the most useful properties of both

fabrication methodologies to be combined together. This dissertation describes a method to rapidly speed up and control the self assembly of nanoparticles with specific binding properties through the use of applied electric fields in solution. By applying electric fields we are able to rapidly move particles through a solution to a desired location, in our case, a surface containing one half of a highly specific ligand binding pair mechanism (biotin/streptavidin, DNA hybrids).

The core of our technique rests on the fact that all ligand binding pair mechanisms act proportional to the rate that each component is present. By doubling the concentration of a reactant, you will double the rate at which binding events occur. By using electrophoresis we can take charged particles located in a diffuse solution and increase their concentration by orders of magnitude near a driving electrode. This method, described in detail in chapter 2, allows for the rapid and specific driving of the binding reaction simply though the rapid increase of the local particle concentration. Through this method we can make use of high fidelity binding mechanisms such as DNA or the biotin/streptavidin system while at the same time allow large scale control and patterning of these nanoparticles. By using electronically switched, current controlled electrodes, we are able to control the deposition rate of particles at specific locations. The particles bind at a vastly accelerated rate in the electronically activated locations due to their greatly increased concentrations, and bind at a trivially low rate in all other places, due to the low background concentration of particles. This process allows for the rapid

deposition of any water soluble, selectively bindable particle, and a high “contrast ratio” between deposited (specific) and non deposited (non specific) regions.

Where would such a methodology be useful? We believe that the utility comes from applications where the end product (materials, devices, systems) must be of macroscopic dimensions, but requires nanoscale patterned fabrication. What we believe to be a current failing of fabrication technologies is that there is no bridge between the precise handling and fabrication of nanocomponents, and their assembly into a higher order manufacturable product. The process described in this dissertation has relatively fine control of nanoparticles in the z dimension (approximately able to fabricate a single layer of particles), with an x and y resolution limited to roughly the dimension of the electrodes used to concentrate the nanoparticles. Since arrays of microelectrodes can be easily fabricated on a macroscopic scale, the ability to scale up devices fabricated in this manner is already possible. Because of the general nature of electric field based assembly, we believe its main strength arises from the ability to integrate a wide range of different nanocomponents (as well as microcomponents), and to rapidly assemble them in a reconfigurable manner, simply by changing which electrodes are activated. Quantum dots, nanowires, tubes, proteins, metallic nanoparticles, and even semiconductor liftoff devices could be integrated together into a complete system. This technique could have applications in advanced fuel cells and photovoltaics, highly integrated

biological and nanosensors devices, and rapid assembly pick and place systems for heterogeneous integration.

1.2. Scientific contributions

In this dissertation I present research on electric field manipulation of self assembling nanoparticles to form higher order structures. I demonstrate the use of this technique to rapidly manipulate and assemble these particles as well as show the methods used in characterizing the process.

In chapter 2, the process is explained, and results of directed self assembly fabrication are presented for biotin and streptavidin nanoparticles. Parameters for the determination of the fabrication of single monolayers and the methodology for determining the level of interparticle stringency are also demonstrated. Using the combinatorial ability of our devices to test a wide range of deposition parameters simultaneously during a single experiment allowed us to determine the optimal deposition parameters. Using those parameters, I demonstrated the ability to perform up to 100 layer depositions.

Chapter 3 discusses the use of this technique on a wider range of other nanoparticles. DNA nanoparticles are examined in a similar manner to the biotin/streptavidin particles in chapter 2. Additionally, quantum dots, and various combinations of large and small particles are discussed in regards to the electric field deposition process. Finally the phenomenon of nanolayer liftoff is presented.

Chapter 4 discusses at length the physical nature of the nanoparticle deposition process, and why the nanoparticles tend to deposit in the manner they do. Various physical effects are examined, and compared with electrical current flow simulations to understand what drives the uniformity of the deposited layers.

Chapter 5 introduces the use of long range dielectrophoretic effects for carrying out high conductivity cell sorting. Results for particle trapping from preliminary experiments are presented along with comparative simulations for those systems. The simulations strongly agree with experimental data, though higher conductance systems show issues with heat dissipation, an issue we intend to address in future work.

1.3. Background

The work in this dissertation focuses on the use of direct electric fields to direct and accelerate the rate of nanoparticle binding to specific locations on a substrate device. There are however, a wide variety of methods for the fabrication or assembly of nanostructures and the placement of nanoparticles. As a way of introduction to the electronic forces used in this work, I will briefly cover a range of these methods. In addition I will describe the windows in which they are applicable.

1.4. Prepatterning/lithography

Many of the most functional advances in the field of nanofabrication come from the microelectronics industry. Using the process of photolithography there has been an inexorable crawl to smaller and smaller feature sizes for fabricated components. In a very general sense photolithography works by the sequential optical patterning of a "resist" layer which is then used to control the etching or deposition of a layer of a material of interest. A premade mask is used to block and shape incoming light which then hits the photosensitive resist, a material which changes properties when exposed to light. The usage of masks typically requires prefabrication, though various methods have been developed to use optical switches in their place(9). The resist is then "developed" through the exposure to a solution that removes either the exposed or unexposed regions (depending on the resist), which leaves the resist patterned. This pattern is transferred to materials beneath by subsequent etching steps in which the material under the exposed resist is removed, while the resist protects the unexposed regions. The end result of this process is a stack of independently patterned material layers. By changing the wavelength of the light used, the size (and shapes) of the features on the mask, and the nature of the resist, the ultimate patterned features can be reduced in size. There are subtle caveats and variations for every process step depending on the materials being patterned, but that is beyond the scope of this discussion. Current photolithography methodologies are expected to produce features below 50nm in size(10,11). While

photolithography is a general method in that a number of materials can be patterned through the process, the nature of the materials is somewhat limited. Typically, for each patterned layer, the entire system is exposed to the photoresist, the light used to pattern the resist, the chemical used to develop the resist, the method used to pattern the material beneath the resist, the chemical used to remove the remnants of the photoresist. This requires that after multiple layers have been deposited and patterned that previously deposited layers are not etched significantly in subsequent patterning steps. This has been most successful in the fabrication of layers made from semiconductors and metals, which are typically resistant to the photoresist chemistries. This process however may not carry over as well when multiple patterned layers of organic filled materials are desired.

Other lithographic methods have emerged for the patterning of materials without resorting to as many chemical processing steps. Imprint lithography can use a stamp (12,13) to place down materials directly, or a mold (14-19) to physically deform a material deposited on a surface. Such methods allow the use of premade high resolution stamps to directly pattern a surface (as opposed to intermediate patterning methods such as with photolithography). The resolution therefore is set by the size of the mask, and care must be taken to avoid physical mask damage (especially with the molding processes). Similar to the stamping methodologies is dip-pen lithography, where a tip deposits a small amount of a fluid or particles onto a

specific location on the surface to be patterned (20-24). Dip pen lithography allows for the precise reconfigurable placements of individual particles.

1.5. Self assembly

Key to the idea of bottom up fabrication processes is the self assembly of individual components. Self assembly is when two or more objects come together and bind in a specific manner due to inherent physical properties of their structure. Self assembly encompasses a very broad range of phenomena. Protein folding, DNA binding (25), antibody attachment(26), charge coupling, and even standard chemistry (27) fall within some form of self assembling systems. Self assembly encompasses a range of geometries that lie from molecules aligning in sheets on surfaces (28-31) to complicated structures forming in solution (32-37). Self assembled processes are typically involve structurally complex molecules but are not controlled. This is in the sense that binding events between two systems often have a high degree of specificity (see DNA and antibody binding to complementary molecules) due to their complex physical and electronic structure but the binding events the particles go through are unplanned and uncontrolled. If two bindable molecules come into close contact, they will bind together with some energy dictated by their physical structure and compatibility. This is the nature of bottom up interactions; they are entirely local and determined by the geometry of the surrounding systems. For the most part, the only way that different local areas can interact is by changing or depleting the nature

and number of the self assembling particles that might diffuse between them. Self assembly therefore excels (at least in principle) at putting a small number of components together well, and doing this in a massively parallel manner. All that needs to be done is to add the components together in the correct ratio and conditions, and the products will form. Where it is less successful is when complicated larger scale structures need to be fabricated. While it is possible to build relatively large objects from self assembled building blocks, those larger objects are not themselves highly complex. As the number of different objects increases, the time and concentration required to find the correct spot to bind will inexorably increase. While cells rely on the highly specific binding specific binding properties of various biomolecules, they do so by localizing them in small, contained regions.

Self assembled structures are only as good as the molecular systems they are fabricated from. In certain cases, such as with tailored DNA systems, the results can be highly precise nanostructures. However, this need not be the case. All self assembly really requires is the presence of two specific binding domains, but those domains can be associated with a larger structure in a fundamentally random manner. For example, much of the work in this dissertation involves nanoparticles covered in biotin or streptavidin. The biotin streptavidin system is a workhorse of self assembly, the bond between the two molecules is rapid and strong, and they can be easily chemically attached to a wide range of of particles or molecules. However, particularly in the case of particle attachment, the number of biotin and streptavidin

attached to a given system is essentially random within some statistical window, as are the spacing and orientation between various copies on a single particle. So while a biotinylated particle will bind strongly to a streptavidinated particle, it will do so only in some range of possible ways. However the biotin and streptavidin themselves on the particle surface will always bind together in the same manner. Therefore while self assembly is intrinsically accurate, it needs to be seen in context of the whole system it is attached to, which is often far more inaccurate. Therefore, we believe that the overall ability of self assembled systems to reach some fabrication goal will be limited by the structural components that are to be linked together.

Further issues with self assembly arise with the idea of "nonspecific binding". For example, while in certain conditions two short DNA stands can be made to bind or not together based on the complementarities of their sequences, this is not always the case(38). As sequences grow in length, or solution conditions are changed towards stabilizing conditions, the presence of a small number of mismatched DNA basepairs becomes less important in controlling the conditions in which the two sequences will either fail to hybridize or to come apart. Specifically, the conditions that promote the rapid binding of two complementary sequences, will also allow the binding of two partially matched sequences. Furthermore, the conditions that remove the majority of nonspecifically or semi specifically bound sequences will also remove a large fraction of the specifically bound sequences. This will be true of all self assembled systems, and will place some limit on the number of

different but similar molecules that can bind together at any one time in a solution. Care must be taken therefore, to minimize the amount of nonspecific interactions in a given self assembled system.

1.6. Layer by layer deposition

Layer by layer deposition is a specific class of self assembly process, which is heavily related to the work done in this dissertation. LBL involves the creation of alternating layers of nanoscale layers formed by a series of self assembly processes. LBL systems have been studied for such topics as drug delivery (39,40), fuel cells (41), batteries (42), nanosensors and biosensors (43), solar cells (44), and tissue engineering (45). In general, layer by layer assembly (LBL) starts with a seed of some sort (typically a particle or surface) which has been coated with a self assembly molecule (46). Most often the molecules involved are merely charged, but any self assembly system can be used (47). The starting seed is then exposed to a solution containing the complement molecule of the self assembly system, which will then form a self passivating layer around or over the initial seed layer. The complementary portion of this bound layer is connected to some secondary linker (nanoparticle, polymer backbone, etc) which has a large number of the complement molecule attached. Some fraction of these will be bound to the surface forming the layer, while another fraction will be pointed up into solution. At this point, the solution is then washed of excess complementary material, and a second solution is added. This

solution contains material complementary to the second layer (typically the same material that made up the first layer), which binds with the second layer to form a third layer. Once bound, the system is again washed and the process is repeated as many times as desired. The end result is a stack of layered materials of alternating binding properties (for example, positive/negative/positive, or biotin/streptavidin/biotin, etc). More complicated materials can be introduced into this stack by using them as the substrate to which the binding system is attached (for example biotin or streptavidin coated nanoparticles)(48). The materials introduced this way do not need to be the same between layers (or even in the same layer) they merely need to be coated with the binding molecule. In principle this allows for the formation of structures with one dimension of variation (along the deposition growth direction) incorporating any materials that can be chemically linked to the binding mechanism.

Layer by layer systems can be patterned, typically by limiting or controlling where the initial seed layer begins, such as with lithographic methods (49), but in doing so the process is limited to the same growth pattern throughout. Without extensive spatial blocking and deblocking steps, LBL is limited in its ability to change its deposition pattern from step to step, since any exposed active area will be deposited upon. Because the process is ultimately driven by the amount of the reactants in the depositing solution, the concentration tends to be high to drive reaction speeds, which tends to be somewhat wasteful of materials. This also tends

to drive nonspecific binding effects if they are relevant to the situation. It is the ability to use low solution concentrations and the desire to pattern the formed layers that provided our motivation to extend the layer by layer process with electric field based assembly.

1.7. Electrophoretic deposition

Electrophoresis is the movement of charged particles due to the influence of an applied external voltage. Electrophoretic deposition (EPD) is the use of electrophoresis to pull particles to a deposition location where they bind(50). This is typically distinct from electrochemistry because the binding is not necessarily due to electron exchange, and the objects being moved are larger than ions or small molecules. Electrophoretic deposition is a continuous growth process, as long as current is running through the system, the deposition will continue, the transport mechanism of which will be discussed further on. Since the particulates used in the solution are charged, they make up part of the solution current, and thus are transported towards the appropriate electrode. The continuous growth means that layer control is a matter of solution concentration and applied voltage. As particles come to the deposition surface, they stick down and extend the surface, to which more particles then can bind. This is different than in self assembly and layer by layer type methodologies, because in those cases, binding will only (in principle) occur to surfaces that contain the appropriate binding substrate, and therefore stops once all

the binding sites have been consumed in a single cycle. The technology discussed in this dissertation is therefore a combination between layer by layer assembly, and electrophoretic deposition since we used electric fields to draw specifically labeled particles to a complementary surface where self assembly could occur. Typically EPD processes are run in non aqueous solutions to avoid electrolysis, whereas the processes in this dissertation were explicitly done in such solutions but at lower voltages in buffered solutions. The general principle between the two methods is similar however, so this discussion is to partially motivate the electronic layer by layer process.

Diverse materials such as silica(51), luminescent particles, nanorods and nanowires(52), carbon nanotubes(53,54), ceramics, superconductors, piezoelectric materials, and more have been deposited as films using this process(55). Applications such as photovoltaics(56,57), fuel cells(58), porous coatings and composites(59), gas diffusion sensors(60), and substrates for biomedical applications(61). Due to similarities in the techniques, we believe that application for both LBL and EPD methods can be utilized using our methodology, but with the added benefit of speed, controllability, lower material usage, and potentially finer layer control.

1.8. Electric field driven movement in liquids

Electronic forces in a liquid are varied in form and function. While they all arise from the basic physics of electronic forces, they are made complicated by the

chemistries of the liquid, the nature of fluid/electrode interface, and the manner in which they are applied. Forces in a liquid are usually seen as the result of a few basic situations, with side effects rising from the vagaries of the liquid itself. Liquid electronics typically involves a regime of little or no fixed charges, low carrier densities, omnipresent dipoles, acid/base reactions, and large amounts of electronic and fluidic drag. These effects typically act with different strengths and in differing geometries. Choosing an appropriate method to move a particle depends heavily on where and how far you want to move it, how fast it needs to be moved, how large it is, and what other particle types are coexist in solution. In discussing these forces and effects, I mean them as examples of how the electronic driven movement in solutions is both complicated, and allows for fine levels of particle control at a large number of lengths scales.

1.9. Electric Forces

In the following sections I intend to mathematically describe and motivate the usefulness of a number of electronic forces in solutions. Due to the regimes we worked in, and technical limitations of our equipment, we focused primarily on electrophoretic driven movement. However, future work is expected to incorporate and integrate some or even all of the forces discussed here in detail. Thus, full understanding of the potential electronic toolkit is desirable, and further uses and discussions of these forces will be discussed further on in the simulation section.

1.10. Electrostatics

Free space is a clean place. Fixed electric charges sitting by themselves can be felt at great distance. The strengths of an electric field for a point charge falls off as the inverse square of the distance, a line of charge as the inverse, and a plane of charge is felt uniformly throughout space. The strength of the electric field is proportional to the charge itself. In general, the free space force felt in some position x_1 by a a generalized chunk of electric charge is

$$F(x_1) = \iiint \frac{q(x)}{(x - x_1)^2} . \hat{s} dx$$

Once things get messy (such as in a solution of electric charges), however, everything changes. Mobile charges and polarizable materials respond to the electric fields produced by other charged particles and tend to redistribute themselves in a manner that tends to locally cancel out the original fields. These redistributions make a particle appear to have lower total charges at a given distance. The length that these redistributions take place over vary depending on the available solution charge, and the charge of the initial particle itself. However, in general mobile charge will tend to minimize the system entropy. The manner in which it tends to do so is not analytic except in simple cases. However, since ionic solutions are typically charge neutral over sufficient distances but actually composed of equal amounts of positive and negative charge, the final system is where net fields are countered by the driven separation of positive and negative ions.

In ionic solutions, this leads to a tendency that there are little to no electric fields in a bulk solution (since the free charges will have redistributed to cancel it). Thus, there are (at least to some threshold, discussed in the next section on electrophoresis) no currents or forces when a voltage is applied across a solution, except for transients ones in the period of charge redistribution. Charge only moves as far as is necessary to produce a counter electric field that nullifies an applied voltage or charge. The type of system is essentially a capacitor (and has found some applications as such(62)). Regions near to fixed charges are typified by ever increasing counter charge densities with the electric field falling off exponentially faster than it would in free space. The electric forces thus become much shorter range, and tend to be less effective as the density of ionic charges in solution increase. In aqueous solutions, the electric fields are limited further due to the voltage restrictions imposed by the electronic breakdown of water. These forces are useful for holding objects in direct contact with electrode surfaces, and the breakdown of water can be inhibited by thin passivation layers. The use of electrostatic charge for the long range movement of particles in aqueous solutions is difficult, however for the reasons given.

1.11. Electrophoresis

Electrophoresis is typified by the steady state electric field driven movement of charge in a liquid solution. The key difference between the

electrostatic situation described above and electrophoresis lies in the behavior of the electrode fluid interface. In a true electrostatic situation as voltage is applied to a solution electrode, electrons or holes will pile up on the surface of the electrode, and counter ions will move out of the bulk solution to create an opposite electric field. Theoretically, this situation would continue on regardless of voltage until the point where the accumulated charge on the electrode is greater than the charges in solution. In this simple case, eventually an electric field would be felt in solution, but the voltages required would be large. In such a situation, there is no charge transfer between the electrodes and the bulk solution, so current conservation is only satisfied by the accumulation of solution charges at or near the electrode. This is because the current carriers in the electrodes are fundamentally different than the current carriers in the solution, and are not freely exchangeable.

For true active electrophoresis to take place at reasonable voltages and ionic solution densities there must be some form of charge transfer between the solution and the electrodes. This charge transfer is the subject of the field of electrochemistry, and a full treatment is beyond the scope of this section. In summary however, three possibilities exist for this charge transfer. Firstly, the electrode itself can dissolve into solution in the form of ions to carry charge. Secondly ions in the solution can react and adhere to the electrode and donate or accept electrons, becoming part of the electrode. Finally, the molecules in solution can donate or accept electrons at the electrode, become charged, and become the

charge carrier in solution. For the electrophoresis that we do, we use the third method, since the first two involve the consumption or degradation of the electrode surface.

In aqueous electrophoresis using non-polarizable electrodes (the electrodes are not consumed, typically involving gold or platinum) charge is introduced into solution by the electrolysis of water in two reactions, one at the positive electrode, and the other at the negative electrode.

$$2H_2O(l) \rightarrow O_2(g) + 4H^+(aq) + 4e^-$$

$$2H_2O(l) + 2e^- \rightarrow H_2(g) + 2OH^-(aq)$$

These reactions involve the removal or addition of electrons to portions of a water molecule, and consequently have an energy of activation to complete (of about 1.23 V). Total voltages applied between the two electrodes less than the two half cell reactions will not result in current because there is insufficient energy to perform the two reactions, and the system will behave as in the electrostatic case since there will not be current moving between the electrodes and the solution. This voltage loss at the electrode increases with the current density, and takes the form at each electrode as

$$\nabla V = A \times Ln(\frac{I}{I_o})$$

Where I is the current, with A and I_0 are constants of the particular electrode reaction. This voltage dependence on the system current merely means

that the system current is not a simple function of the applied voltage, since the available voltage in solution is also related to the current.

For a given charge in solution, the current will be (as a function of the actual voltage) across the solution(63)

$$I = V * L$$

Where L is the system conductance, and is related to geometric factors and proportional to the specific conductance κ. With

$$\kappa = F \times \sum_i c_i \mu_i$$

Where F is the faraday constant, c is the concentration and μ the mobility of each charged species in solution. The mobility is a factor taking into account the charge and drag of a given particle type. It should be noted that because it is derived from a balance of drag and electrical forces, the mobility of a particle is dependent on the surrounding medium, and the mobility of two different charged species might not scale proportionately between two different mediums. This reaches an extreme where one species is physically size excluded from entering a given medium (such as a gel), but another is not. In such a case the current is made up of one set of charged particles in the gel and a greater set outside the gel.

Taking into account the overpotential at the electrodes, to solve for the current of a solution in a one dimensional case at a given voltage we have the equations

$$V_{total} = V_{cathode}[I] + V_{anode}[I] + \frac{I}{L}$$

Which for given electrode/solution parameters we can solve numerically for the current at a given voltage. The situation becomes significantly more complicated however, with electrodes in three dimensions and as the number of activated electrodes grows. Turning on additional electrodes to a given voltage will modify the electric field distribution across the solution in a way that changes the currents coming out of the original electrodes.

Control over electric field driven particles requires a controllable and uniform movement, and the deposition of particles requires a uniform and predictable deposition rate. In practice, this requires a flow of particles into the electrode, regardless of the total activated electrode configuration. The solution to the multiple electrode problem lies with reformulating the manner in which we consider the charged particles moving in solution.

The movement of a single particle is related to its fraction of the total mobility, the total number of charges in solution, and the total current. From this we determine that to maintain a stable particle deposition rate, regardless of the electrode configuration, we need to drive the electrodes at a constant current. With a system which automatically drives voltages to different levels to create the appropriate current, we can control the particle deposition rate for a given particle concentration in a given ionic solution. In comparison to the electrostatic situation, the range of the electrophoretic force lies anywhere between the driving electrodes,

allowing for long range movement of particles, with speeds controllable by increasing currents and voltages.

Complications to the electrophoretic process arise from the manner in which we drive the current through the electrode/liquid interface. The products of those reactions are hydrogen and oxygen gas, as well as the ions H+ and OH-. At low currents, the gaseous byproducts tend to dissolve into solution and dissipate away from the electrodes, but at higher currents, the production is done at a high enough rates to form bubbles on the electrode. Given the currents and geometries we worked with, it was found that the bubbling threshold was above the particle deposition threshold, so this was not a significant issue.

1.12. Dielectrophoresis

Dielectrophoresis (DEP) is the movement of particles in solution towards or away from concentrations of electric field gradients (64). DEP has found applications in the sorting and sensing of nanoparticles(65), cells, nanotubes(66,67), DNA(68), gold particles(69), and the assembly of various nanocomponents(70-74). Its primary advantage lies in the fact that it can be performed at high frequencies (and therefore has no issues with acid or base creation at the electrodes), and because a single particle will move towards or away from an electrode at different frequencies related to the makeup and geometry of the particle, allowing for complex separations to be performed. For our work, these separations involve the

distinguishing of various closely related cell types, and the separation of various high molecular weight cellular fragments from blood. The work described in this dissertation involves mostly methodologies towards allowing DEP separation of high conductivity samples, which has been traditionally a difficult problem.

This DEP effect occurs due to differences in the dielectric constants of the solution and the particles that reside within it. Because the dielectric constants are a function of the applied electric field frequency and the material makeup, it is possible for a particle to exhibit both positive (moves towards high field gradient regions) or negative (moves away from high field gradient regions) DEP merely by changing the operating frequency of the applied voltage. In a simple sense, force can be though to arise from the alignment of dipoles in the particle being moved vs. the dipoles in the surrounding solution. Depending on how the material of the particle and solution respond to the applied electric field, the dipoles generated will either be in or out of phase, causing the net charge on the particle caused by that field to be in or out of alignment with the dipoles in the solution. In the limit where spherical particles are small compared to the local change in electric field gradient, the dielectrophoretic force on a particle can be approximated as

$$F_{dep} = 2\pi\epsilon_0\epsilon_m r^3 Re[K(\omega)]\nabla E^2$$

Where ϵ_m is the relative dielectric constant of the surrounding medium, r is the radius of the particle, and K(ω) is the Claussius-Mossatti factor, a dimensionless quantity which for spherical particles of a single material is given as

$$K(\omega) = \left(\frac{{\epsilon_p}^* - {\epsilon_m}^*}{{\epsilon_p}^* - 2{\epsilon_m}^*} \right)$$

Where ϵ_m^* and ϵ_p^* are the complex dielectric constants of the medium and the particle, which for the frequencies of interest for this kind of application is given by

$${\epsilon_x}^* = \epsilon_x - \frac{I\sigma_x}{\omega}$$

With σ = the conductivity of the material and ω is the angular frequency of the electric field. The change from positive to negative DEP is caused therefore by the change in the real portion of the dielectric constant as a function of frequency, or the falloff in the importance of the conductivity portion of the dielectric constant as the frequency rises. It should be noted that K(ω) is a function of the geometry, both radial, and angular, and the form given is only true for uniform spherical particles. Because for a given particle and electric field geometry, all other quantities in the force equation are fixed, the K(ω) term controls the magnitude and direction of the force at any given point. While it always is a dimensionless number between -1 and 1 (the actual range for a given particle is particle geometry dependant), its frequency dependence (and thus the direction of particle motion) will vary wildly with particle geometry. It should be noted that while a particle can have a maximum force applied to it (when K(ω) =+1 or -1), the force can be very small as well as K(ω) approaches zero. It is these regions where particle separations become most relevant between

similar particle types, so the strength of separation between two particles becomes important.

Where the electrophoretic force is proportional to the electric field strength, the dielectrophoretic force is proportional to the gradient of the electric field squared (which is in some sense a measure of electric field energy density). The particle can be seen to be rolling down a hill created by the shape of the electric field. Because the DEP force is so strongly geometry dependant (since it is based on gradients), the strongest force locations are where the electric field concentrates and turns corners as rapidly as possible.

Chapter 2: Electric Field Directed Self Assembly

2.1 Introduction

The work contained in this section is both the experimental and philosophical core of this dissertation(75). The *key* goal of this work was to demonstrate the viability of using electric fields to manipulate and assemble nanoparticles into higher order forms and structures. Our work focuses on what we believe to be one of the core problems of nanofabrication, namely how nanocomponents of various types and forms can be rapidly, controllably, and manufacturably integrated together in a single system. Our aim is to create a general method to bridge the gap between self assembled nanoparticle structures and the mass patterning methods typically used in MEMS and *CMOS* circuit fabrication. These methods should be general enough that any type of nano or microparticle can be a subject for deposition, ranging from small lift-off electronic devices hundreds of microns across, to particles a few nanometers across. It is our belief that this work demonstrates the viability of this method.

The ultimate technology and platform that this work would lead to would look different than the system presently being used. The system used for layer fabrication was originally designed for DNA diagnostics. Because of this (as described in the next section), the electrodes used for layer deposition were not suitable for the fabrication of fully “filled” surfaces (layers fabricated on one electrode do not physically touch those fabricated on an adjacent electrode due to the system

geometry). The system allowed for the determination of optimal parameters for z-dimensional nanoparticle deposition, but it does not allow for the demonstration of a fully x-y patterned surface. However, this is not a fundamental limitation of the techniques, but rather was a limitation of the available equipment.

The work herein primarily deals with methods to determine the optimal fabrication parameters of electronically assembled nanolayers. There are a wide variety of possible nanoparticles of interest, and it is unlikely that the optimal parameters for the deposition of each particle type are identical. However, the general methods used to determine those parameters should be similar to the methods described herein. The particles used in this work were chosen more for their optical detectibility and surface properties than any other intrinsic properties, but they provide a useful test case of the general electronic layer by layer assembly method. The experimental methods in this section involve using electric fields to direct the deposition of particles suspended in a buffered aqueous solution down to a binding surface. Both the nature of the binding surfaces as well as the properties of multiple nanoparticle layers were studied in this work. A brief study of the properties of the nanoparticles themselves was conducted to determine the suitability of the particles for forming layers in general.

2.2 Equipment

2.2.1 Nanogen ACV400

Nanogen has designed and developed several DNA diagnostic systems. The principle behind these systems is to use DC electric fields to concentrate DNA probes to specific locations (electrodes)(76-78), though similar technology was developed to assemble mesoscale components(79). By increasing the concentration of the DNA at the target location, binding is accelerated, and background crosstalk is reduced. The system we had access to was a development model which allowed direct access to a mounted but unpackaged CMOS microarray (normally the CMOS microarrays are further packaged to include a sealed fluidic system).

The CMOS microarray consists of 404 electrodes built on top of a CMOS system that simultaneously and independently measures and controls the voltage of each individual electrode. Four large voltage controlled counter electrodes surround a grid of 400 smaller (55 micron) current and voltage controllable deposition electrodes. The larger electrodes can go between 0-5 volts, and allow the electric field to access most of the solution. They are further divided into two subgroups, the long (those on the top and bottom of the array), and the short (those on the sides of the array). The electrodes in each of the groups are controlled together (in practice all 4 counter electrodes were always set at the same voltage). The inner electrodes are arranged in a 25 x 16 grid. Each of these inner electrodes are 55um in diameter and are spaced 180 μm apart, center to center (for a fill factor ~7%). They can supply between 0-5 volts, and can source between -1 to 1 uA of current (for a maximum

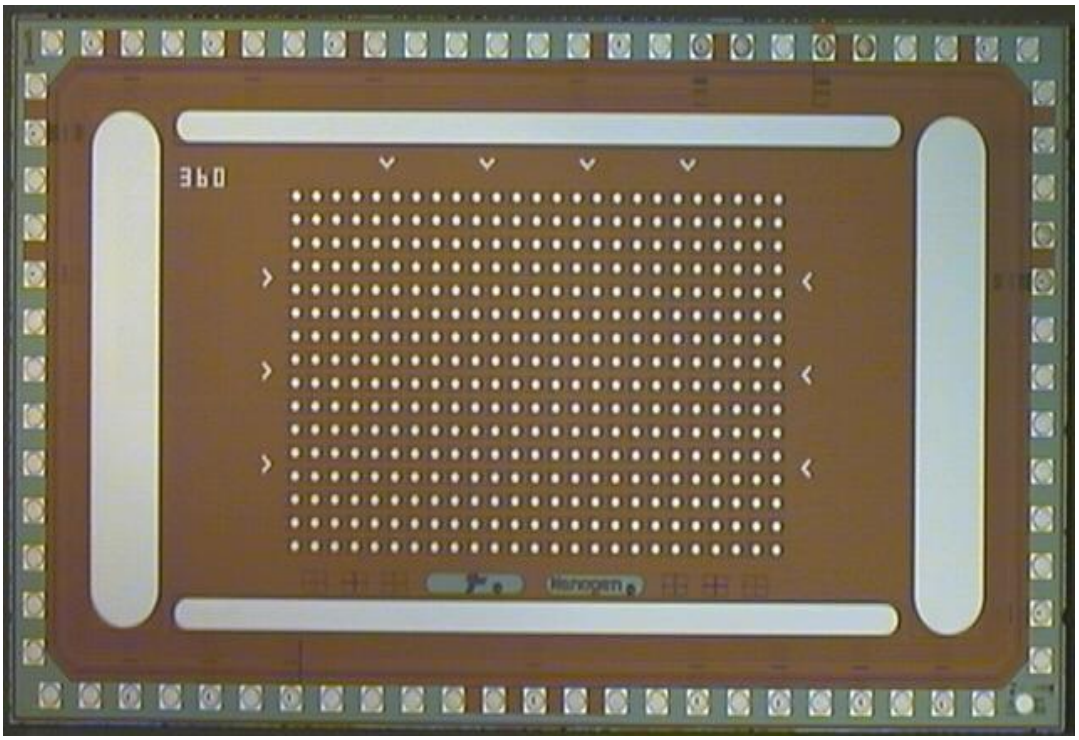

Figure 2.1: The Nanogen 400 site chip used for the experimental work.

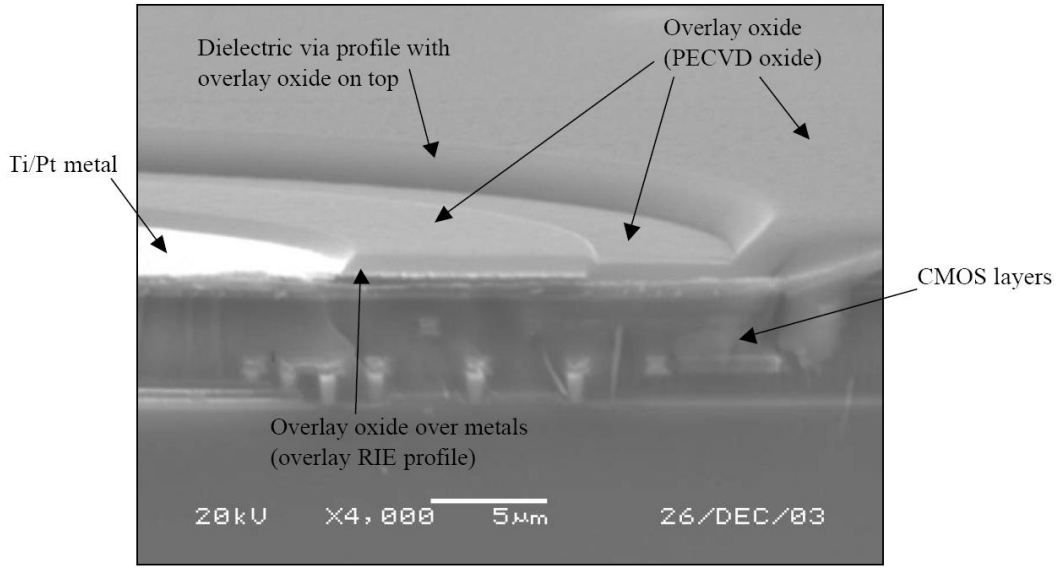

Figure 2.2 : SEM closeup of the electrode structure

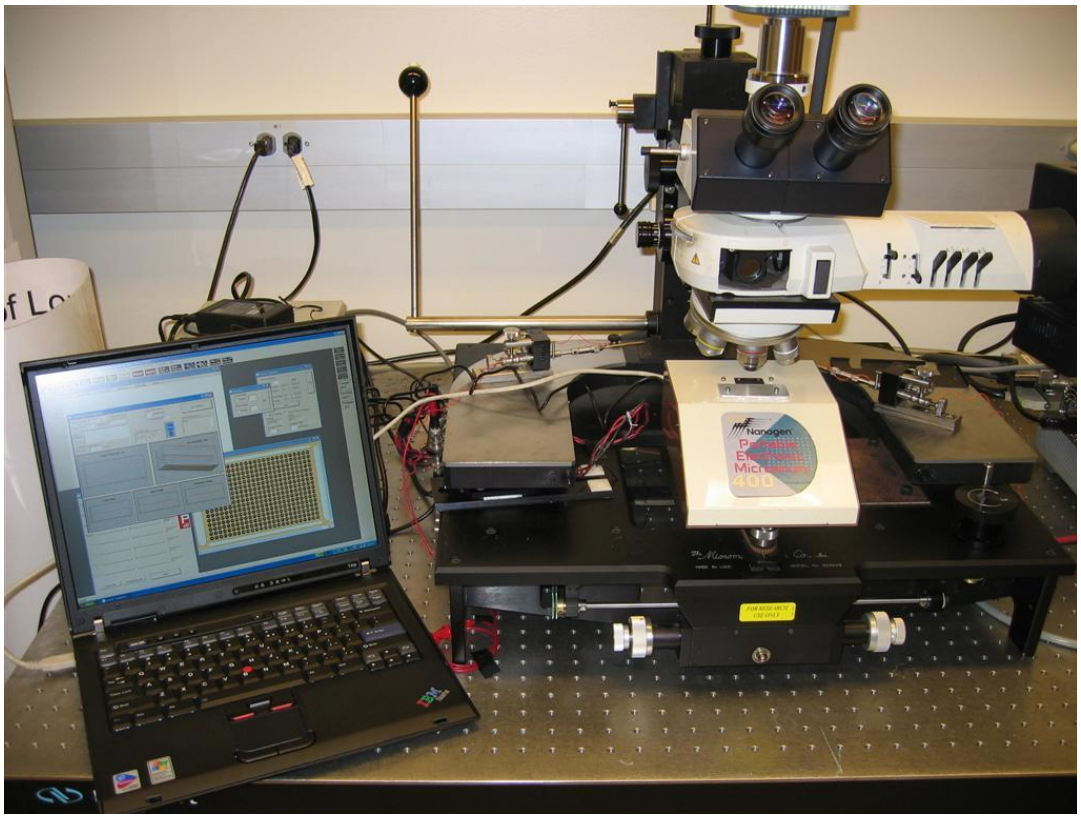

Figure 2.3: The experimental setup

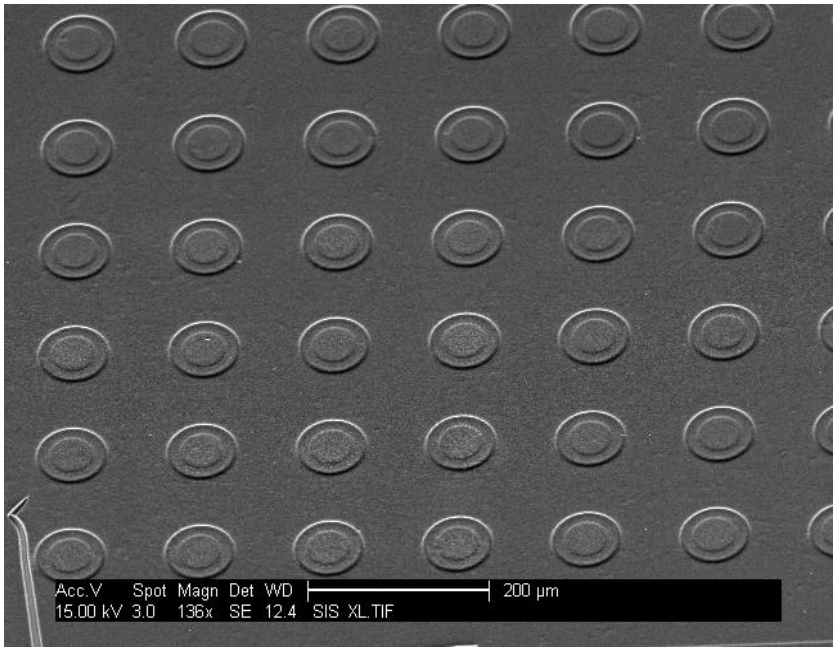

Figure 2.4: SEM image of electrode array

current density of 420 A/m^2). The chip can reliably source current with at least a 25nA resolution. Each inner electrode can simultaneously be run at a different voltage or current level. These current and voltages can be programmed through a computer interface to a control board, allowing the pattern of activation of the electrodes to be changed during an experiment in complex manners (as described in the further sections). Each electrode has a current feedback system that monitors the current and adjusts the voltage continuously to maintain the desired level. The system takes on the order of two seconds to achieve the desired current level.

The electrodes are made of platinum, and are passivated at the edges with a layer of silicon dioxide to prevent liquid from flowing underneath the electrode, preventing de-lamination of the electrode and damage to the electric circuitry. The inner area of the microarray with the 400 small electrodes is covered with a 10 um layer of polyacrylamide gel containing streptavidin. This gel was designed to bind biotinylated DNA probes internally in its volume, but in our present work served as both a passivation (protective) and binding surface layer (the necessity of the passivation layer will be described in a later section).

The microarray itself is mounted inside a larger package of ceramic. This package contains a series of contact electrodes which lead to the active microarray (chip) itself. These electrodes/wires are not directly in contact with the electrodes of the chip itself, but rather contain power, temperature sensors, and data lines which are used to control the chip through digital means. Previous iterations of the system

had a single wire running to each electrode, but the system used in these experiments were all run though intermediate circuitry. Since all this work involves direct electrophoretic attraction of charged nanoparticle to the electrode, this setup was preferable because of the level of control it allowed. However, other work done by our group involves the AC dielectrophoretic (DEP) attraction of nanoparticles to an electrode surface, which this chip (400 site CMOS) cannot perform due to its relatively long switching times. The 400 site CMOS chip is mounted to the bottom side of the ceramic package, with a hole cut into the ceramic above the main area of the chip. This creates a well that holds around 20ul of fluid above the electrodes when the fluid surface is flat with ceramic surface, though up to around 40ul of fluid can be placed in the well if fluid flatness is not desired.

In many ways this chip proved to be ideal for our purposes. The ability to simultaneously control the current of every electrode at different levels across the chip allowed us to in essence conduct up to 400 different experiments at the same time. The optimal current and voltage range found for particle deposition turned out to be well within the range provided for the chip. The presence of the surface gel was instrumental to the success of this work, since it protected the fabrication process from the direct effects of electrochemistry as well as providing a substrate to build the layers off of. However, it should be noted that the device has a relatively low fill factor and no electrodes are physically adjacent, so it is impossible to fabricate structures that are continuous across the array. A full fill factor is a feature we'd like

to engineer into future revisions of this technology. The data in the results section should be viewed in the context of the geometry of this device.

2.2.2 Microscopy

To image the deposition of the nanoparticles in this work, we extensively used fluorescent microscopy. A mercury arc lamp was run through a fluorescence filter set which selectively allowed excitation light to impinge on the nanoparticles of interest and collect the emission light from those particles. Images were captured from the microscope with a Orca-ER camera from Hamamatsu. Our filter sets were sensitive enough that we were able to distinguish between the fluorescence of the different particles we used (see next section). By switching between filter sets we could image all particles of one type independently of the other particles. By measuring the fluorescent intensity at a particular electrode, we were able to measure the relative number of particles at the electrode. This allowed us to take real-time measurements of layer growth during the experiment, rather than having to resort solely to post experiment measurements such as an SEM.

2.2.3 SEM

For this work, extensive use was made of SEM imaging to examine the surface characteristics of the deposited layers. This was a complement to the optical methods since the fluorescence was used to determine the amount of particles deposited with low spatial resolution, whereas the SEM was used to examine the

properties of the surface at high resolution but with no ability to view into the sample. The SEM used was a Phillips XL30 ESEM. All samples were coated with a thin layer of gold or chromium to increase contrast under the SEM. Some samples, most notably areas with bare gel or a small amount of deposited beads would spontaneously “bubble”. In such a situation, a large deformation would occur which would destroy the quality of the local image. This was mostly avoided by focusing in a nearby region, then moving to the region of interest while the scanning electron beam was off and taking a single still shot. For the most part, however, all regions where more than a monolayer of beads had deposited down were impervious to this problem.

2.3 Materials

Beads

For these experiments, four types of nanoparticles were used. Of these there were two sizes (40 nm and 200 nm diameter beads), and each of these groups contained both a biotin functionalized and neutravidin functionalized beads. The beads were all purchased from Invitrogen and were as follows

- FluoSpheres® NeutrAvidin® labeled microspheres, 0.04 µm, red fluorescent (580/605) (Invitrogen F8770)
- FluoSpheres® biotin-labeled microspheres, 0.04 µm, yellow-green fluorescent (505/515)) (Invitrogen F8766)

- FluoSpheres® NeutrAvidin® labeled microspheres, 0.2 µm, yellow-green fluorescent (505/515) (Invitrogen F8774)
- FluoSpheres® biotin-labeled microspheres, 0.2 µm, yellow-green fluorescent (505/515) (invitrogen F8767)

All nanoparticles came in a stock solution containing 50mM NaCl, 50mM Sodium Phosphate, 0.02% Tween 20, 2-5% Sodium Azide, in a pH 7.5 solution. The beads themselves were listed as 1% solids making the undiluted concentration 500nM for the 40nm beads and 4nM for the 200nm beads. The beads were chosen for several reasons. First, they were of the size range we were interested in (in the tens to hundreds of nanometers). Secondly, they were available in both biotin and neutravidin subtypes, which would allow for specifically complementary binding of one particle type to another. Finally (at least for the 40nm beads) they came in different colors, which allowed for our microscope system to fluorescently resolve them into the separate subtypes. The 40nm Neutravidin beads were red fluorescent, and the 40nm Biotin beads were yellow green fluorescent, which allowed for us to detect the accumulation of a single type of bead at a time, even when both types were down on the same surface.

Streptavidin

Streptavidin is a four subunit protein that strongly binds to the small ligand molecule called biotin. Each subunit is able to bind a single biotin molecule,

allowing a single streptavidin protein to bind up to four biotins. We used streptavidin (Roche 11721666001) extensively in our experiments to provide an active binding surface for our beads. The use of this will be described in the methods section.

Biotin Dextran

Biotin dextran is a polymeric molecule containing several biotins coming off of a dextran backbone. For our work, we used (Sigma-Aldrich, B9264) which contains on average 20 biotins per molecule (with an average molecular weight of 80,000). We used the biotin dextran to crosslink streptavidin surfaces and provide more streptavidin binding sites. The full description of this work is found in the experimental descriptions.

L-Histidine

L-histidine is an amino acid we used extensively as a buffer for all of the following experiments (Sigma-Aldrich, H6034). It was chosen because it is a zwitterionic buffer. In other words, it is able to prevent changes in pH to the solution, while having a net charge of zero. Because it is uncharged, when an electric field is applied to the solution, the zwitterionic histidine itself does not contribute to the conduction of current, allowing the charged particles of interest to move much more rapidly. The histidine only moves when it picks up a charge as it acts as a buffer (when it associates with the hydrolysis products H+ or OH-). This action slows down

the electrolysis products as compared to an unbuffered solution, once again allowing the nanoparticles to act as a greater portion of the current. The typical concentration of l-histidine used in solution was 50-100mM

2.4 General experimental methods

This section describes the general methods used in the experiments reported in this study. However, while it is general, the methods used in various other experiments vary in a few details. For the most part, these details vary only in the arrangement and configuration of the various active electrodes at each stage of the experiment. It will be noted in each experimental section as to where the differences lie. It should also be noted that the methods used here are the result of various optimizations from our earliest work. The earlier methods leading up to those described here will be discussed in a later section, but are not directly relevant to the results presented in this section. Therefore they are placed later in the text for pedagogical clarity.

2.4.1 Chip preparation

The experimental process is divided into two stages. The first stage is always the same between experiments and involves the preparation of the chip for the experiment. The second part involves the experimental deposition steps and is

where the variances lie, but in general involves repeated deposition steps with various electrode configurations.

Experimental setup preparation

1) The chip is visually inspected for any gross defects (such as a torn gel layer).

2) The chip is mounted and leveled on the controller box.

3) The chip is electronically tested while dry. A small fraction of the chips exhibited a behavior where they would have an uncontrollably high leakage current, rendering them unsatisfactory for further operation. Such chips were remounted, and if this failed to resolve the leakage issue, they were discarded.

4) The chip sample well was repeatedly washed of preservatives. These preservatives consisted of a protective sugar (arabinose) used to prevent the gel from cracking when it is not hydrated (stored). The amount of washing would vary between chips since they had different amounts of preservative on them. In general the washing consisted of repeated pipettings of 40 µl of Millipore filtered water, each of which was agitated across the chip surface 10 times using the pipette. This was repeated until the sugar was all dissolved, and then cleaned two more times to remove any excess sugar.

5) 20 µl of a 2 µM biotin dextran solution in water was allowed to react with the gel surface for 30 minutes.

6) After step (5) the chip was washed (as in step (4)) 5 times with Millipore water to remove unbound biotin dextran.

7) 20 µl of 100 µM streptavidin were allowed to react with the surface for 30 minutes.

8) The chip was washed 5 times using 100mM L-Histidine solution. This is to equilibrate the chip with L-histidine buffer for the experimental procedures. The chip is left with 20 µl of buffer until right before the experiments begin. The experimental portion usually took place immediately after chip preparation, and the chip was always kept hydrated in buffer until the experiments began.

The end result of this process is a chip consisting of multilayer porous materials with a final surface binding layer. The first layer is the electronic and electrode layer, terminating in the platinum electrode at the chip's surface. On top of that is the 10 µm thick Polyacrylamide/Streptavidin gel layer. Next is a layer of Biotin-Dextran which is bound to the gel through interactions with the interior streptavidin as well as possible nonspecific interactions. Finally, there is a layer of streptavidin which crosslinks the biotin dextran layer together and provides the basic binding layer for the fabrication process (see later chapter on initial work). The chip is now ready to be addressed with the first layer of biotin nanoparticles.

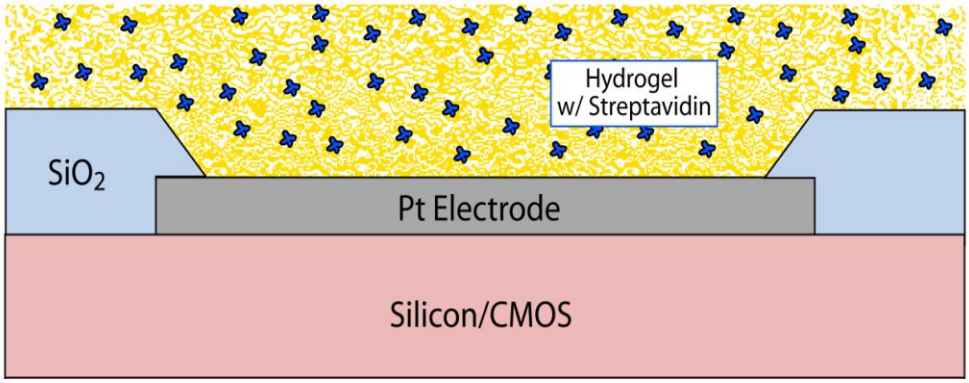

Figure 2.5a: A diagram (not to scale) of the electrode gel interface before surface modification

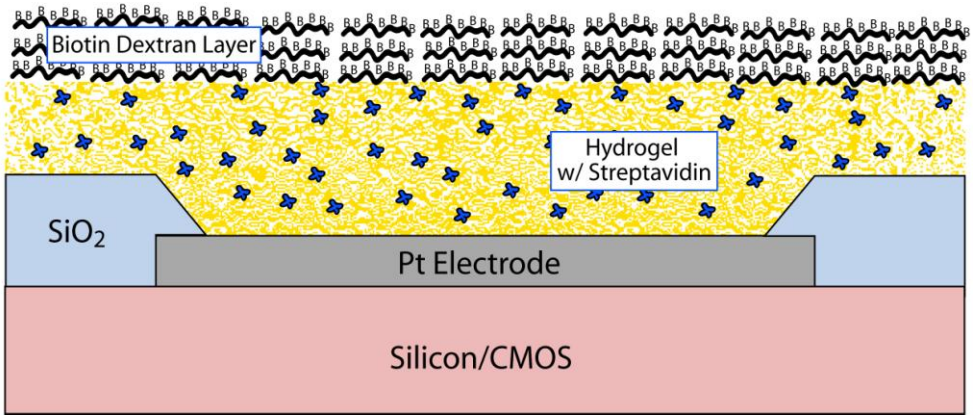

Figure 2.5b: A diagram of the electrode after modification with biotin dextran

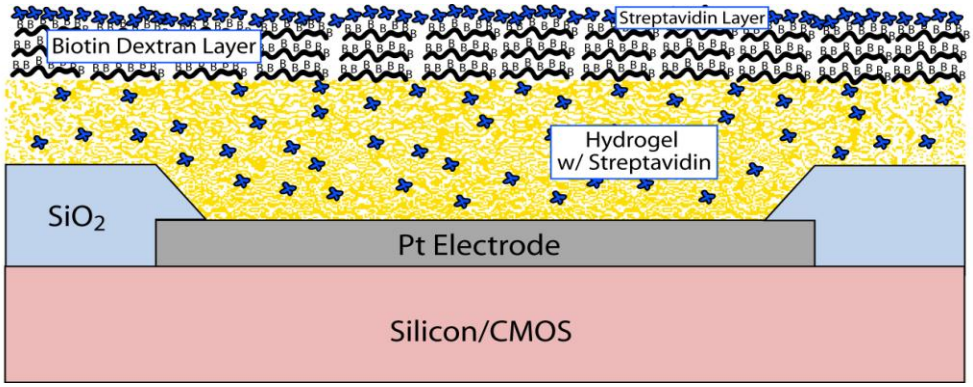

Figure 2.5c: A diagram of the electrode after the final modification with streptavidin.

2.4.2 General Experimental Procedure

1) A 1/100 dilution of the beads is prepared. This is typically 10 µl of bead stock into 990 µl of 100mM L-histidine buffer. For most of the experiments reported here, the beads used were 40nm biotin (yellow green fluorescence) and 40nm Neutravidin (red fluorescence) beads.

2) Any excess liquid is pipetted from the chip and 20 µl of the biotin bead solution is placed in the chip's well.

3) The geometric pattern for electrode activation for biotin beads is run through the computer controller, and the negatively charged beads are electrophoretically attracted to the electrode surface (see figure 2.6a).

4) The chip is gently washed with a solution of 100mM l-histidine buffer until no beads appear to wash from the surface of the electrodes. This usually takes 5 washes (figure 2.6b).

5) The appropriate fluorescent filter set is set in place to view the biotin beads, and an image is recorded into the computer. It should be noted that the same gain settings were used throughout the entire experimental run to preserve consistency between images. The gain settings were chosen so that there was appreciable data from single monolayers, but when a large number of layers were deposited >50, the image was not saturated.

6) Any excess liquid is pipetted from the chip and 20 µl of the biotin streptavidin solution are placed in the chip's well.

7) The pattern for electrode activation for streptavidin beads is run through the computer controller, and the beads are pulled down to the electrode surface (see figure 2.6c).

8) The chip is gently washed with a solution of 100mM l-histidine buffer until no beads appear to wash from the surface of the electrodes. This usually takes 5 washes (figure 2.6d).

9) The appropriate fluorescent filter set is set in place to view the streptavidin beads, and an image is recorded into the computer.

10) Steps 2-9 are repeated multiple times (usually between 10-50 times). The number of layers quoted in various sections counts biotin and streptavidin particles depositions as individual layers (see figure 2.6e)

11) The remaining liquid is removed from the chip after the final wash step. The chip is not washed in unbuffered water for reason discussed in the lift-off section.

The electrode activation pattern used varied from experiment to experiment. Typically it consisted of multiple columns of activation patterns, with each row in a column having a different activation current, and each column being activated for a different time, or not at all during a particular particle deposition. Due to technical reasons, to vary the deposition times of various electrodes, the chip was activated in one pattern for a set period of time, and then a new electrode pattern was loaded that was similar to the first pattern but with one or more columns turned off. The new pattern was then run for a period of time until a new pattern was

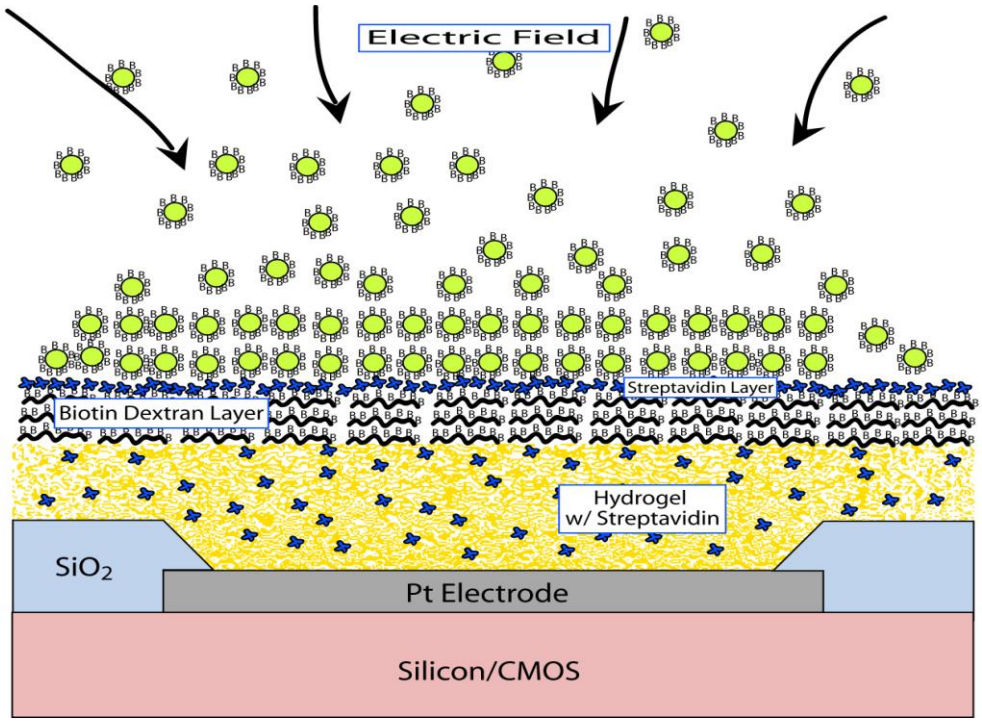

Figure 2.6a: Initial particle deposition

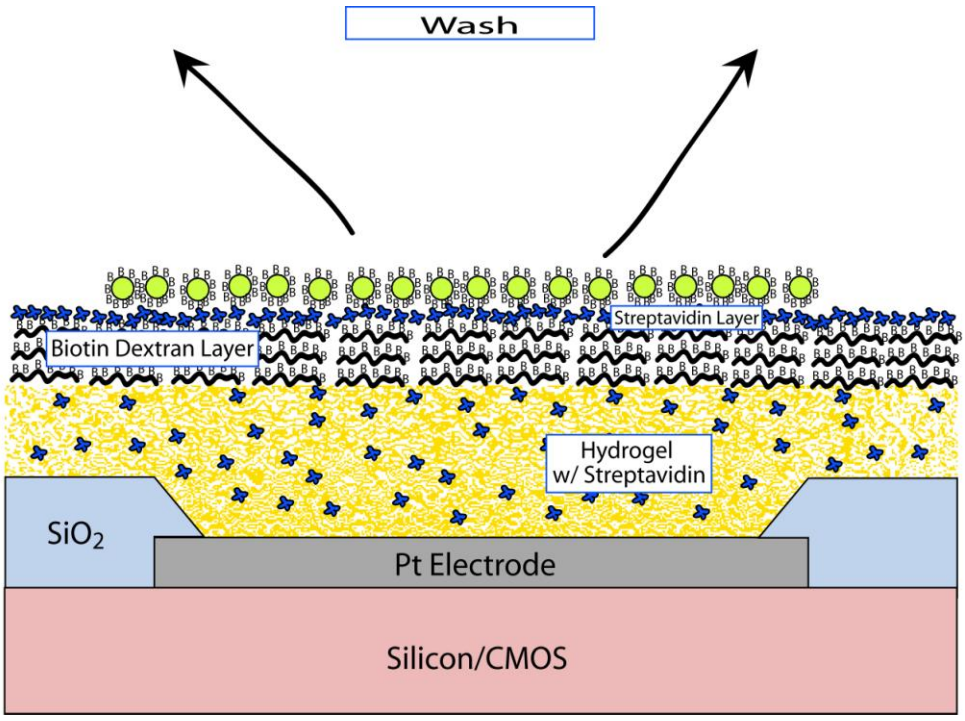

Figure 2.6b: Particle wash leaving single monolayer

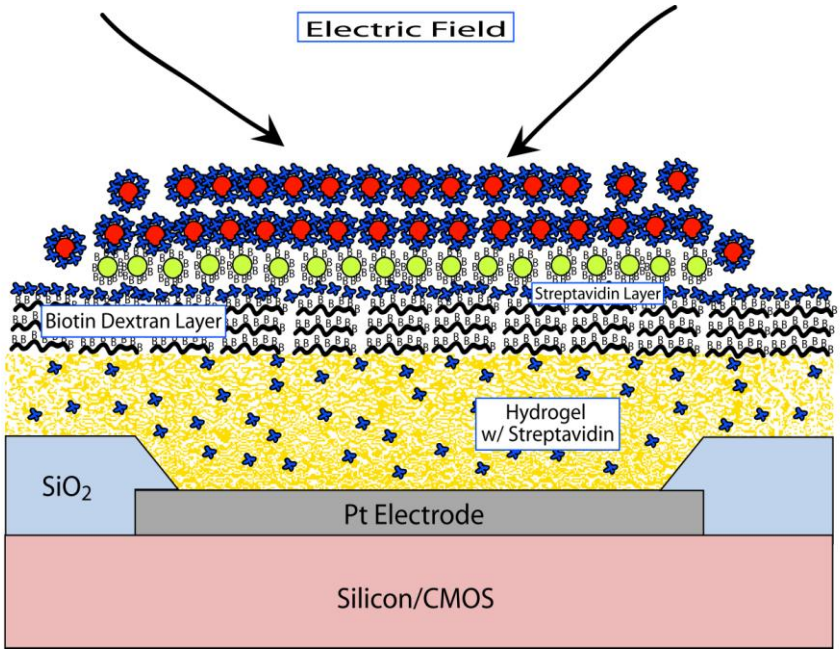

Figure 2.6c: Second particle layer deposition

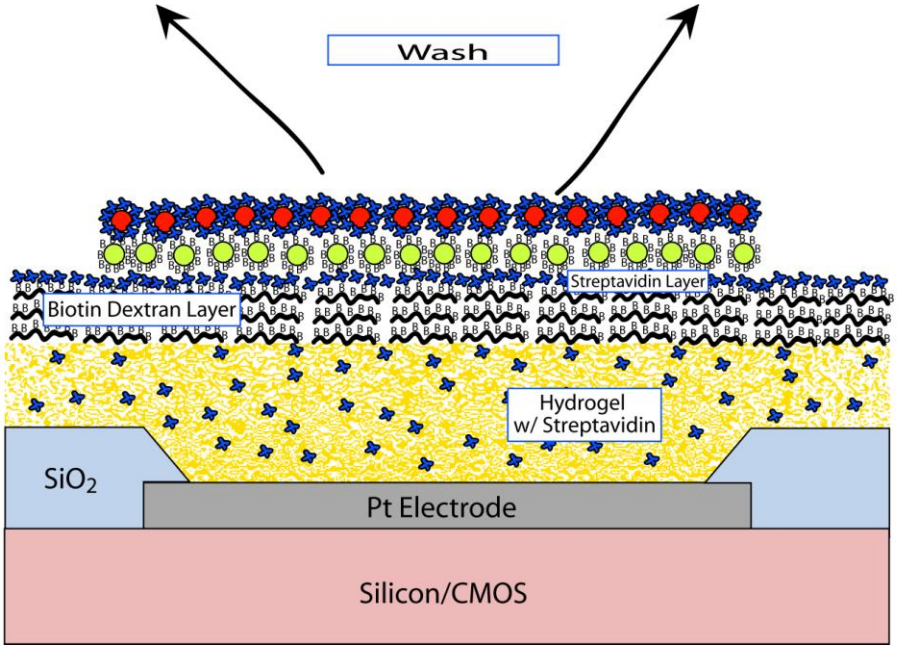

Figure 2.6d: Particle wash leaving second monolayer

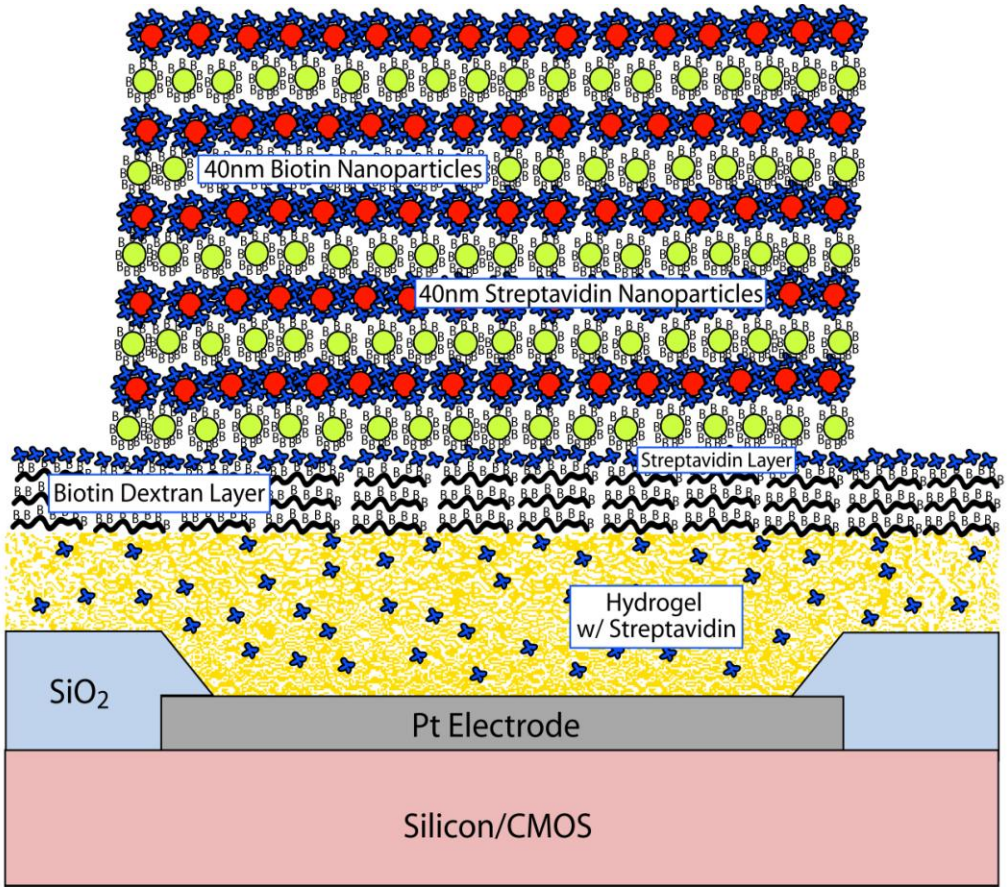

Figure 2.6e: Diagram of nanoparticle layer stack after repeated depositions.

A	1	2	3	4	5
1		0.025	0.025	0.025	0.025
2		0.050	0.050	0.050	0.050
3		0.075	0.075	0.075	0.075
4		0.100	0.100	0.100	0.100
5		0.125	0.125	0.125	0.125
6		0.150	0.150	0.150	0.150
7		0.175	0.175	0.175	0.175
8		0.200	0.200	0.200	0.200
9		0.225	0.225	0.225	0.225
10		0.250	0.250	0.250	0.250
11		0.275	0.275	0.275	0.275
12		0.300	0.300	0.300	0.300
13		0.325	0.325	0.325	0.325
14		0.350	0.350	0.350	0.350
15		0.375	0.375	0.375	0.375
16		0.400	0.400	0.400	0.400

B	1	2	3	4	5
1			0.025	0.025	0.025
2			0.050	0.050	0.050
3			0.075	0.075	0.075
4			0.100	0.100	0.100
5			0.125	0.125	0.125
6			0.150	0.150	0.150
7			0.175	0.175	0.175
8			0.200	0.200	0.200
9			0.225	0.225	0.225
10			0.250	0.250	0.250
11			0.275	0.275	0.275
12			0.300	0.300	0.300
13			0.325	0.325	0.325
14			0.350	0.350	0.350
15			0.375	0.375	0.375
16			0.400	0.400	0.400

C	1	2	3	4	5
1				0.025	0.025
2				0.050	0.050
3				0.075	0.075
4				0.100	0.100
5				0.125	0.125
6				0.150	0.150
7				0.175	0.175
8				0.200	0.200
9				0.225	0.225
10				0.250	0.250
11				0.275	0.275
12				0.300	0.300
13				0.325	0.325
14				0.350	0.350
15				0.375	0.375
16				0.400	0.400

D	1	2	3	4	5
1					0.025
2					0.050
3					0.075
4					0.100
5					0.125
6					0.150
7					0.175
8					0.200
9					0.225
10					0.250
11					0.275
12					0.300
13					0.325
14					0.350
15					0.375
16					0.400

Figure 2.7: Electrode activation templates for a 4 column activation process (values are in μA). (A) is run for 10 seconds, (B) and then (C) for 5 seconds each, and then (D) for a final 10 seconds, giving 10, 15, 20 and 30 second activation times

loaded. By repeating this process a few times, it was possible to vary the run times of electrodes across the chip.

Figure 2.7 shows the activation pattern for a 5x16 section of the electrode array. A typical activation pattern would sequentially have **A** running for 10 seconds, **B** and **C** for 5 seconds, and **D** for 10 seconds. The value listed in each cell is the intensity of the current in μA. Blank cells are unactivated (not set to zero volts, but left floating). This would mean column 1 is left as an unactivated control, while columns 2-5 run for 10, 15,20, and 30 seconds respectively. Columns 6-25 are repeats of columns 1-5 and are used to examine cross chip variation. The outer four counter electrodes are set to 0 volts. The activation pattern shown here is used in the upcoming section on determining the optimal deposition time and current. In that system, both particles use the same deposition pattern over the same electrodes.

2.4.3 Stringency determination experiments

In a layer by layer deposition process, there is an implicit assumption that as you place down a layer, you do so in a controlled manner. The layering process is assumed to be self passivating. That is, there is a property of the surface that causes binding to occur with some aspect of the solution above it. Once some amount of binding occurs, that property is consumed, and further binding is impossible until the surface has been refreshed by the subsequent layer. If this assumption fails to hold, that is a single kind of particle can bind to itself in a form of

A	1	2	3
1		0.025	0.025
2		0.050	0.050
3		0.075	0.075
4		0.100	0.100
5		0.125	0.125
6		0.150	0.150
7		0.175	0.175
8		0.200	0.200
9		0.225	0.225
10		0.250	0.250
11		0.275	0.275
12		0.300	0.300
13		0.325	0.325
14		0.350	0.350
15		0.375	0.375
16		0.400	0.400

B	1	2	3
1	0.025	0.025	
2	0.050	0.050	
3	0.075	0.075	
4	0.100	0.100	
5	0.125	0.125	
6	0.150	0.150	
7	0.175	0.175	
8	0.200	0.200	
9	0.225	0.225	
10	0.250	0.250	
11	0.275	0.275	
12	0.300	0.300	
13	0.325	0.325	
14	0.350	0.350	
15	0.375	0.375	
16	0.400	0.400	

Figure 2.8: Electrode activation templates for a stringency determination process. (A) is run for 15 seconds when the biotin beads are present on the chip and (B) is run for 15 seconds when the streptavidin beads are present on the chip. Values Listed in μA.

continuous growth, then the system is less controlled. In such a system control of layer thickness would be achieved more by accurate deposition times and currents than by an intrinsic self limiting process. The method discussed in this section is to determine the intrinsic stringency of the particles used in these experiments, that is, to determine to what degree the particles stick to their own kind as opposed to those particles to which they are expected to adhere to.

Procedure:

1) The chip is prepared for deposition as described in the general method.

2) The chip is activated as described in the general method, except that during the biotin bead deposition pattern A in figure 2.8 is used for 15 seconds, and for streptavidin deposition pattern B is used for 15 seconds.

As can be seen in the figure, the biotin beads are deposited only in columns 2 and 3, while the streptavidin beads are deposited only in columns 1 and 2 (the pattern is repeated every three columns). This means that column one is only directly exposed to streptavidin beads, while column three is only exposed to biotin beads. This experiment is then repeated only with a chip which has a final biotin surface, rather than one with a streptavidin surface. The results for the beads used in these experiments are described in the results section.

2.4.4 Initial monolayers

When this work began, we had several open questions involving the deposition of the particles. One of those was whether or not enough beads were accumulating at the direct surface of the gel to form a monolayer or particles, what is the quality of the monolayer once it has formed, and what deposition conditions were necessary for the formation, assuming it takes place. In the case of less than perfect stringency we would want to know the monolayer deposition conditions to avoid continual growth of unwanted particles. Another question we had was what is the nature of subsequent layers past the initial. Does the rate of particle deposition slow once a few layers are already deposited? While this is not answered directly by the monolayer studies, it plays a part, as shown in the results section.

The procedure for the monolayer studies experiment is the same as described in the general section, except instead of putting down multiple depositions of both types of particles, only a single layer of particles complementary to the surface binding agent is used. In this case biotin particles were used on a streptavidin surface. Once the chip was cleaned and dried, an SEM was taken of the center of electrodes of various times and currents of deposition. From these images a fill factor of beads on the electrodes was determined. The results of these studies are reported in the results section

2.4.5 Optimal Deposition Time and current

From the early experiments in this work, two competing phenomena formed a window in which the experiments were relatively more or less successful. Success was judged by an additional layer being deposited on top of a previously deposited stack while the stack itself maintained its structural integrity. One of the limiting phenomena was insufficient deposition of particles. At low currents and times of deposition, insufficient particles were attracted to an electrode to form a sufficient binding surface for subsequent layers. In the results sections this is detailed more clearly. The other limiting factor was the degradation of the deposited stacks. After some number of layers for a given current and time, the entire layer stack would tend to break off from the surface, with this process occurring first at the highest currents and time. Thus to be able to build as many layers as possible, it becomes necessary to determine what the optimal deposition conditions are.

The process for determining the optimal current and time parameters is given exactly in the general methods section above. Repeated alternate depositions of biotin and streptavidin nanoparticles are layered on the electrodes. This process continues until some arbitrary condition is met, such as some total number of deposited layers or until some fraction of the deposited stacks have become damaged with enough pristine layers remaining for SEM analysis. Typically the number of total layers was between 20-100. See the results section for more details.

These were the baseline experiments used to collect the bulk of the growth data found in results section.

2.5 Results

The results described herein are produced from two different data sources. The first is intensity data from images taken during each deposition step. We make the assumption that the fluorescent intensity measured by the camera (when the background is subtracted) is directly proportional to the number of particles deposited on the electrode (assuming the camera has not reached intensity saturation). The data is extracted by measuring the peak pixel intensity for an electrode when extracting the information in Labview. Photo/thermal bleaching of the particles is prevented by blocking the excitation beam when the image is not being taken. The fluorescent intensity gain at a single electrode from picture to picture is taken to be an equivalent gain in the number of deposited particles. This method leads to quantitative measurements for the changes in the ratios of particles, but it does not allow a direct measurement of the number of particles. Since the optics and gain may vary between experimental runs, the values measured are only to be compared during a single experiment, and are measured in arbitrary units. When a deposited layer stack breaks or comes loose from the surface, that experimental parameter is taken as finished and subsequent points are not reported. Due to the limitation of optical resolution, only large surface details are measured.

The second method of data collection was by examining the deposited layers under the SEM. This method gives us an accurate view of the surface, but is unable to tell us details such as thickness of an individual layered structure. Ten layers of beads looks identical to 2 or 50. Only in cross-sections can an idea of the depth of a structure be determined under SEM, and even then the thickness is only approximate. Due to the nature of the SEM imaging, it is impossible to distinguish between the biotin and streptavidin beads (since they are the same size and mostly the same material) that can easily be distinguished under the fluorescent microscope. The SEM and Fluorescent datasets can be reconciled when looking at single layer studies since the SEM is able to determine at which point a monolayer forms, and one can tie microscope data to determine the fluorescent intensity of a single bead monolayer. Data from both measurement regimes is presented in the following section.

2.5.1 Stringency

Before carrying out fabrication of alternate multilayer nanoparticle structures, we analyzed the tendency of the biotin and streptavidin nanoparticles to self adhere. If layer formation resulted from the continual accumulation of the same kind of nanoparticles through nonspecific binding (biotin to biotin or streptavidin to streptavidin), then this would negatively impact the quality of multilayer structures. Figure 2.9 shows the results for accumulation of biotinylated 40 nm yellow-green

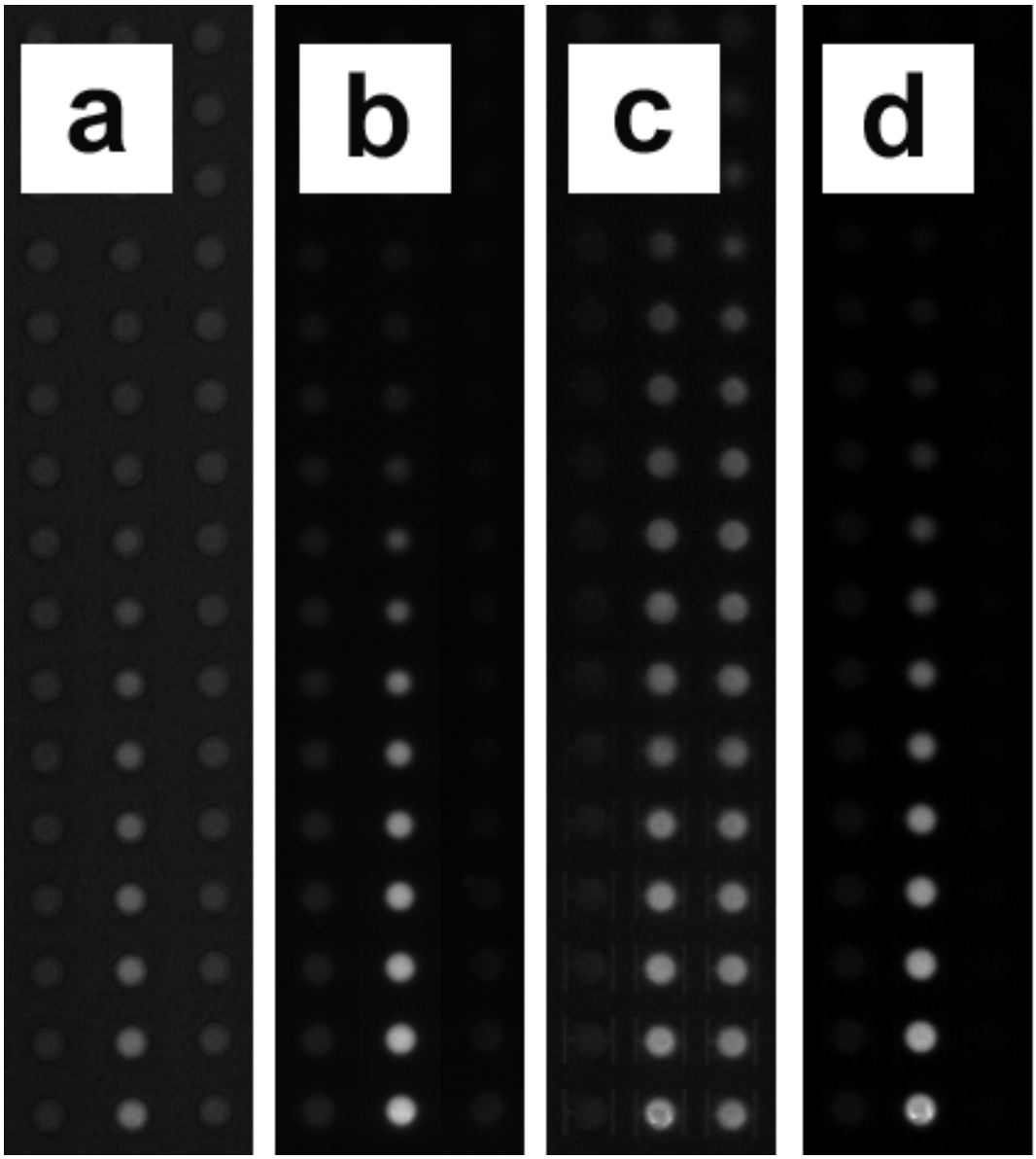

Figure 2.9a-d: stringency experiments under different conditions. (A) Shows biotin bead fluorescence on a biotin surface, (B) shows streptavidin bead fluorescence on a biotin surface, (C) shows biotin bead fluorescence on a streptavidin surface, (D) shows streptavidin bead fluorescence on a streptavidin surface,

fluorescent (Em max 540nm) nanoparticle and streptavidin 40 nm red fluorescent (Em max 615 nm)nanoparticles, starting on both a biotinylated (microarray) surface and the high density streptavidin surface. Since the biotin (yellow-green) and streptavidin (red) nanoparticles have little overlapping fluorescence spectra, it is reasonable to assume that most of the fluorescence signal in the image is due to either the biotin or streptavidin nanoparticles. Figure 2.9b, and and 2.9d show that streptavidin nanoparticle self adhesion is very low, as the only case where streptavidin nanoparticles strongly accumulate is where biotin nanoparticles have been previously bound. As can be seen in Figure 2.9c (biotin nanoparticles on a streptavidin surface), it appears that biotin nanoparticles do have some tendency to self adhere, however this accumulation is still relatively minor when compared to what is observed for the alternating biotin/streptavidin structures. The accumulation of the particles in the overlap deposition column is not explainable solely by the perpetual deposition particles. However, due to the better stringency of streptavidin particles, they are the one with the later accumulation data will be reported. This may lead to a slight discrepancy with the monolayer fabrication data, which due to the nature of the chips surface is based on biotin particles.

2.5.2 Monolayers

Initial experiments were carried out to determine the optimal electrophoretic conditions necessary to create a single monolayer of nanoparticles.

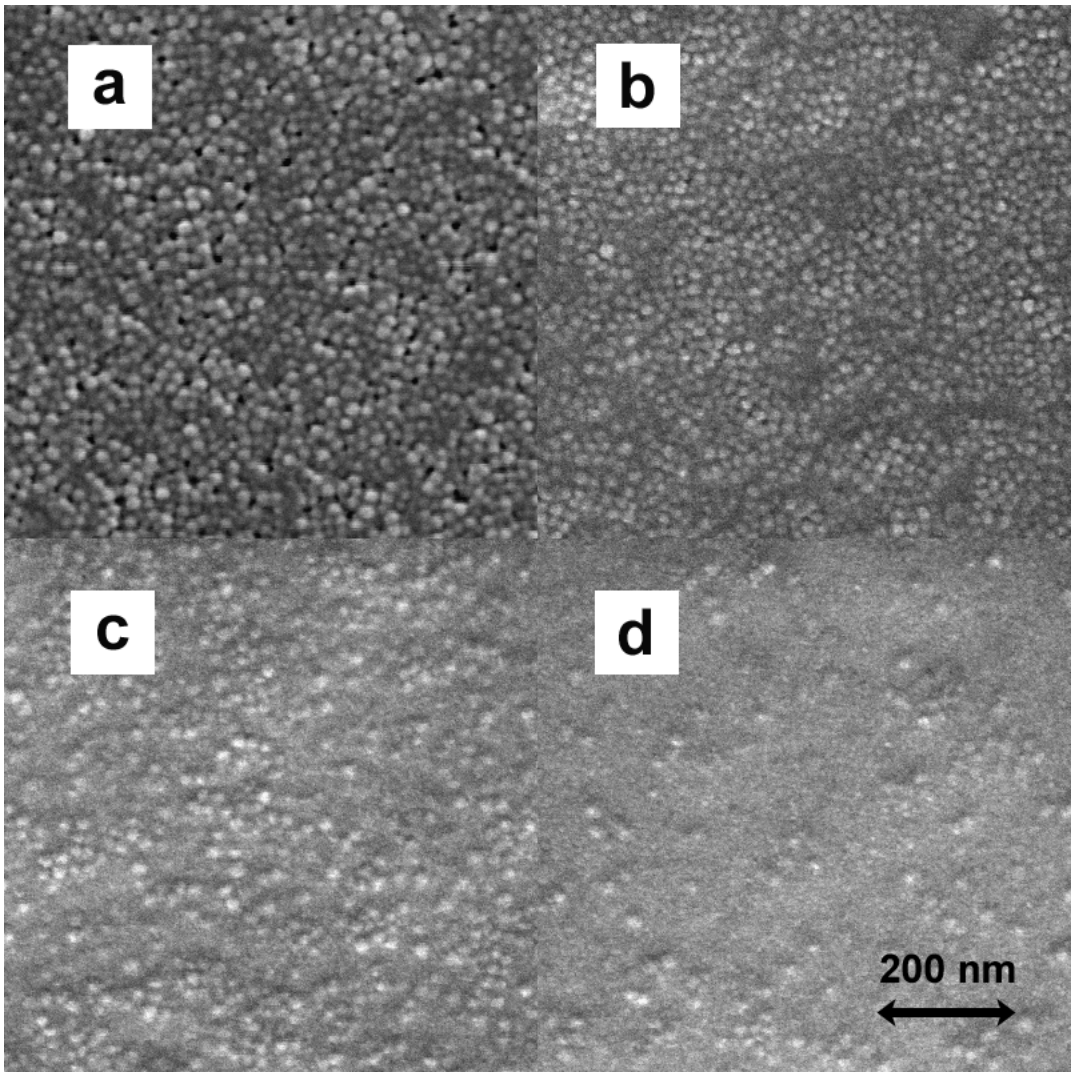

Figure 2.10a-d: SEM images of the initial deposition of 40 nm biotinylated nanoparticles on a streptavidin modified surface at (a) high (20s, 0.4uA), (b) medium (15s, 0.3uA), (c) low (5s 0.2 μA), and (d) no current.

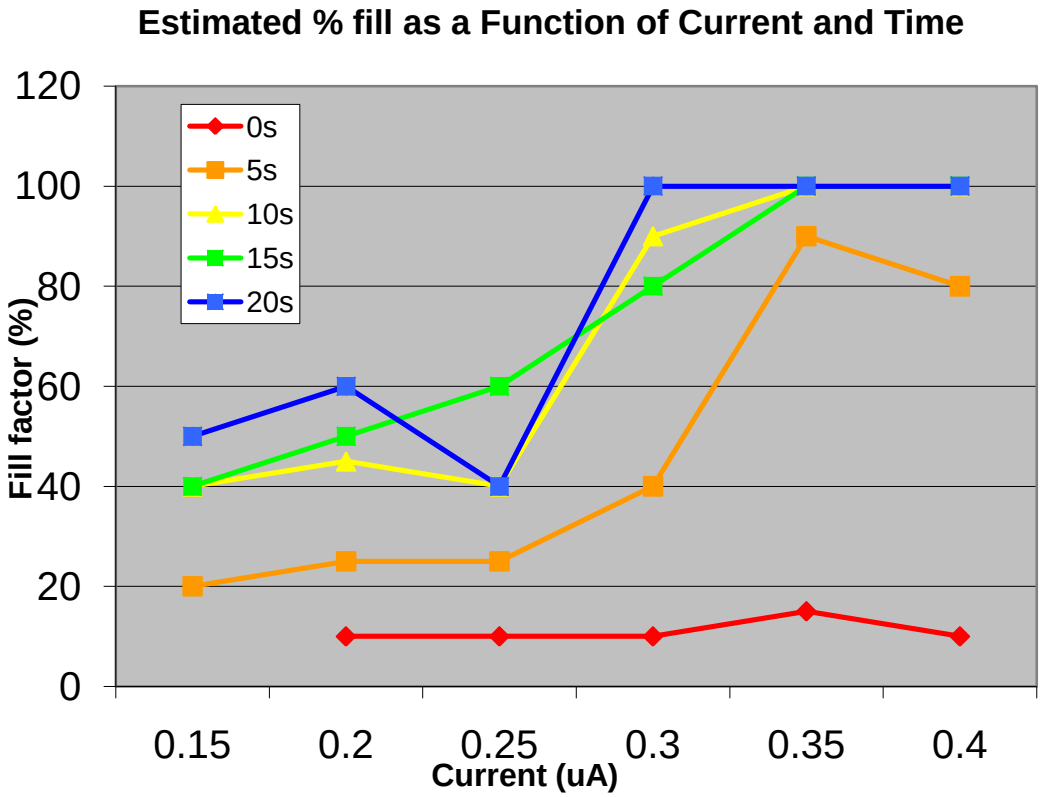

Figure 2.11: Monolayer formation as a function of deposition condition.

We defined the ideal deposition conditions as those which formed a single monolayer of nanoparticles without gaps greater than ~40nm. We found that the surface binding activity and the various electric field parameters (voltage, current, time) were critical to the formation of high quality nanoparticle monolayers.

As can be seen in the SEM images in figure 2.10, there is an increase of biotin nanoparticle density as the active deposition time and DC current levels are increased. Figure 2.10a clearly shows that a complete monolayer of biotinylated 40 nm nanoparticles has been formed at the optimal deposition conditions. Background nanoparticle binding was less than a few percent, and a rapid increase in layer formation is observed between 0.2 and 0.25 μA and 10 or more seconds of deposition time. Due to technical issues, the resolution of electrodes which have less than a full layer of beads are only approximate. Without a full layer of beads the gel layer has a strong tendency to bubble. What can be measured (by SEM imaging) is the transition point between a full monolayer of beads and less than a monolayer. Density counts are made by manually counting the number of beads in a subfield, but this count is approximate due to poor image resolution.

2.5.3 Optimal deposition time and current

In this work, we were looking for the ability to deposit a large number of particle layers in a reasonably quick period of time. Since this work hinged on number and thickness, in this context we take “optimal” to mean the conditions in terms of

Figure 2.12a: 4 layers

Figure 2.12b: 14 layers

Figure 2.12c: 34 layers

Figure 2.12d: 54 layers

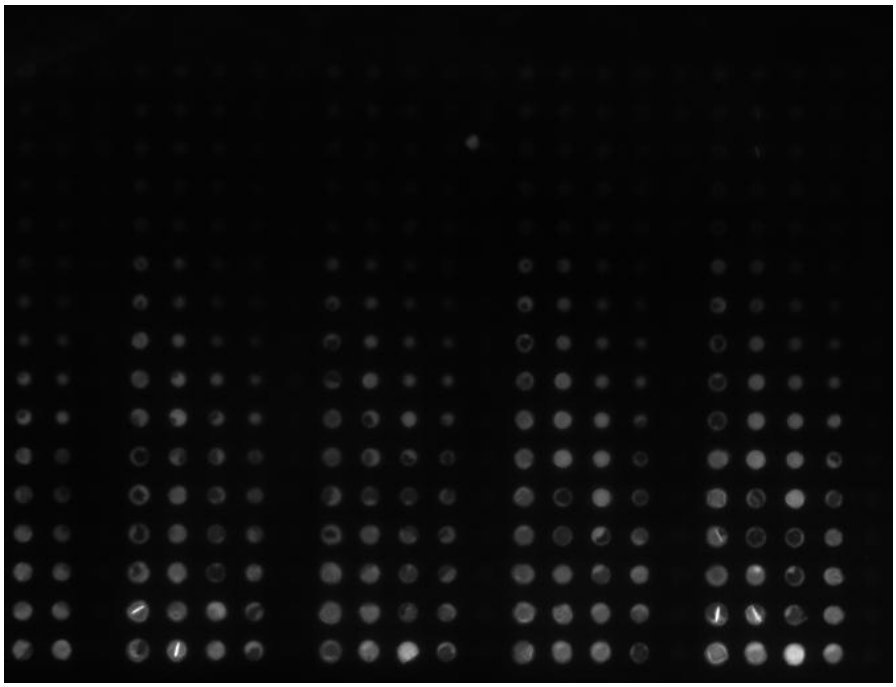

Figure 2.12e: 94 layers

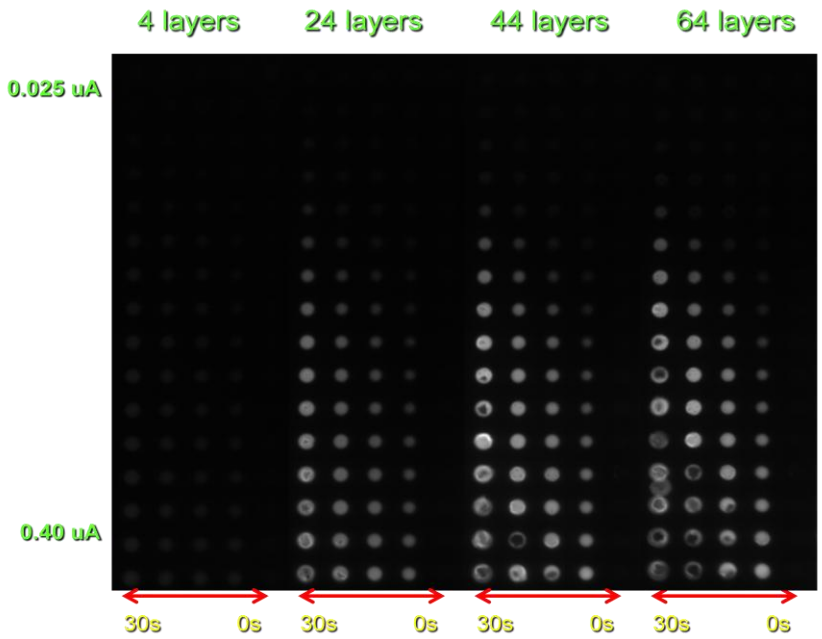

Figure 2.12f: composite image of a subset of the same electrodes at 4, 24, 44, and 64 layers

current and deposition time which produce the greatest number of deposited layers before structural defects occur in the fabricated structure. This is not to say that other layer parameters (such as uniformity or speed) are uninteresting, but rather they were outside the scope of this work. In the case where a lower number of layers is desired (such as in a specifically designed structure using the Electronic Layer By Layer technique), other such parameters may be of interest. In any case, as the main variables of control are the currents and times of deposition, the methods would remain identical; merely the choice of data interpretation would change at the end.

Given that our criteria for failure was the point at which critical flaws appear in the layer structure, our analysis for this portion is mostly by examination of the images taken after each layer has been deposited. Since, often around 100 layers were deposited, only a subsection of the images will be displayed herein. For consistency between the data reported here and in the next two sections, the number of layers shown is for every 10^{th} deposited, starting at the 4^{th} layer (This is the point at which 2 streptavidin layers have been deposited, and where layers become reasonably distinguishable on an unaltered picture)

As can be seen in figure 2.12, there is a period of increasing layer brightness as the number of layers increase. However, as the number of layers increases, the optimal fabrication window discussed in the methods section becomes apparent. No layer forms below ~0.15-0.20 μA (depending on deposition time). In addition, the layers at higher currents and times begin to degrade with increasing

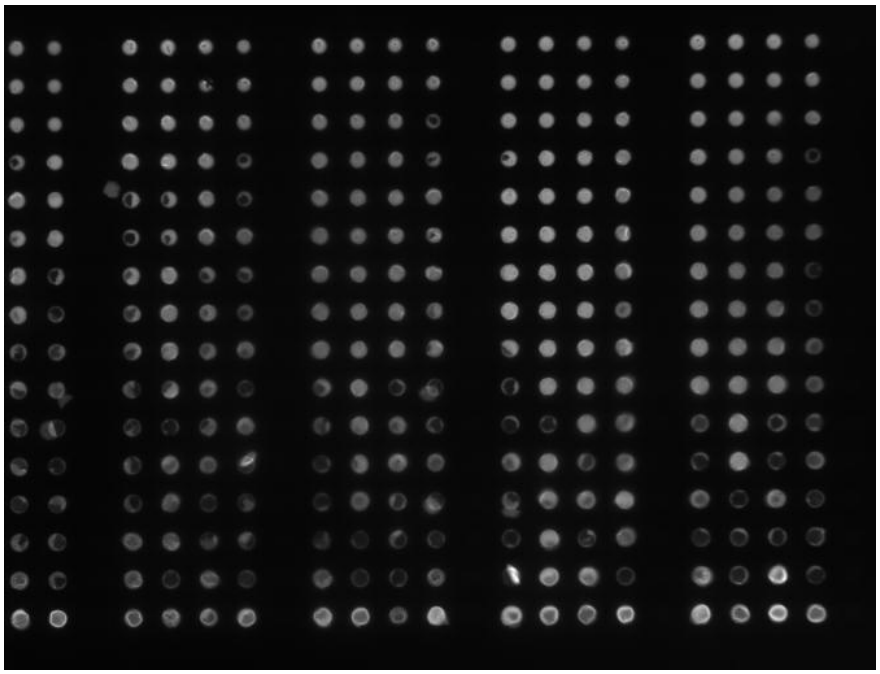

Figure 2.13a: 54 layers

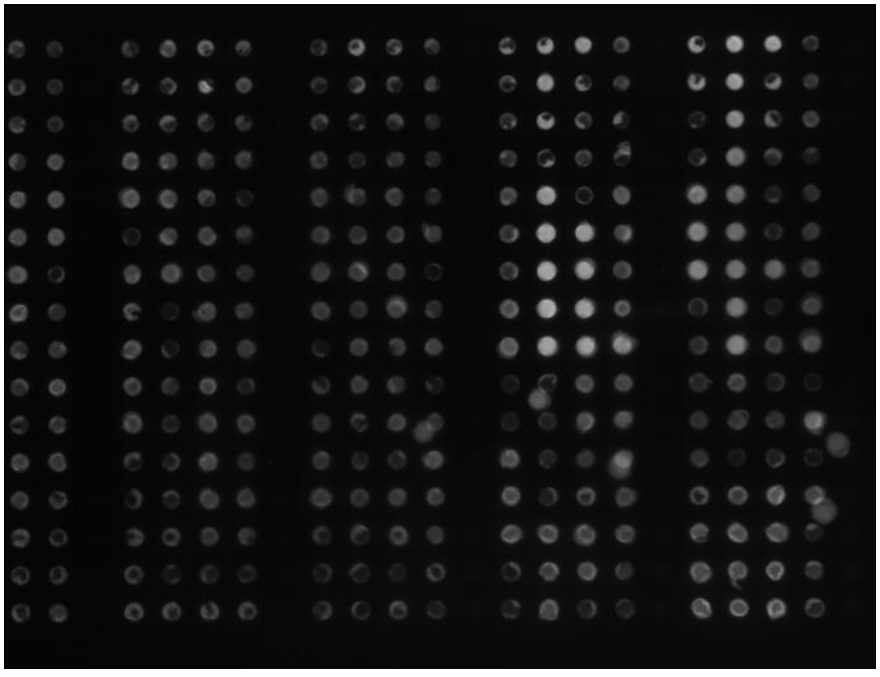

Figure 2.13b: 94 layers

depositions. It should be noted that even after the deposited layer breaks off and floats away from a deposition site, particles are pulled down in further depositions. Therefore, there is a tendency for even broken deposition sites to continue to grow additional layers and increase in brightness. In analyzing the images we can see that the best surviving layered structures after 94 deposited layers lies around 10-20 seconds of deposition time, and 0.2-0.3 uA. Since the granularity of this experiment is too large to determine an optimal deposition time, we conducted a second experiment identical to the first except that the times and currents of deposition were in a narrow range. Instead of a current range between 0.025-0.4 in 0.0.025 increments at 10,15,20, and 30 seconds, the second experiment had current ranges from 0.2 to 0.3 μA at 11,12,13, and 14 seconds. The results of the second experiment are shown in figure 2.13. As can be seen, the results are more uniform (since the conditions are in a narrower range), and the optimal deposition conditions are seen to be at 0.225-0250 μA, at 12-13 seconds.

These conditions should be understood in the context of this particular experiment. The beads used were 40nm biotin and streptavidin nanospheres of a $1/100^{th}$ stock dilution in histidine buffer. By performing this experiment we have determined the optimal way of depositing these particles in the maximum number of layers achievable. In the case where we change the particle size or type, it is entirely possible that different parameters would be required (for example see the results of

the deposition of 200nm beads in chapter 3). The method reported here is a general way for determining the optimal deposition parameters for nanoparticle layering.

2.5.4 Layer growth rates vs. deposition

When this work began, we were confident that nanoparticle layering would at least be successful enough to deposit a single layer of nanoparticles. However, we did not have any idea of how the presence of additional layers would influence the deposition rates of subsequent layers. It was plausible that the presence of a few layers of deposited nanoparticles would passivate the surface of the gel and prevent further current from passing through the layered stack. In such a case, the particles would mostly pile up at the edge of the previously deposited layers. Fortunately, this is not the case, and the reasons why are addressed in the chapter 4. Once it became clear that layer growth was forming, and that SEM had validated the presence of at least a monolayer of particle growth, the next question was how constant the layer growth is. There are a few boundary phenomena that might have some level of influence on the situation

1) Previously deposited layers could cause a drop in conductance through the stack which prevents particles from depositing there at a constant rate between layers.

2) As suggested in the methodology section, more particles are pulled down to a single electrode than are needed to form a single monolayer of particles

(this is borne out by experimental observation, far more beads are pulled down to a single site than remain there after washing).

3) Given a sufficient level of interparticle stringency, we would expect at most only a single monolayer of particles to be deposited during each deposition step.

In the case of point 1, we would expect the growth rate of the layer stack (as measured by fluorescent intensity) to go down with subsequent layers. That is, as the number of layers increase, the change in brightness from one layer to the next would go down. Eventually once the layer reaches some saturation point no more particles would be deposited on the surface, and the brightness at the center of the stack would remain constant between deposition steps (though the size of the structure would probably increase radially as particles are attracted to the outer edge where current still flows. We would expect this effect to be inevitable for a couple of reasons. Firstly, eventually the layer would become thick enough that current cannot flow through it compared to alternate paths (this is addressed in chapter 4). As long as adding more layers to the stack tends to increase the total resistance of ions passing through it, this must eventually happen. Secondly, we purposely run the system in a constant current mode to compensate the effect adding additional layers has on the system resistance. However, the chip compensates for this additional resistance by increasing the voltage of the electrode, and eventually the electrode would hit its maximum output of 5 volts. So in theory, there should be a maximum

depositable thickness (though given the results in the previous section which involve physical inspection of the layer defects, that saturation point could easily be after the point at which structural defects dominate). To detect this saturation point we merely look for a point at which the fluorescence tends to roll off as a function of increasing layers. The results of looking for growth saturation will be discussed later in this section.

As mentioned in point two, far more particles are pulled from solution to the gel surface above an electrode than actually remain bound to the surface after washing. When watching the deposition process in real time, it is observed that particles continuously are pulled to the surface and remain there for the duration of the electrode activity. During this period they are not observed to be subject to any fluidic turbulence or mixing, they are merely observed to accumulate, with the accumulation being proportional to the current applied at each electrode. Once the electrode has been turned off, some fraction of the particles will drift away through diffusion, though the bulk will remain on the gel until the chip itself has been washed. Mathematically and physically this is not so strange. Given the number of particles in the original solution, and accounting for the dilution and the volume of liquid placed on the chip, there are enough particles present during each deposition step to cover **each** electrode in a pile of beads roughly 100 monolayers thick. Now of course, the distribution of beads is not uniform. Mathematically we expect the total number of beads that are pulled to the surface of the gel to be roughly proportional

to the time integral of the current at the corresponding electrode (that is, the total charge passing through that electrode). The ratio of this charge between the longest time, highest current electrode and the shortest time, lowest current electrode is 48:1. In addition there is the possibility that once beads are pulled down to a surface that has been subsequently turned off, that some of those beads would be able to be caught up by the currents travelling to a still activated nearby electrode. Given the distribution of currents and times, if all the particles were used in the deposition even the lowest deposition time and current electrode would still have 10 monolayers worth of particles (the greatest deposition condition would have around 450 layers worth of particles). While it is unlikely that all the beads get pulled down to an electrode, it should be clear that there are plenty of beads to go around. And since our goal in each deposition is to form a monolayer of beads, it should be clear that there are absolutely enough particles present for that to occur, as long as a secondary binding effect does not come into play.

Given the abundance of particles, as discussed in point 2, and given that we only expect a single monolayer of particles to bind to the surface we would expect to see a relatively high rate of particle saturation. If such saturation is not observed, then we would expect some secondary effect to be taking place. Such effects include

1) Insufficient time for the particles to bind to the surface

2) Local conditions that preclude binding such as small scale turbulence near to the electrode

3) Steric hindrance from previously deposited but unbound particles prevents additional particle binding

4) Stringency of the particles may be insufficient to prevent greater than a single layer of particles from binding to the surface.

5) While similar, the rates of particle deposition for the biotin and streptavidin particles may be dissimilar enough that the monolayer deposition conditions are not identical. The effects listed are not taken to be mutually exclusive, but rather offer insights into why the mere presence of multiple monolayers of particles would not lead to a single deposited monolayer. While the biotin/streptavidin binding mechanism is strong, it is a physical adherence mechanism like Velcro, it does not act at a distance like charge attraction, therefore it is not strange to find there are conditions in which a large amount of particles would not lead to a full layer. While not explored in depth, we believe that a form of "tapping" where an electrode attracts particles down for an extended period of time followed by several repeated short pulses to allow a final rearrangement could change this. In addition, nonspecific binding of nanoparticles is possibly induced at longer times and currents.

As stated previously, the results reported here are shown until the point at which the layer breaks. Past this point measurement is pointless, and fluctuates

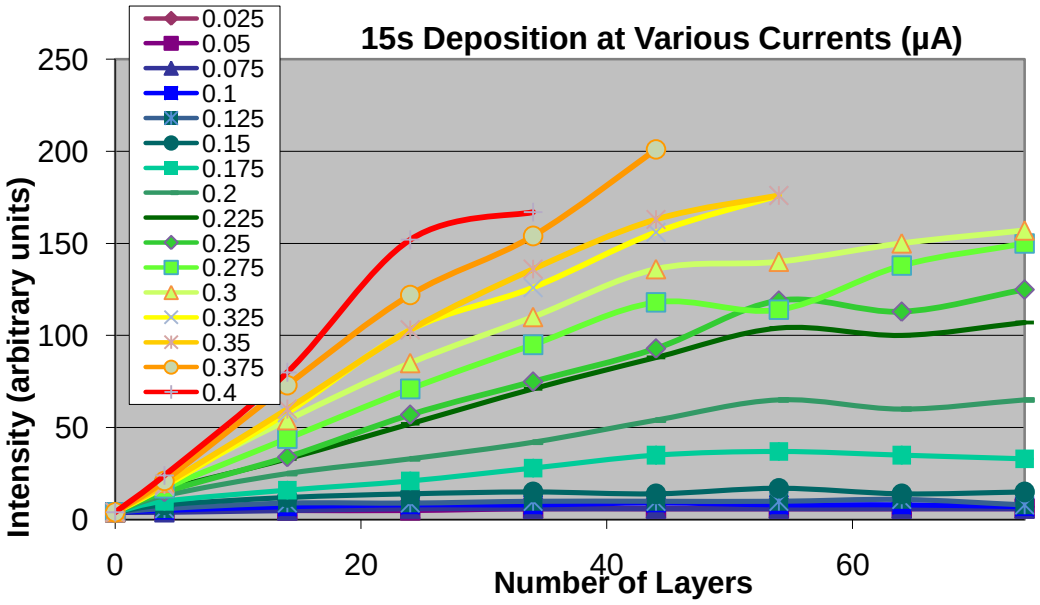

Figure 2.14a: Plot of peak intensity for 15 seconds of deposition at different current.

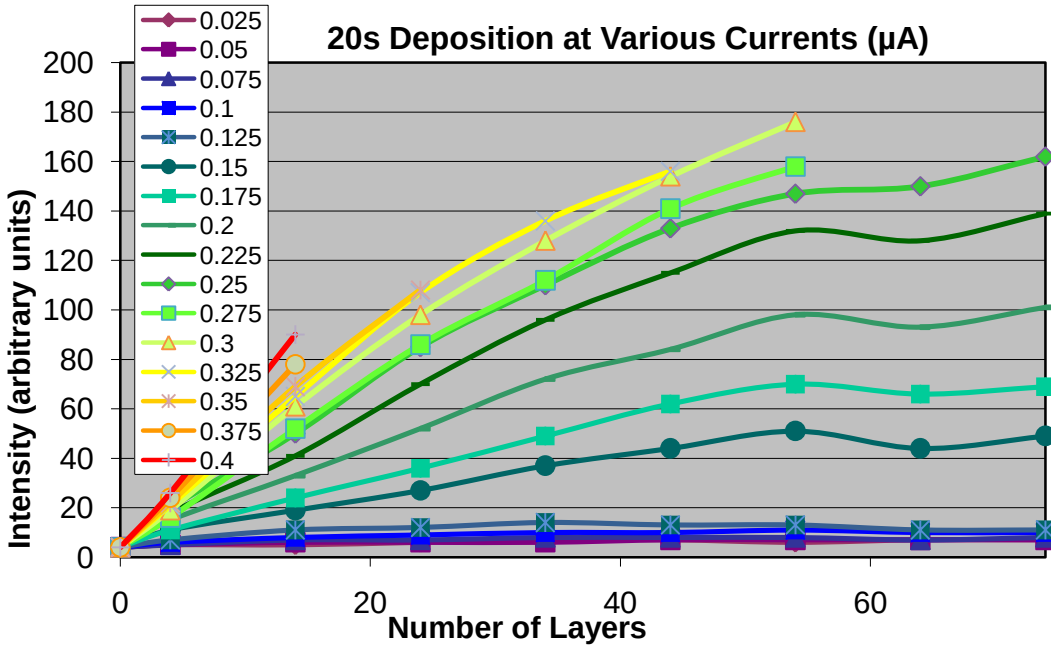

Figure 2.14b: Plot of peak intensity for 20 seconds of deposition at different current.

wildly as additional layers grow on the remaining structure, and has little to do with continued growth. In looking at the growth rates of the undamaged layers we can see many things (figure 2.14). Firstly, and most importantly, we see that even after 50 or more layers of particles have been deposited, there is still accumulation of particles with each additional layer. While there is an eventual falloff in the increase in intensity, it beings to occur after dozens of layers have been deposited. The growth rate remains linear for many layers, and only begins to significantly fall off after 60 or more have been deposited (depending on the deposition conditions). Due to the linear growth rate we can conclude that the resistance offered by the additional layers is low. While the chip compensates for additional resistance by increasing the voltage, too much resistance would cause the current to flow around the layered stack (see simulation chapter). What the data conclusively shows here is that the growth rate is well defined given a deposition parameter (at least for the first few tens of depositions). Also, at higher currents, the growth rate roughly saturates.

Another question we had about this method was how much of a saturation effect there would be as more particles are pulled down to an electrode. As stated previously, there are vastly more particles pulled to an electrode than are needed to cover it, so there would be hopefully some sort of saturation effect. This saturation effect is observed with respect to current (see figure 2.15). Note how the higher current electrodes tend to have the same level of intensity, especially compared to the intensity of the low current electrodes. For a given time of

deposition, there is a clustering of the amount of deposition at higher currents for any given number of deposited layers. Also, as a function of total charge passing through an electrode, there is a rough correspondence to the total amount of deposited particles at a given electrode, at least in the middle of the range of currents and times. It breaks down at the extreme ends likely due to the edges of the deposition windows, as have been discussed previously.

2.5.5 Layer growth rates vs. condition

The data discussed in the previous section is shown as fluorescent intensity as a function of applied depositions. This view is useful to see how a layer grows over time at a given condition, but makes it difficult to determine the differences between different growth conditions. The graphs shown in this section show deposited particles vs. current at a single deposition time (with different lines representing different numbers of total depositions). In these plots, we can see the direct effect that varying the current (and thus the number of particles pulled to the surface) has on the thickness of the deposited layers. For a given time of deposition (as is represented in these plots) the number of particles pulled down to a given surface should be linear with the current. Since the beads make up a proportional amount of the solution charge, doubling the amount of current doubles the amount of particles pulled down to the electrode (within reasonable limits, as discussed in the theoretical section). However, due to the aspects of binding discussed in the

previous section, we would not expect there to necessarily be a linear increase in the number of bound particles, especially as the number of layers increases. With respect to current we would expect this to occur for a number of reasons

1) If insufficient particles are bound to the surface of one type, there will be an incomplete binding surface for the next deposited layer.

2) More current pulls more particles down to the electrode, but the particles close to the electrode experience more force due to greater electric fields.

3) Increased force on particles may cause a greater degree of nonspecific binding

4) Previously deposited layers of particles retain their charge, and experience a force as a result of the applied currents.

In looking at the data of intensity vs. current we can see many regimes. These regimes shift depending on the length of the applied current, but there are general features found in each of the different time parameters. First at low current there is a regime where almost no particles are deposited and no successive layers are formed. This is consistent with the monolayer SEMs that show very few particles at lower currents and times. This threshold ranges from ~0.1 to ~0.2 μA depending on the time of deposition. The knee observed in the data at this point is clear proof that without sufficient layer formation, subsequent layers are unable to form. While we saw in the previous section that layer growth is constant (linear) from deposition to deposition, it is definitely not linear with respect to increasing current. It is not

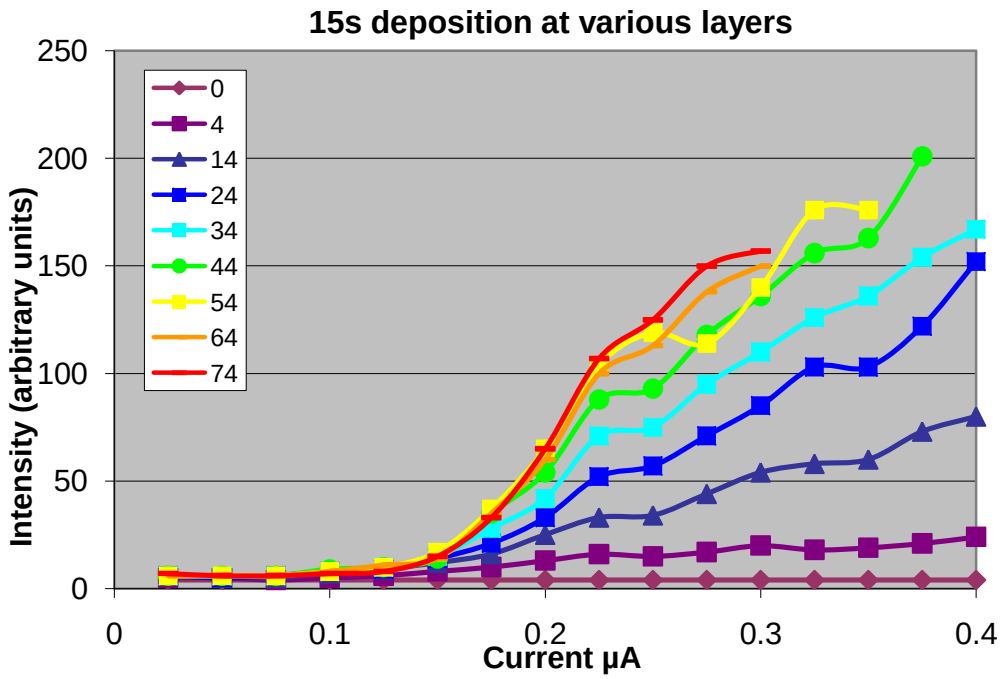

Figure 2.15a: 15 seconds of deposition at various numbers of deposited layers

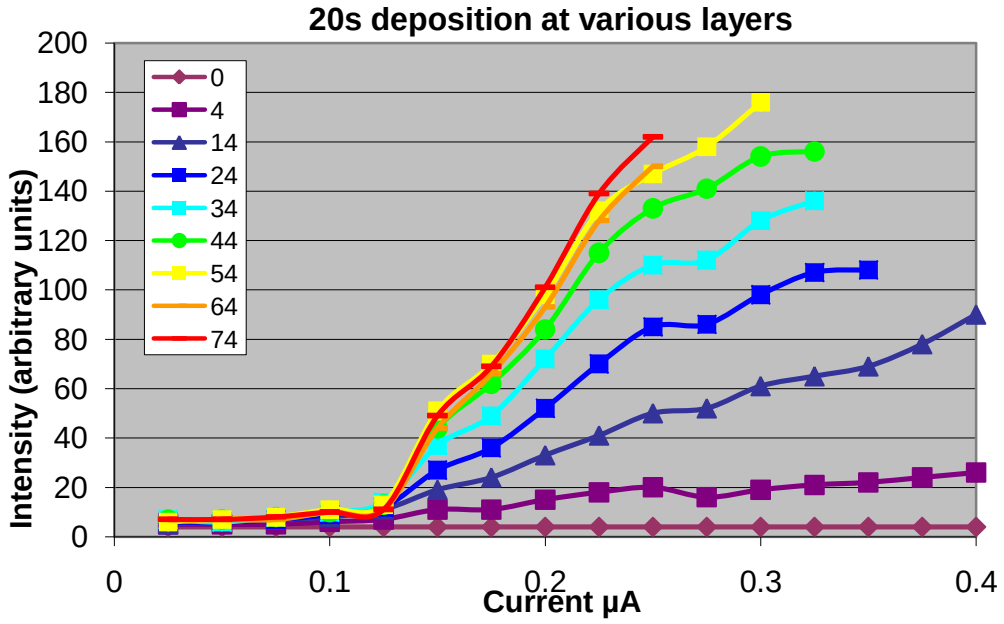

Figure 2.15b: 20 seconds of deposition for various numbers of deposited layers

clear how points one and two above play into this, or even to what degree they can be decoupled. Even if the binding rate to an available surface increased roughly as the square of the current (ie more beads time a stronger force per bead) it is still the case that an insufficiently built binding layer will prevent clean binding from occurring. This is solely due to the lack of binding sites available to incoming beads.

As current increases past the point where layer fabrication occurs, there is a region of greatly increasing growth with respect to current. This increase in growth continues with respect to current till around 0.25- 0.3 μA, at which point there is a small plateau in the data. Not surprisingly, this is around the same current range at which monolayers were observed to form under the SEM. While not a wide window, this plateau implies there is a zone where fully bound monolayers form on the previously deposited stack, and only a single layer remains after washing, independent of the number of particles which are pulled down to the surface. Interestingly, this region of what is surmised to be constant monolayer growth is actually slightly higher in terms of deposition current and time than those determined to be “optimal” for extended long term layer growth.

Finally there is a current regime past the plateau point where the layers continue to grow thicker as the applied current increases. Since we know that this is the point where monolayers are forming, any additional growth in this range must be due to some form of nonspecific interparticle binding between like particles. As seen from the stringency studies, the streptavidinated particles have a relatively high

stringency compared to the biotinylated particles (which is why the fluorescent study is exclusively looking at rates of streptavidin particle accumulation). This discrepancy is interesting because it implies that the supposed nonspecific rate of particle accumulation increases in the presence of particles of a complementary binding at higher currents. The reason for this is not entirely clear.

One effect observed to be related to the current is the deformation of the fabricated layer. As the current is increased, the fabricated layer can be seen to compress towards the electrode. The charged particles making up the fabricated layer experience a direct electronic force and compress the gel in response. While it is not surprising that charged particles can experience a force in the presence of an electric field, it does lead to an insight into the nature of why the layers tend to degrade as a function of both the number of layers, as well as the deposition current and time. More generally, there are 3 probable causes of the layer degradation

1) Electrochemical/pH/osmotic effects cause the disintegration of the fabricated layers

2) Gel Compression during the deposition step causes a built in stress to form in the layers

3) Surface adhesion to the gel is unable to withstand the stress from repeated compression cycles

We believe there is evidence of all of these effects, though more direct evidence is presented in a subsequent chapter. Since these effects all should grow

along with the increase in current, it is unsurprising that the physical degradation occurs from the highest current settings towards the lowest.

2.5.6 SEM surface and cross-section views

SEM imaging was extensively used as a complementary confirmatory tool in this work. The particles used were far below the wavelength of light, and are therefore unresolvable. While the particles themselves can be detected on the fluorescent microscope, the resolution at which we can see them is poor, and thus any form of fine structure on the scale of the particles themselves is impossible to observe. The microscope is able to differentiate gross geometrical differences across a single electrode (such as radial intensity changes), and is thus able to get some measure of 3D information, but never on the level of single particles. The SEM, however is both more and less powerful.

The SEM runs a scanning electron beam across a surface and records scattering data from each beam position in a 2D plot which is then viewable as an image. Depending on the beam voltage and the materials under inspection, objects can appear opaque to semi-transparent. In our case, we were observing small organic molecules suspended on an organic surface. To observe such a surface, you either need to use a very low beam power, at the expense of resolution and contrast, or to coat the sample in metal. Given that our particles are a small size (and semi-transparent under the SEM) all our samples were coated in gold prior to viewing.

Most of our conclusions about this process were informed by our SEM images. However, all the images, by their nature are of a single surface. The SEM process mostly only shows surface topographies, and in the case of where particles are transparent, the images come out as a pile. In addition, many of the samples we observed reacted poorly under the SEM. The process of scanning would heat the underlying gel to the point where it would rapidly expand, creating a bubble in the region where we were trying to observe. This effect only occurred in regions where gel was the main constituent of the image. Mostly, this was on only control electrodes where no beads had been pulled down, the gel between electrodes, and electrodes where less than a monolayer of beads had been deposited. In the regions where stacks of particles were deposited, there was enough cohesion that no bubbles would form. As a result, it was easy to take pictures of the surfaces of bead stacks, but was more difficult to image monolayers or less of beads, or control areas free of beads. In those cases, usually an image had to be taken by zooming to a region while the beam was off, after focusing on a nearby region, and then quickly taking an image. Even in this case many bubbles formed, but a fraction of the images came out clear. Unfortunately this process meant that the resolution of these quickly taken images was poor, since focus was obtained on areas where bubbles had already formed, and the image was taken on areas without a first inspection. The images displayed here should be viewed in the context of this process.

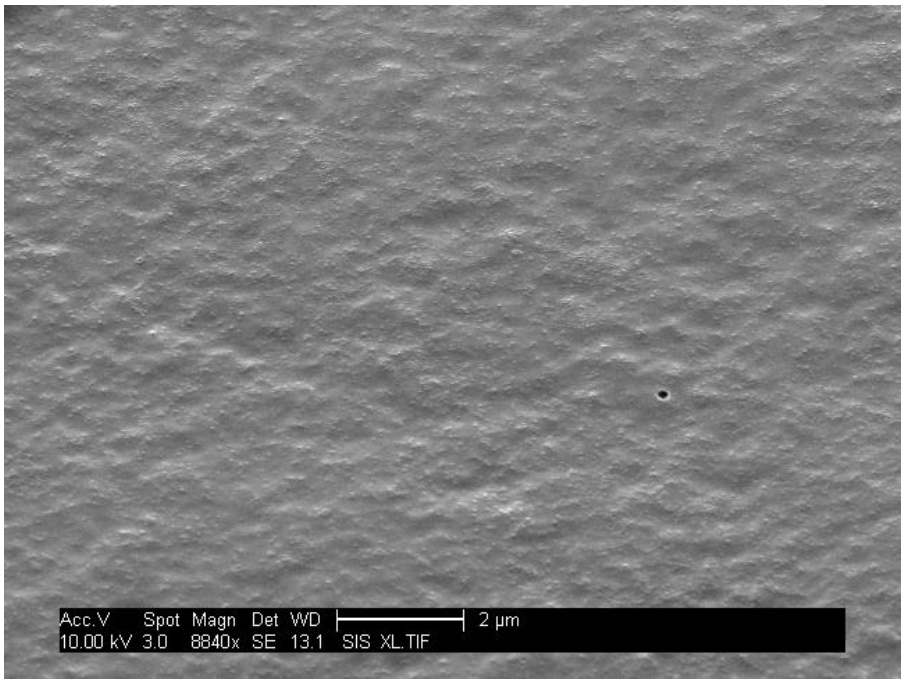

Figure 2.16: SEM of background non activated gel

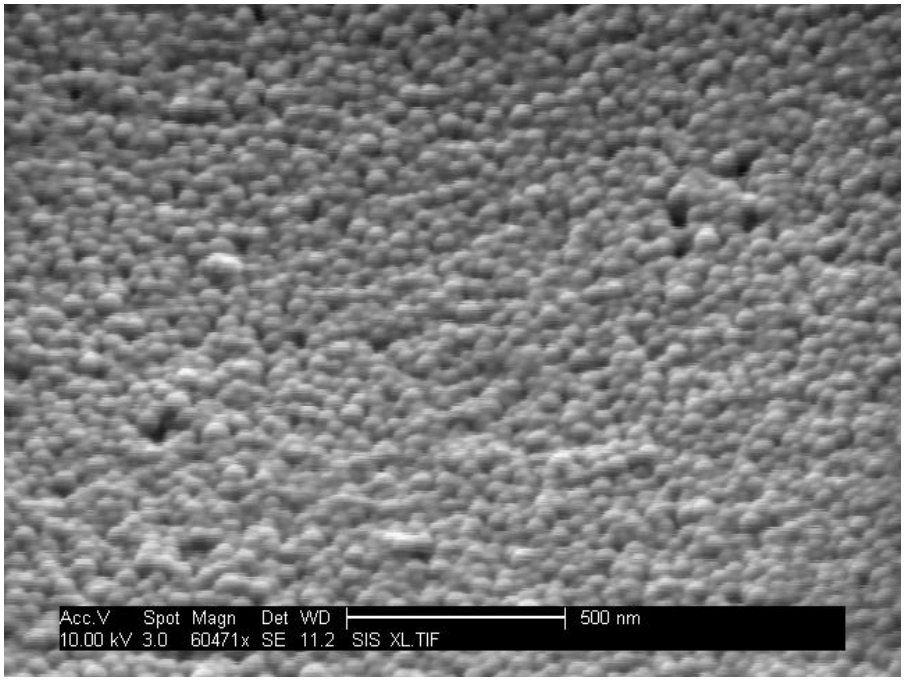

Figure 2.17: SEM of top of 40 layers of deposition

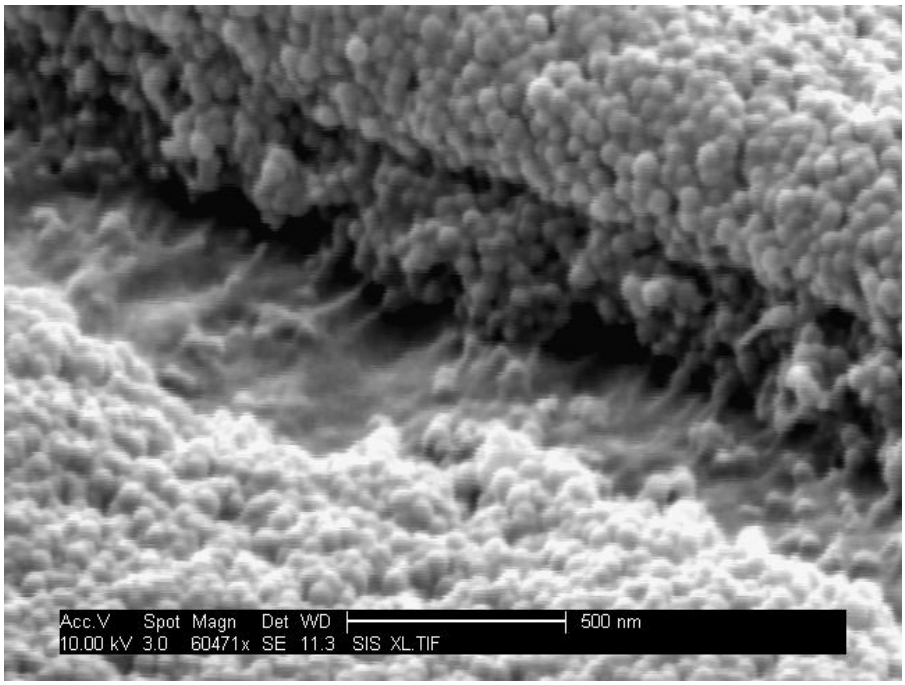

Figure 2.18: SEM of crack in a stack of 40 layers

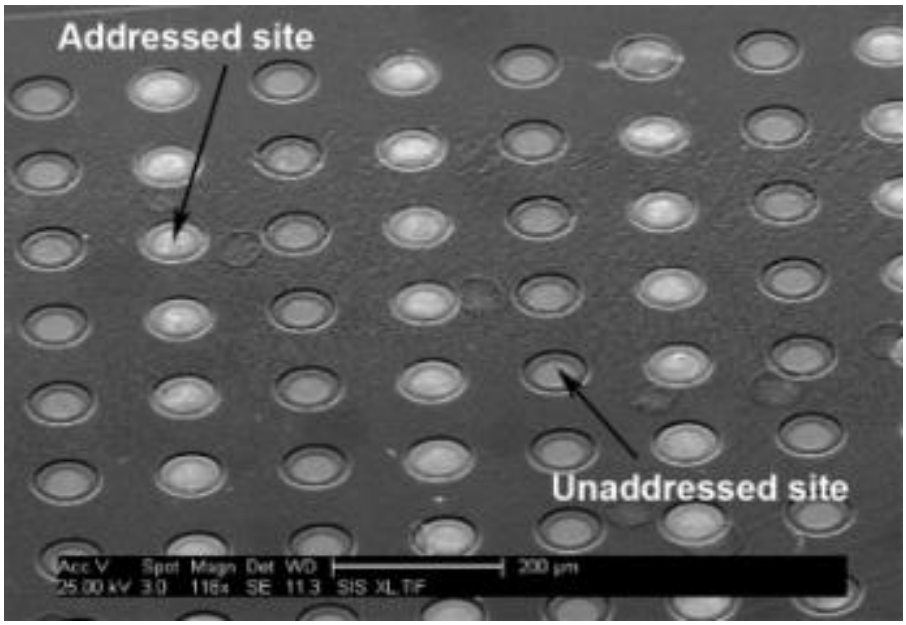

Figure 2.19: SEM of alternate addressed and unaddressed sites

Under the fluorescent microscope, the particles we used are distinguishable. That is, if the proper filter sets are used, we can view both sets of particles to the exclusion of the other. This is how the stringency data was acquired, since we could independently observe the accumulation of both particle types and conclusively know that accumulation on the single particle type control rows was only a single type of particle, and not influenced by nondirected binding of the other type of particle. However, the SEM is only able to measure surface topography. To some degree it can detect the composition of that surface by contrast differences (such as between metal and organics), but since both our biotin and streptavidin particles were basically identical in their underlying size and composition, there is no way to distinguish between them under the SEM. Therefore, the images presented here are mostly surface images consisting of round 40nm beads. Included are some cross-sectional images, but as stated, there is no way to distinguish between separate layers given the nature of our particles. (In the additional results section there are some images of both 40nm and 200nm particles layers).

In the images presented here we can see several things. Firstly, the layers as formed by this process are relatively flat. While by no means a crystalline lattice, the end result of the surface shows no sign of being composed of or forming large clusters or mounds of particles. While we are unable to see how turbulent the surface is during the deposition stage, the result is relatively clean. Due to the random nature of the deposition process, lack of any constraining forces, and

nonuniformities in the particle size, we had no a priori expectation that there would be any order or crystalline packing of the beads. Therefore, it is in fact somewhat surprising that the bead layers are as flat as they are observed to be. While there is some surface roughness, most of it is on the order of the size of the beads used. There is no direct evidence that larger impurities are incorporated into the resulting layered stacks in any large number. While some of the deposition conditions leads to what appear to be blowholes in the surface of the layers, that surface not severely impacted until catastrophic failure occurs.

Another observed feature is the low level of background observed on the surrounding gel as opposed to the amount of particles deposited during electrode activation. Despite being exposed to the same solution as the electrodes, and despite having an equally bindable surface, the unactivated gel has a very low rate of particles sticking to it. This shows that the electric field concentration effect not only is able to form particle layers on the gel surface, but is also able to do so from a solution containing minute numbers of particles. As was mentioned previously, since there two orders of magnitude more beads in solution than is actually necessary to cover the electrodes, it is possible that even lower numbers of particles could be made to bind to the surface, merely by lowering the solution concentration.

As seen in the cross-sectional SEM figure 2.18, the stacks can get quite deep. This is further confirmatory evidence that repeated layer depositions are possible, and that the increase in layering resistance does not inhibit the further

deposition of particles interestingly, the cross-section images were taken during an earlier version of the binding layer process. Earlier methods of binding the layers to the surface had weaker levels of adhesion, so the fabricated layers would tend to crack down the middle after sufficient depositions. After the binding layer method was changed, the adhesion and layer stability increased. This had the side effect of not allowing us easy cross-section views.

2.6 Constraints

This section has extensively discussed the benefits of the electronic layer by layer process. The ability to rapidly and controllably deposit particles from a low concentration solution allow for the patterning of a large range of particle types. This technique is both flexible and powerful, though it is subject to its own constraints. These constraints occur due to the nature of the electrophoretic process. They are in summary

1) The particles must be water soluble (or dispersible)
2) The particle must be sufficiently charged
3) The particles should not be prone to aggregation
4) The particles need a complementary binding surface layer
5) The particles should have a low amount of nonspecific and self binding
6) The particles must not be susceptible to due to changes in pH.
7) The particles need to be stable in the buffer

8) The buffer needs to be of low ionic strength

9) The resolution of the fabricated structure is limited by the control electrodes

10) The electrodes need to be current controlled to a sufficient current density

11) The electrodes need to be coated in a gel

Most of these limitations are aspects of the same few problems. Namely that you must pull a large number of particles down to a surface in an aqueous solution using electric current, and have only a single, complete layer remain. This is not by any means an insurmountable problem, and we have demonstrated its feasibility using not only the 40nm fluorescent polystyrene particles used in this section, but also with gold, DNA coated particles and larger sized beads as well. Due to these constraints, particles in nonpolar solvents won't work, and non aqueous polar solvents are likely to cause significant problems. It should be noted that aqueous solutions allow a large range of particle types. A vast array of nanoparticles and biological molecules of interest are soluble under the conditions which are allowed by the constraints above, and it is these particles in particular which drove our interests in this technique to begin with. The ability to integrate the products of nanotechnology and the results of biotechnology are one of the key goals of this project.

2.7 Conclusions

In this work we demonstrated many important features of the electronic layer by layer methods. Overall, the method has been established as a viable method of fabricating multiple stacks of nanoparticles in a rapid and controlled fashion. In particular, we have demonstrated many different aspects that contribute to the fabrication process. First, we demonstrated that the process allows the deposition of nanoparticles in an amount controlled by the deposition time and current. Second, the amount of particles deposited under certain conditions is sufficient to form a monolayer of particles over a given electrode. Third, the rate of deposition of particles in subsequent layers remains constant for a given deposition time and current for a large number of layers. Finally we have shown that the process can be tuned to a point where a large number of layers can be deposited at a single point in a rapid period of time.

Chapter 2, in part is a reprint of the material as found in Small: Dehlinger, D.A., Sullivan, B.D., Esener, S. and Heller, M.J. (2007) Electric-field-directed assembly of biomolecular-derivatized nanoparticles into higher-order structures. *Small*, **3**, 1237-1244. The dissertation author was the primary investigator and author of this paper.

Chapter 3: Particle interactions and layer fabrication parameters

3.1. Introduction

This chapter will describe additional work done during the time of this dissertation. The work is directly related to the topics discussed in chapter 2, but is related here because it is not directly relevant to the narrative of the work told there. Mostly these experiments involved secondary materials and methods which extend the process or were involved in earlier procedures. In addition, interesting experimental results observed in the mainline experiments will be mentioned here. The focus of this section is to understand what happens to the process when changes are made to the layering materials. As we saw with the biotin and streptavidin nanoparticles, there was some degree of nonspecific binding which placed limitations on the overall process. In this section we will explore the behavior of different types, sizes, and coatings for the nanoparticles used for the layering process.

3.2. DNA Layers

3.2.1. Introduction to DNA layering

The experiments and results described in chapter 2 were conducted entirely with biotin and streptavidin coated nanoparticles. It was the biotin streptavidin bond which both held the different types of particles together, and

mostly kept the same type of particle apart. While the biotin/streptavidin system allows for a fast and strong bond between two particles, it suffers from certain limitations. At the core of these limitations is the fact that the “lock and key” nature of the bond is not extensible. That is, there are not really multiple types of biotin that each bind to their own form of streptavidin. Of course, there are many types of binding systems, ranging from chemical to biological, to physical methods. Of these we chose to work with DNA binding systems. The reasons for this choice were many. Our lab has extensive experience and resources for dealing with DNA binding so in many ways it was a natural choice. There exist a wide array of biochemically derived tools for modifying and working with DNA. DNA itself is “programmable” based on its sequence in that it will bind most strongly with its specific complement. Because we can easily design and purchase whichever sequence we want, with a wide array of chemical modifications, we are able to have a wide potential array of various binding molecules. This allows for the design of a set of DNA nanoparticles that can specifically bind to one or more other nanoparticles without gross physical differences between them.

3.2.2. DNA materials

With all this in mind, we wanted to see if the experimental work that we performed with biotin and streptavidin beads could be replicated using sets of beads coated with coated in complementary DNA strands(80). In this work, the two

different sets of streptavidin nanoparticles and the electronic microarray binding sites were derivatized with target and complementary 24mer and 51mer DNA oligonucleotides. Through a rapid series of DC electric field (electrophoretic) directed depositions, accelerated hybridizations and washing steps, a layered nanostructure material was assembled using complementary DNA oligonucleotides as a structural binding material in the same manner as the experiments described in chapter 2, with minor variations to account for the different binding substrate. The complementary DNA derivatized nanoparticles were specifically concentrated and hybridized (in zwitterionic histidine buffer) to the target DNA sequences bound to the porous hydrogel surface above the microelectrodes (see Figure). The DNA sequences and derivatized nanoparticles used in the experiments are shown below:

24mer and 51mer Oligonucleotide Sequences and Derivatized Nanoparticles

5’-Biotin-GAA-CAG-CTT-TGA-GGT-GCG-TGT-TTG-3’ (24mer target sequence bound to microarray)

40nm Streptavidin Nanoparticle-5’-Biotin-CAA-ACA-CGC-ACC-TCA-AAG-CTG-TTC-3 (24-complementary sequence)

40nm Streptavidin Nanoparticle-5’-Biotin-GAA-CAG-CTT-TGA-GGT-GCG-TGT-TTG-3 (24mer target sequence)

5’-Biotin-GAA-CAG-CTT-TGA-GGT-GCG-TGT-TTG-TGC-CTG-TCC-TGG-GAG-AGA-CCG-GCG-CAC-3’ (51mer target sequence bound to microarray)

40nm Streptavidin Nanoparticle -5'-Biotin-GTG-CGC-CGG-TCT-CTC-CCA-GGA-CAG-GCA-CAA-ACA-CGC-ACC-TCA-AAG-CTG-TTC-3' (51mer complementary sequence)

40nm Streptavidin Nanoparticle-5'-Biotin-GAA-CAG-CTT-TGA-GGT-GCG-TGT-TTG-TGC-CTG-TCC-TGG-GAG-AGA-CCG-GCG-CAC-3' (51mer target sequence)

The DNA derivatized nanoparticles were produced by mixing a stock solution ($6x10^{-7}$M) of 40nm Neutravidin red fluorescent nanoparticles (Invitrogen, #F8770, Ex 580nm and Em 605nm) in a 1:60 ratio with the 5'-biotinylated 24mer and 51mer target and complementary oligonucleotides (synthesized by TriLink, San Diego, CA). Two sets of each of the nanoparticle derivatives were prepared (see above). After gentle mixing for an hour to allow sufficient time for the biotinylated DNA to bind to the Neutravidin nanoparticles, the mixture was diluted to 1/100 with 100 mM zwitterionic histidine buffer (pH 7.6) and 20 mM NaCl. The zwitterionic histidine acts as a low conductivity buffer for electrophoresis and promotes hybridization at the positively activated microarray sites under low NaCl concentrations. The microarray surface for binding the biotinylated oligonucletides was prepared by first washing the 400 site electronic microarray (Nanogen, San Diego, CA) several times with 18 MOhm water. 20ul of a 2uM solution of biotin dextran (sigma B9264) was applied to microarray and allowed to bind to polyacrylamide/streptavidin surface for 30 minutes. The microarray was then washed repeatedly with 18 MOhm water, and then a solution containing 1mg/ml of

Streptavidin (Roche Applied Science 11 520 679) was allowed to bind to the surface for 30 minutes. The microarray was again washed repeatedly with 18 MOhm water. For experiments involving the 24mer DNA sequence and derivatized nanoparticles, a 10 μM solution of 5'-Biotin-GAA-CAG-CTT-TGA-GGT-GCG-TGT-TTG-3' (24mer target sequence) was electronically addressed across all 400 sites on the microarray for 30 seconds at 0.25 μA per site. For those experiments involving the 51mer DNA sequence and derivatized nanoparticles, a 10 μM solution of 5'-Biotin-GAA-CAG-CTT-TGA-GGT-GCG-TGT-TTG-TGC-CTG-TCC-TGG-GAG-AGA-CCG-GCG-CAC-3' (51mer target sequence) was electronically addressed across all 400 sites on the microarray for 30 seconds at 0.25 μA per site. Finally, the microarray was washed with a solution of 100mM L-histidine and 20mM NaCl.

3.2.3. DNA layering methods

By alternating the deposition between nanoparticles derivatized with complementary and target DNA sequences, a multilayered nanoparticle structure was formed using hybridized DNA as a specific binding agent, rather than a biotin streptavidin bond. The combinatorial methods used to determine optimal conditions for biotin/streptavidin nanoparticle layering were again used to determine the optimal conditions for the DNA nanoparticle layering, i.e., the optimal addressing times and DC current levels. The standard stringent detection methods as described in section 2.5, with the times used being 10, 20, 30, and 60 seconds. Each DC current

level in microamperes (μA) and time condition (10, 20, 30 and 60 seconds) was tested on three sets of electrode columns ("***a", "b",*** *and* ***"c"***). Electronic addressing and hybridization of DNA nanoparticles was carried out in the following manner. A solution of nanoparticles derivatized with the complementary DNA sequence (~600 nM) was first placed on the microarray, and the ***"a"*** and ***"b"*** microelectrode sets across the whole microarray were activated (rows from 0.025 to 0.40 μA and columns at 10, 20, 30 and 60 seconds. The ***"c"*** columns of microelectrodes were left un-activated (neutral). The microarray was then washed with the histidine/NaCl buffer five times. Next, a solution of nanoparticles derivatized with the target DNA sequence was placed on the microarray, and the ***"b"*** and ***"c"*** microelectrode sets across the whole microarray were activated (rows from 0.025 to 0.40 μA and columns at 10, 20, 30 and 60 seconds. Now, the ***"a"*** columns of microelectrodes were left un-activated (neutral). Thus, the **"a"** columns are only activated when the nanoparticles with complementary DNA are applied, and the **"c"** columns are only activated when the nanoparticles with target DNA are applied. This procedure is designed such that DNA nanoparticle layering should only occur on the ***"b"*** columns of microelectrodes, and the ***"a"*** and ***"c"*** columns serve as controls for different types of non-specific binding or hybridization. The microarray was then washed with the histidine/NaCl buffer five times. This process of repeated depositions and washing was carried out 10 times for a total of 20 separate depositions of nanoparticles (10 times for nanoparticles with target DNA sequence, and 10 times for nanoparticles

derivatized the complementary sequences). Separate experiments were carried out for nanoparticles with the 24mer sequences and for nanoparticles with the 51mer sequences. Nanoparticle layering was measured by using an epifluorescent microscope system and CCD camera to monitor fluorescence. Analysis of these results is slightly different from the biotin/streptavidin experiments because only one type of bead was used with so the fluorescent spectra of the target and complement beads were identical.

3.2.4. DNA layering results

The results from the combinatorial electronic microarray DNA nanoparticle layering experiments show optimal growth windows with respect to the addressing/deposition parameters of time and DC current level. As seen in figures 3.1 and 3.2, nanoparticle accumulation (as measured by fluorescent intensity) is strongly affected by the longer addressing/deposition times, higher DC current levels, the total number of depositions and somewhat by the DNA sequence length i.e., 24 mer or 51mer. After 20 depositions figures 3.1 and 3.2 clearly show that nanoparticle layering (by hybridization) only takes place on the column "***b"*** sites, and appears to be most optimal for the 30- 60 second addressing time and at the DC current ranges from about 0.15 to 0.30 μA. Figure 3.1 shows an enlargement of those sites on the microarray which appear to have the optimal nanoparticle layering. Nanoparticle layering on the column "***b"*** sites is the expected result, as nanoparticles with

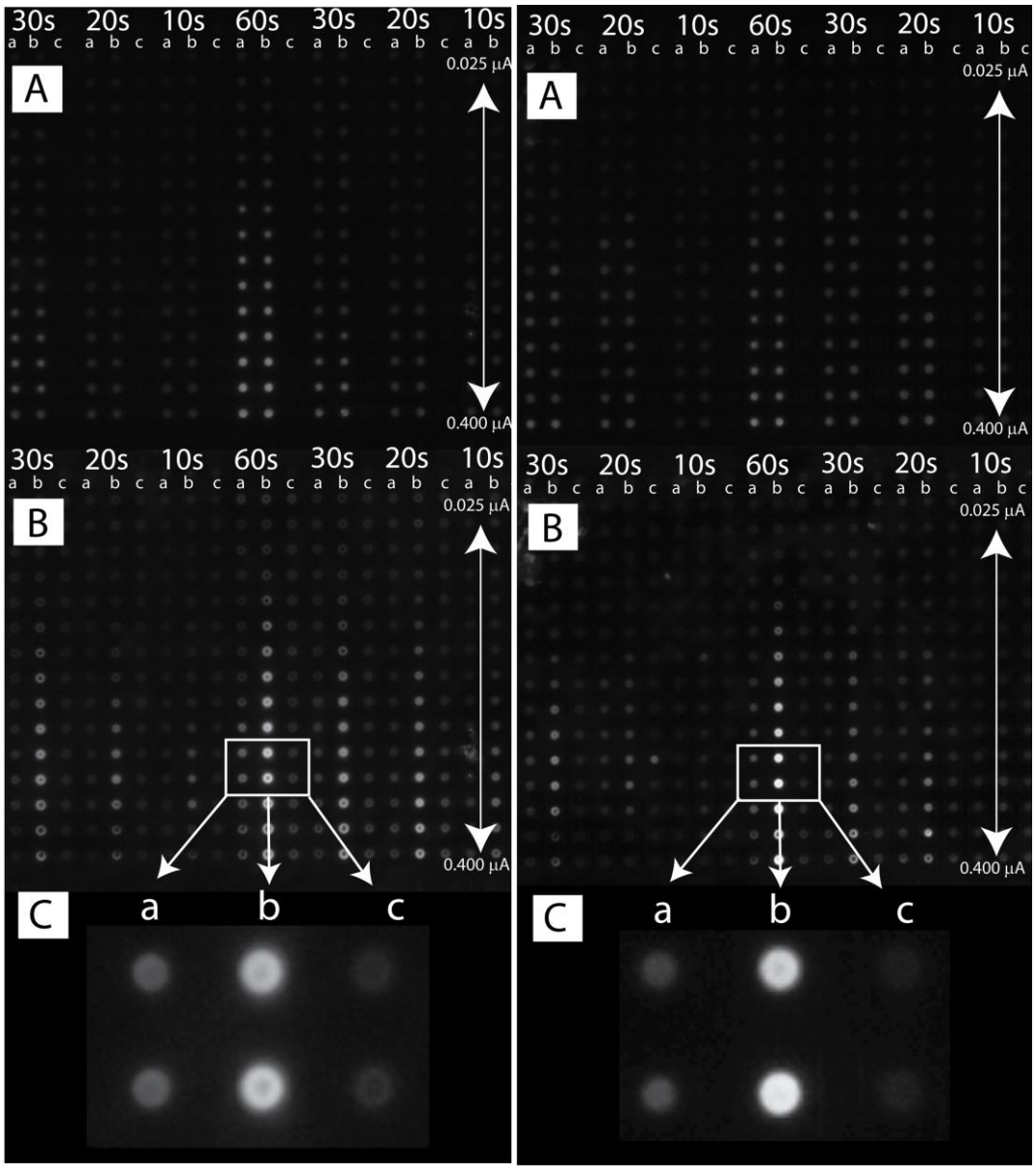

Figure 3.1 (left) 3.2 (right): Fluorescent DNA images. (A) shows one deposited DNA beads layers, (B) shows 20 deposited DNA bead layers, (C) shows a closeup of the optimal deposition window for beads with 24bp DNA linkers (left) and 51bp DNA linkers (right).

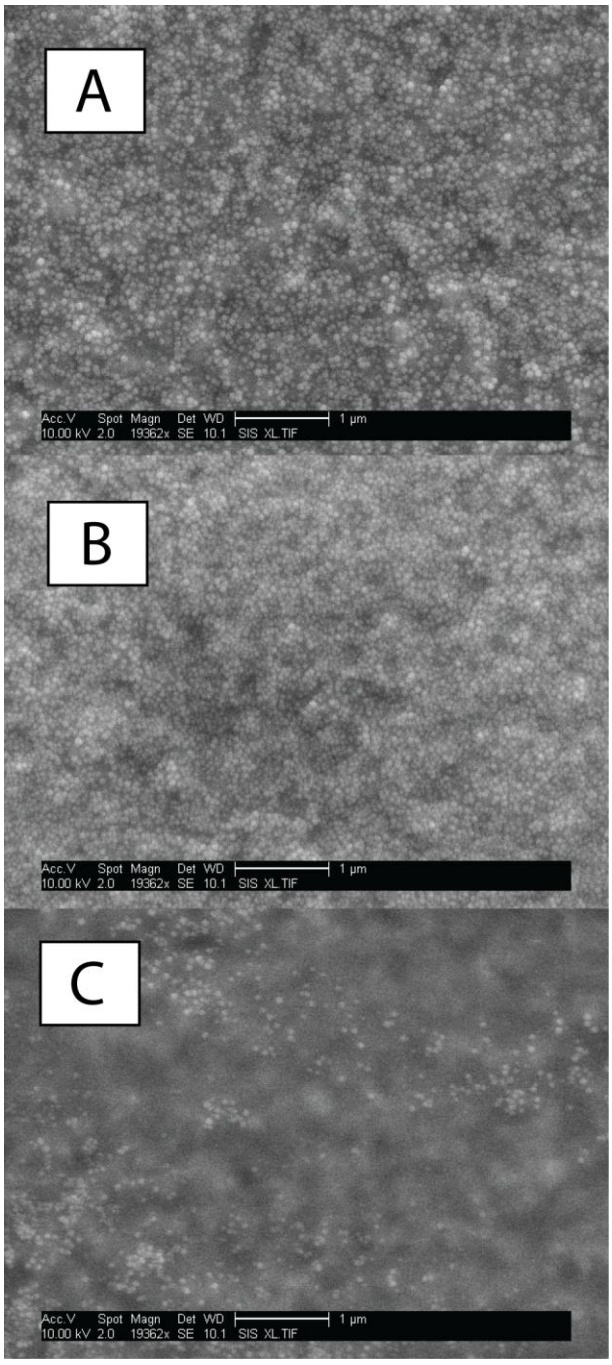

Figure 3.3: DNA stringency study SEM. A, B, and C respectively show the scanning electron microscope (SEM) images of the ***"a", "b",*** and ***"c"*** sites after three alternate addressings of nanoparticles with the 24mer complementary and target DNA sequences for 60 second at 0.25 µA.

complementary and target sequences are addressed to the "***b"*** sites in the proper order. The amount of DNA nanoparticle accumulation on the ***"a"*** and ***"c"*** control columns is significantly less than on the ***"b"*** columns (as seen in figures 3.1 and 3.2, parts B and C). However, figure 3.1A and 3.2A show that after the first addressing of the nanoparticles with the complementary DNA sequence, the ***"a"*** and ***"b"*** sites both show a nearly equal fluorescent intensity signal which is consistent with the fact that target DNA sequence is attached over all sites on the microarray. Site ***"c"*** shows no fluorescent signal because it was not activated during the initial addressing of the nanoparticles with the complementary DNA sequence. After the first addressing, if any significant number of nanoparticles were nonspecifically bound, the fluorescent signal on the ***"a"*** and ***"c"*** control columns would show an increase in fluorescence during the subsequent addressings. While the exact fluorescent intensity levels vary depending on the time and current conditions, after 20 depositions the level of fluorescent intensity (nanoparticle accumulation) on the ***"b"*** site columns was found to be about 25 times higher than that of the ***"c"*** site columns, and more than 7 times higher than the ***"a"*** site columns (which has a first single layer of DNA nanoparticles). These basic results are expected due to the nanoparticle deposition configurations of the ***"a"*** and ***"c"*** columns. The ***"c"*** column is an intended control to monitor nonspecific binding of DNA nanoparticles coming in contact with target DNA on the surface. On the other hand, when nanoparticles are actively addressed to the ***"a"*** column they have the same complementary DNA sequence as the first layer of DNA

nanoparticles hybridized to the site. Thus the ***"a"*** column is more of a control to monitor nonspecific binding of DNA nanoparticles which should not hybridize under active addressing conditions. Due to the low levels of nanoparticle accumulation on the ***"a"*** and ***"c"*** columns after twenty active addressings, nanoparticle accumulation on the ***"b"*** column is most certainly due to the hybridization of the nanoparticles. Figure 3.3 shows the SEM imaging results after three deposition cycles, which includes six alternate addressings of complement and target DNA nanoparticles onto the ***"a", "b",*** and ***"c"*** sites at optimal conditions of 60 seconds and 0.3 μA. Figure 3.3C shows that the ***"c"*** site is almost completely devoid of nanoparticles, while figures 3.3 A and B shows the ***"a"*** and ***"b"*** sites are completely covered with at least one or more monolayers of DNA nanoparticles. (The exact thickness of the DNA nanoparticle layer on the ***"b"*** site is not determinable by this surface SEM image).

The relative rate for fluorescent DNA nanoparticle accumulation (hybridization) is clearly a function of both the addressing time (seconds) and DC current (μA) level applied during the deposition process, as shown in figures 3.4 and 3.5. While the rate of DNA nanoparticle accumulation (hybridization) appears to be roughly constant for a given time and current level, this is subject to various deposition windows. In addition, the nanoparticles with the 51mer DNA sequence behaved slightly differently than those with the 24mer DNA sequence. DNA nanoparticle layer deposition appears to be relatively constant as the number of layers increases for nanoparticles with the 24mer DNA sequence (figure 3.4),

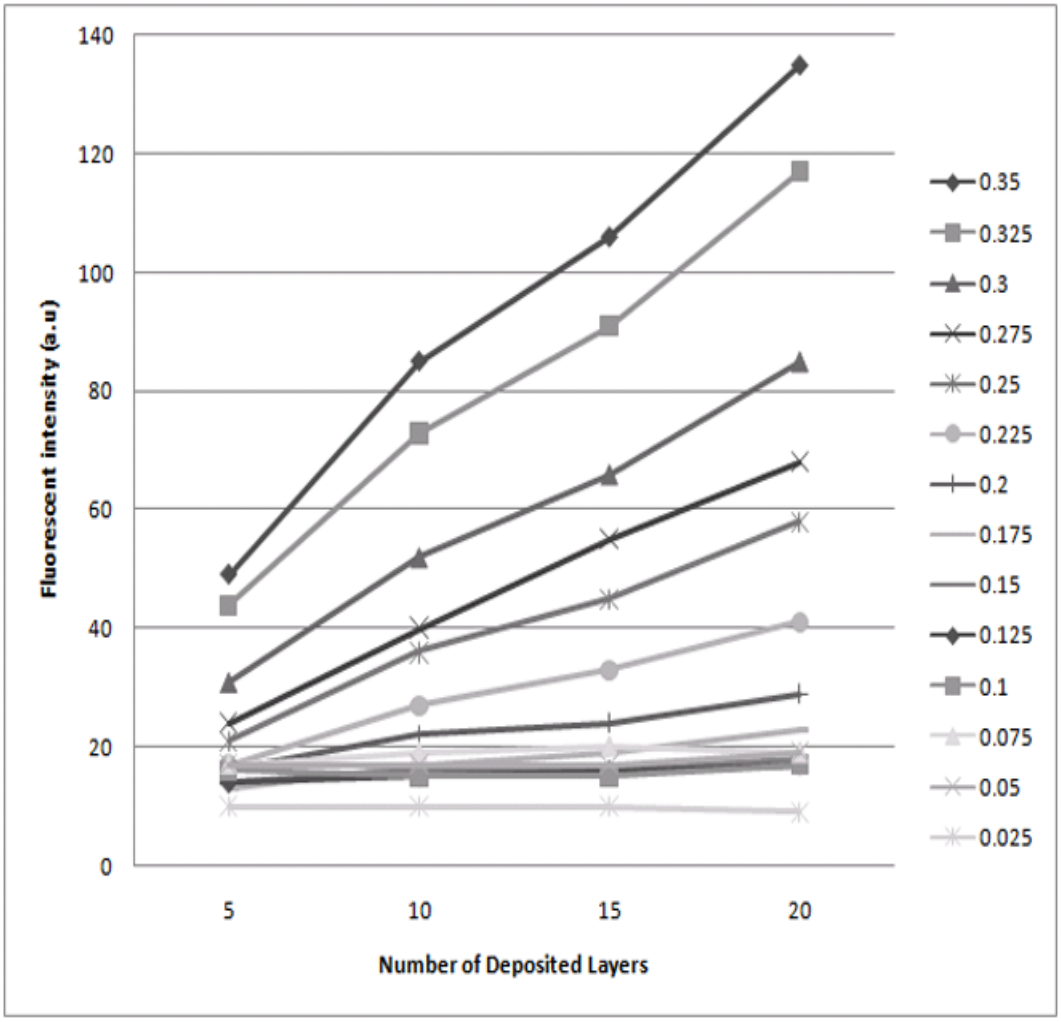

Figure 3.4: A plot of fluorescent intensity versus number of depositions (layers) for each of the DC current levels from 0.025 to 0.35 μA (applied for 60 seconds) for the 24mer DNA nanoparticle layers.

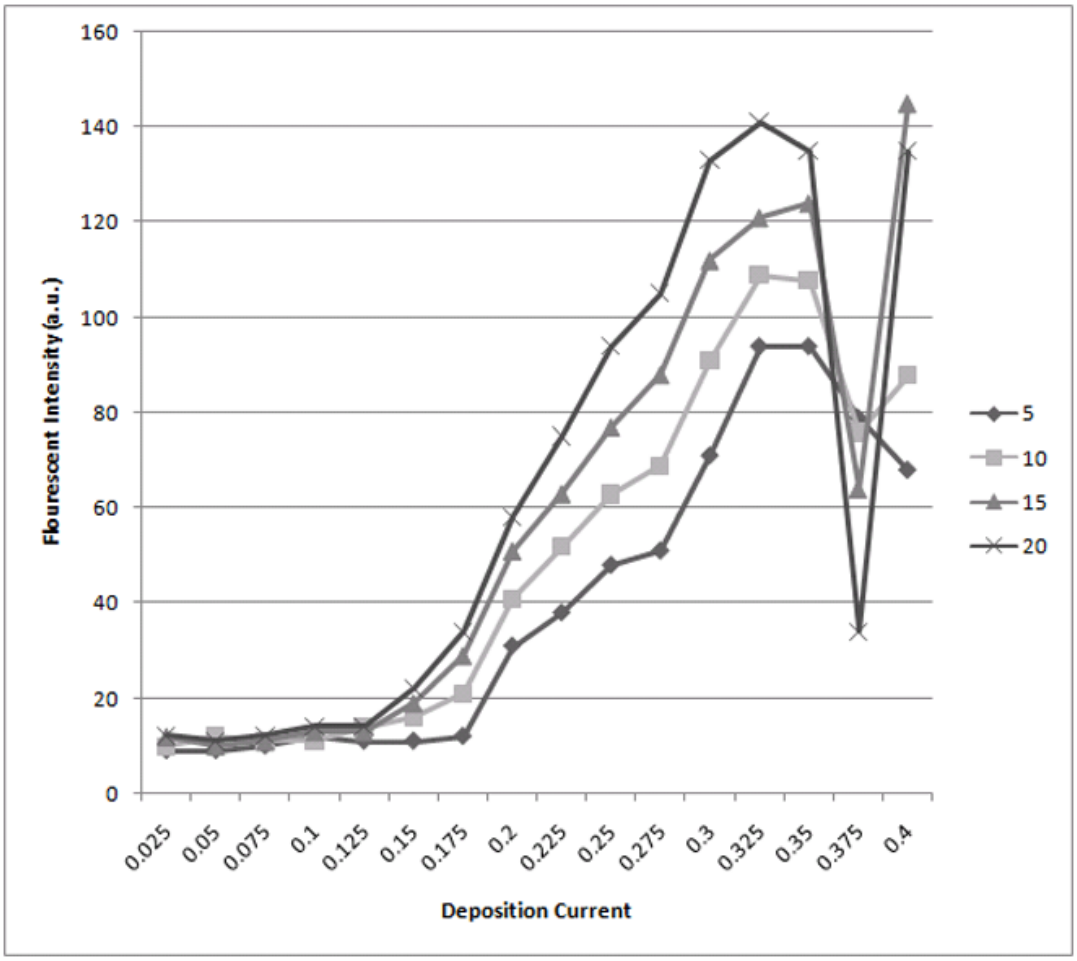

Figure 3.5: A plot of fluorescent intensity versus DC current levels from 0.025 to 0.35 µA (applied for 60 seconds) for 5, 10, 15 and 20 depositions (layers) for the 51mer DNA nanoparticles.

whereas nanoparticle layers with the 51mer DNA sequence grew more quickly in the initial first 5 depositions, and then at a slower and more constant rate for the later 15 depositions. The nanoparticle layer growth rate itself is not a linear function with current. For a given deposition time there appears to be a minimum current cutoff point. For any current level applied beneath this threshold, no layers appear to be formed. Once past the threshold point, the nanoparticle layer growth appears to be roughly linear with increased current levels. However, at higher currents levels (0.35 to 0.40 μA) and at longer times (60 seconds) the nanoparticle layers fail to form properly (see figures 3.1B, 3.2B, and 3.5). As the upper limit of the DNA nanoparticle deposition window is reached, the layers begin to form "donuts" and are unstable (this donuting behavior is visible in figures 3.1B and 3.2B). As an example, the data shown in figure 3.5 has a minimum deposition current around 0.125μA, which increases linearly with current levels up to 0.3μA. After 0.3μA, the layers are unstable and a significant reduction in fluorescent intensity is observed.

Our results show that hybridization (increasing fluorescent signal) occurs only on the ***"b"*** sites, in spite of the fact that all 400 sites on the microarray have target DNA sequence attached and have been exposed passively to ten additions of the complementary DNA nanoparticles. This is consistent with the fact that the passive hybridization of the DNA nanoparticles to the microarray is not likely to occur at the relatively low DNA nanoparticle concentration (50 nM) and under low ionic strength conditions (20 mM NaCl). The exception being the initial addressing of the

"a" sites with complementary DNA nanoparticles where hybridization is observed and equal to the initial fluorescent intensity on the ***"b"*** sites. Overall, the electronic hybridization was at least two orders of magnitude faster than the passive process, considering the total time the microarray sites were exposed to DNA nanoparticles was 20 minutes. Additionally, further controls for electronic addressing indicate there was relatively little DNA nanoparticle nonspecific binding when the same DNA derivatized nanoparticles were electronically addressed to sites (***"a"*** *and* ***"b"***) with similar DNA nanoparticles. Even more convincing are the SEM images of the ***"a", "b"*** *and* ***"c"*** sites after 20 addressing of DNA nanoparticles. These images show very few DNA nanoparticles attached to site ***"c"*** which was electronically addressed 10 times with target DNA nanoparticles and passively exposed to 10 additions of the complementary DNA nanoparticles (figure 3.3).

This work demonstrates many interesting things. Foremost of course, is that DNA coated particles can be used as binding material between nanoparticle layers, even in conditions where DNA would not traditionally bind (low ionic strength solutions), due to the acid products at the electrode. While this effect has been known to promote DNA interactions, this is the first demonstration of the effect to bind particles together. But DNA has been shown to be more than merely a general binding material; it has been shown to be a selective binding material under the electrophoretic deposition conditions. Beads coated with a single type of DNA strand only bound in significant numbers to bead layers that had the complementary strand

exposed. Layers that had noncomplementary strands did not cause binding, even though the other conditions were identical. Of course, DNA was chosen because it has these properties in general, but the successful confirmation of this effect allows us to use a wide array of different DNA strands to selectively bind various other particles.

Overall the DNA/DNA layers were less stable than the Biotin/Streptavidin layers. This isn't really surprising, since the strength of DNA binding is typically less strong than that of the biotin/streptavidin bond, and the experiments were deliberately run in low conductivity buffers in order to promote particle transport. As the NaCl concentrations in solution were increased in preliminary experiments, the movement of nanoparticles vastly diminished (as expected), and eventually the electrodes would begin to bubble significantly. Possibly various other buffer combinations would be able address this problem. In addition, the binding between beads with 51bps compared to the binding of beads with 24 bps was different. Geometrically the placement of the DNA binding regions may have been suboptimal. Physically the DNA would have the best binding if the beads were spaced apart by the length of the double stranded DNA (since both the complement and target DNA had a 5' biotin). However, the beads were likely pulled directly together by the electric field, making full binding more difficult. A 3' biotin on either the complement or target stand may address this issue.

3.3. 200nm bead layers

The beads we used in these experiments were mostly determined by what was commercially available. The beads were purchased from the molecular probes division of Invitrogen, mostly because their color, size, and molecular coatings were useful to us for these experiments. However, the availability of particles limited us to only be able to use the 40nm particles in the main experiments. Mostly this was because 40 nm particles were the only ones available in different fluorescent colors for the different binding surfaces. The only other sized beads offered were 200 nm yellow green beads in both biotin and neutravidin coatings. Because the colors of these beads were the same, we felt that it would be more difficult to run the same series of experiments we did on the 40nm beads because we wouldn't be able to distinguish them fluorescently. However, we did do a few confirmatory experiments on the 200nm beads to determine their basic viability. In these experiments, $1/100^{th}$ dilutions of the beads in 100mM L-Histidine were made. The beads were NeutrAvidin® labeled microspheres, 0.2 µm, yellow-green fluorescent (505/515) #F-8774 and biotin-labeled microspheres, 0.2 µm, yellow-green fluorescent (505/515) #F-8767. The experimental procedure was roughly the same as the "stringency test" procedure described in chapter 2.5. The chip surface was prepared in the usual fashion, and alternating layers of 200nm Biotin and streptavidin particles were laid onto different sections of the chip, leaving a region with only biotin particles, one with only NeutrAvidin particles, and one with an alternating combination of biotin

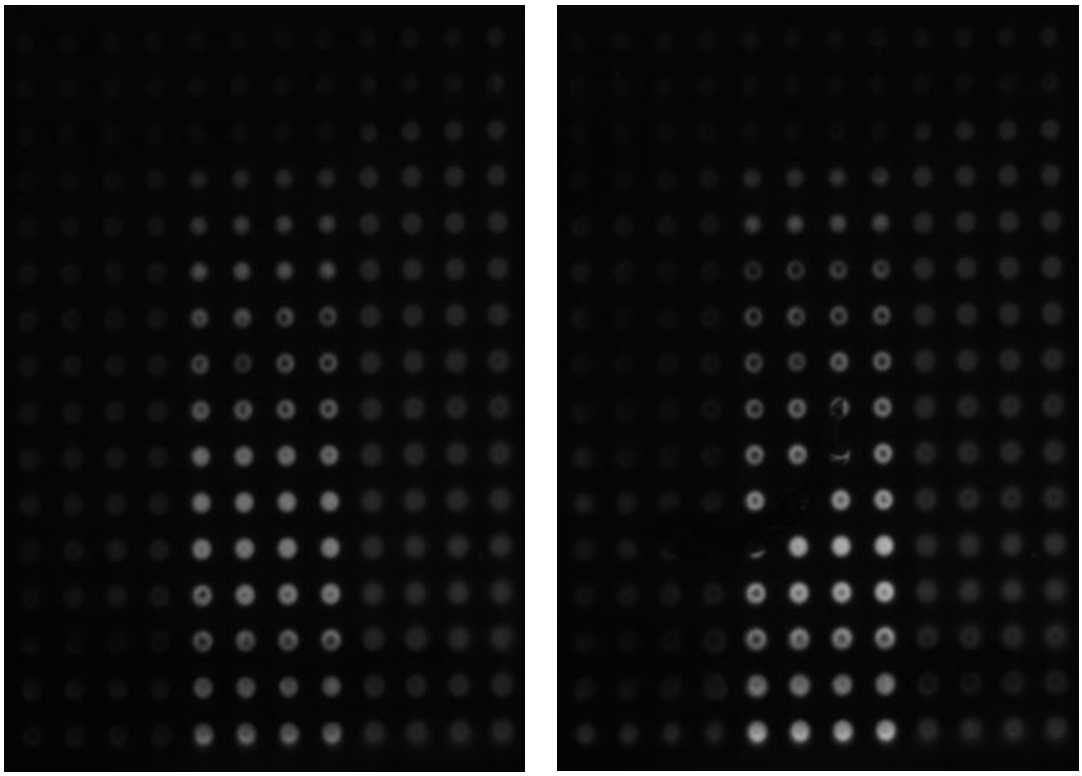

Figure 3.6: 200nm bead stringency tests. Left-200nm beads at 6 layers. Right-200nm beads at 9 layers.

and NeutrAvidin particles. The rows are arranged in a current ramp from 0.025 μA to 0.4 μA, in groups of 4 identical columns for each condition. Each pad was activated for 15 seconds apiece. Due to the particles all being the same color, individual particle types have to be inferred rather than detected directly.

As can be seen in figure 3.6, there is a reasonable level of particle stringency. One set of columns has a low level of accumulation (the column where the beads are of the same binding type as the surface), one set has a moderate level of accumulation (the region where the beads have complementary binding to the surface), and one region where there is continual accumulation (where both types of beads are layered). One interesting feature of the 200nm beads is that they appear to form layers on the surface at much lower currents and times than the 40nm beads, even despite the fact that there are roughly 125 times as many beads in a solution of 40 nm particles than in the 200nm particle solution. However, the 200 nm beads appear to have a worse level of adhesion, since the fabricated layers appear to be heavily breaking up after around 9 deposited layers. Likely the 200nm particles have a greater amount of charge per particle, allowing them to approach the surface more easily, but due to their larger size, the resulting structure has less binding contacts (since the volume ratio of the binding layer compared to the bead volume decreases). Overall, the 200 nm particles were less suitable for use in the larger series of experiments carried out on the 40nm particles. However, they saw some use due

to their size difference from the 40nm particles which allowed us to get a level of contrast under the SEM. This is discussed in the next section.

3.4. Structures formed from particles of various sizes

As was discussed in chapter 2, the 40nm particles used in this work are fluorescently distinguishable, but identical under the SEM. Given that the particles themselves are too small to be observed individually under a microscope, we took to extensive use of SEM imaging to observe the finer scale structures on the surface of the electrode. However, due to the identical size and shape of the 40nm biotin and neutravidin particles, the SEM was unable to resolve individual layers of particles. In an attempt to resolve this problem, I deposited down alternating regions of 200nm and 40nm particles. Ideally, particles of a closer size would be used. In the case of 40nm and 200nm particles, the topographic variations of the spherical 200nm particles are larger than the 40nm particles themselves. Thus the nature of the fabricated layers would be inherently “dirtier” than that of the alternating 40nm particles.

The chip surface was prepared with biotin dextran and streptavidin as normal. The layers were deposited as follows. First 4 layers of 200nm particles diluted by 1/10th in 100mM L-histidine were deposited, alternating layers of biotin and streptavidin particles. Then 6 layers of 40nm particles 100mM L-histidine diluted by $1/10^{th}$ were layered with alternating biotin and streptavidin. Then the whole

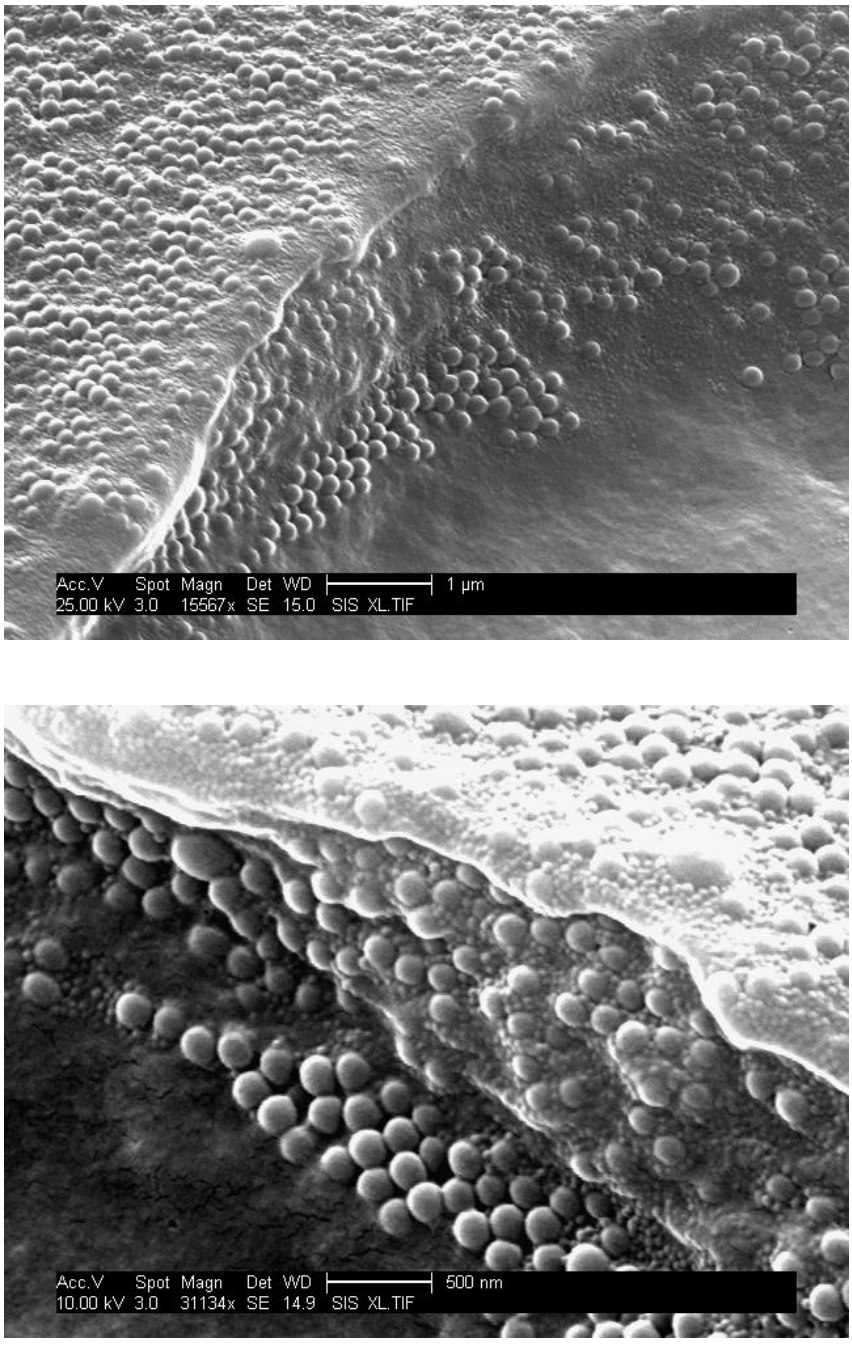

Figure 3.7 SEM images of multiple sized bead layers. A(top) and (B) bottom: SEM image of multiple alternating layers of 200nm and 40 nm particles.

layering process was repeated. This gave a total of 20 layers, 8 200nm bead layers and 12 40nm bead layers, with 10 total biotin layers, and 10 total streptavidin layers. All the deposition conditions were the same at 15 seconds activations, 0.25 μA current.

After layering, the chip was scratched with a probe tip to attempt to expose the deposited strata, and the resulting scratches were viewed using SEM imaging. As can be seen in figure 3.7, there are somewhat distinct strata, but the upper levels of particles appear to be intermixed.

3.5. Quantum dots

When we first began the work on nanoparticle layering, we considered switching to working with quantum dots. Ultimately chose not to, chiefly because they gave inconsistent results due to their smaller size. We used CdSe quantum dots purchased from the Quantum Dot corporation. Similar (and somewhat superior) to the 40nm fluorescent particles we used in the experiments reported in chapter 2, we were able to purchase a wide variety of colors and surface coatings for these particles. Due to previous work in other areas, we had some biotin and streptavidin quantum dots with red and yellow/green fluorescence.

For our experiments we performed the usual stringency tests on the particles as has been described previously (section 2.6). These experiments were performed before we had settled on the biotin Dextran followed by streptavidin

surface. The surface was modified only with biotin dextran, and the first layer pulled down was composed of streptavidin quantum dots. A 1/1000th dilution of quantum dots was prepared in 100mM L-Histidine. The quantum dots were pulled down in the usual 3 column setup to determine particle stringency with the usual 0.025-0.4 μA current ramp. The activation times of the columns were 45 seconds. Images were taken through the fluorescent microscope using appropriate filter cubes that allowed the imaging of a single species of quantum dot independent from the other. Due to the small size of the quantum dots, they were not resolvable under the SEM.

The observed results were interesting. On the columns where both streptavidin and biotin quantum dots were pulled down to the surface, the fluorescent intensity slowly increased over time, as we would expect. For the columns with only streptavidin quantum dots, the initial layer was the same brightness as the back and forth column, but only doubled in fluorescent intensity after the first layer and the last deposited layer (20 depositions), whereas the back and forth layer exhibited a streptavidin quantum dot fluorescent increase of 8 times. Because we weren't able to SEM the quantum dots (due to their small size and organic coatings), we can't tell if this additional intensity is due to particle stacking or a more complete filling in of an initial monolayer. However, the bulk of the streptavidin quantum dots were deposited in the first deposition. This implies a low level of streptavidin quantum dot interparticle non specific binding, as few additional particles were deposited to the surface even though they were pulled down to it. The

biotin quantum dots were different, however. Since they had a biotin coating, and the surface had been coated with biotin dextran, we would expect that they would only bind to the main experimental column where the streptavidin quantum dots had been previously deposited. For those columns the biotin quantum dots did indeed deposit, and did so in a uniform manner (see figure 3.8). However, the columns where only biotin quantum dots showed what appeared to be a high level of nonspecific binding. In fact, the biotin quantum dot accumulation in those columns was actually much higher than in the regions with both biotin and streptavidin quantum dots, even though there was ostensibly nothing for them to bind to. However, the spots on the biotin only regions exhibited a strange secondary characteristic; they were much smaller than the spots on the other regions. All the particle intensity was gathered near the center of the electrode, rather than spread uniformly across it, as is seen with the streptavidin only and the streptavidin plus biotin regions. Indeed, the biotin quantum dots layered on top of the streptavidin quantum dots behaved as we would expect them to. Due to this we were unable to determine the actual amount of nonspecific binding the biotin quantum dots exhibited.

What was the cause of this behavior? Why would biotin and streptavidin quantum dots behave differently, except due to the effect their surface coatings? The problem is of course, is that these particle aren't really identical at all. The core part of the quantum dots are similar, except for small size variations which allow the

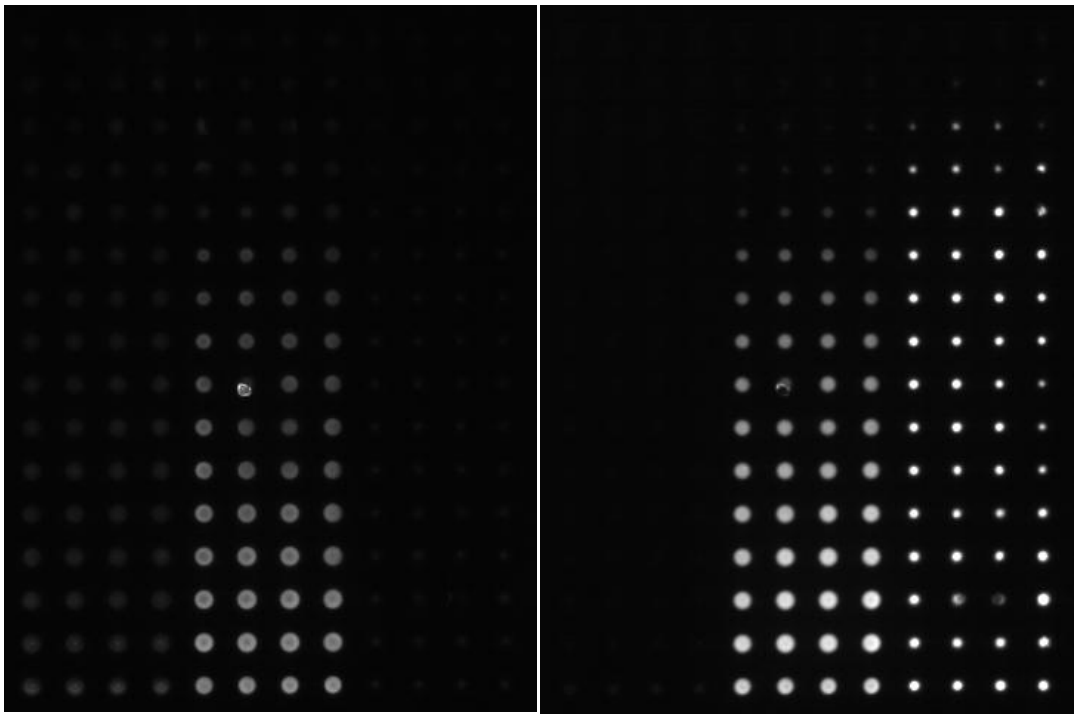

Figure 3.8: The standard stringency experiment repeated for biotin and streptavidin coated quantum dots. The four left columns are streptavidin qdots only, the middle four are both streptavidin and biotin qdots, and the left four are biotin qdots only. (left image) Shows the fluorescent image for the streptavidin quantum dots at 39 total depositions and (right image) shows the fluorescent image for the biotin quantum dots at 40 depositions. Note the size difference in the intensity for the right control columns in the biotin image vs. the deposited intensity for the actual experimental columns.

quantum dots to fluoresce at different colors, but the surface coatings are radically different. Biotin is a small molecule consisting mostly of a couple of atomic rings. Streptavidin is a protein roughly 55kd in mass and 3-4 nm across. The addition of the streptavidin layer around the quantum dots would roughly double the radius of the particle. Therefore the main difference between the biotin and streptavidin quantum dots is simple; the biotin quantum dots are physically much smaller. Once we understand this, the observed differences the results are pretty intuitive. The biotin quantum dots are evidently small enough to move into the gel itself, which was purposely designed to allow small particles to enter into it (since the chip was designed with DNA hybridization inside the gel in mind). The streptavidin nanoparticles with their greater radius were above the size threshold to enter the gel, and therefore remained on the surface. In the region where both quantum dot types were pulled down to the gel, the streptavidin coated quantum dots went down first and created a layer to which the biotin particle could not penetrate. Therefore in that region the biotin particles behaved as they would expect. One of the more interesting points was that the biotin quantum dots accumulated in the electrode center, a matter which will be dealt with in depth in chapter 4.

The work with the quantum dots brings up an important constraint on the nanoparticle layering system. We find that the gel itself has several important properties that make it necessary to have present in the system. However, the size of the porous regions in the gel itself must be smaller than the particles we hope to pull

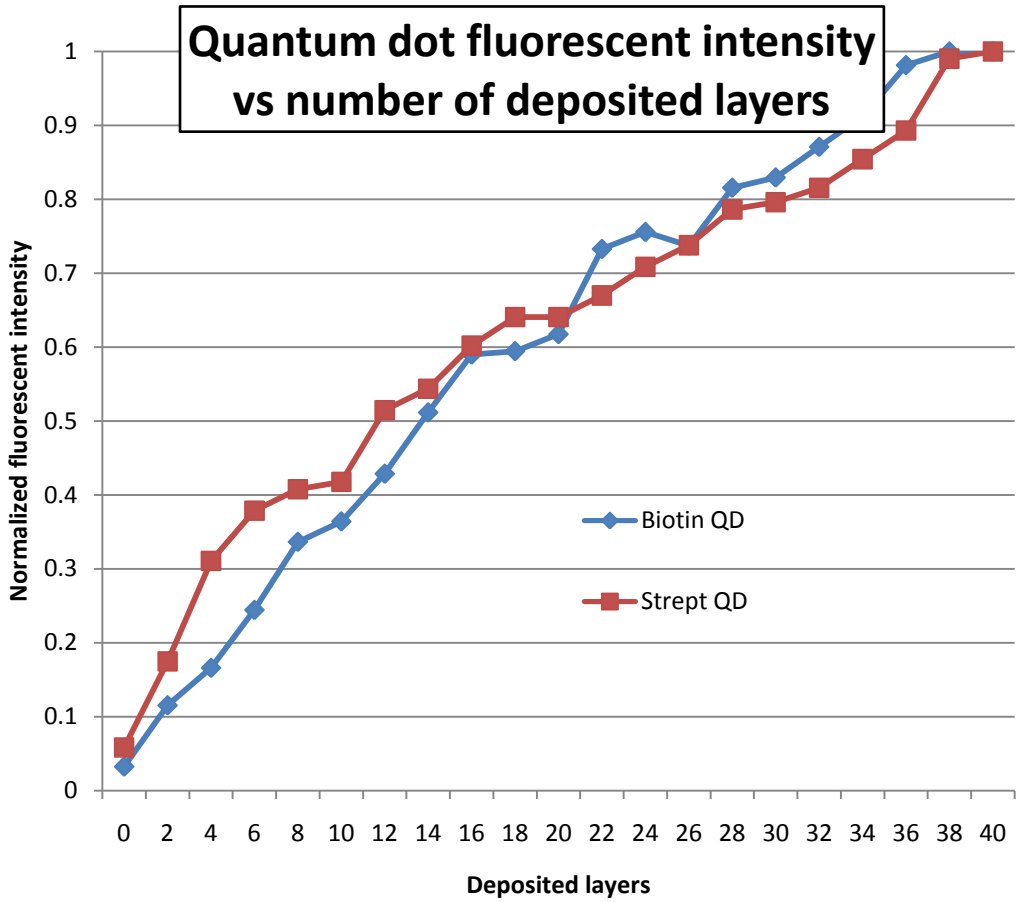

Figure 3.9: Normalized quantum dot intensity compared to deposited layer number.

down. Otherwise the gel goes from being a neutral support system for the growth of nanolayers to effectively a molecular sieve. Any future devices will have to take the intended size of the deposited particles into account when designing the electrode standoff layer.

In spite of the fact that we couldn't determine the level of biotin quantum dot stringency, we were able to observe the relative rate of particle layer growth for both types of quantum dots. The growth rate appears to be roughly constant until around 20 deposited layers, at which point is seems to slow down, though particle accumulation continues to the final 40^{th} deposited layer. Comparing the normalized intensity of the biotin and streptavidin quantum dots show that the relative rate of fluorescent intensity is roughly the same between the two populations. Neither population stops growing, nor does the ratio of growth from one layer to the next drastically change (see figure 3.9).

3.6. Liftoff of layers

While developing the initial process, I used to finalize the chip for SEM analysis by washing away excess L-Histidine solution with washes of 18 MOhm water. This was done under the assumption that the histidine might cause detrimental crystallization once the remaining water evaporated from the chip. However, when we did this we observed that the fabricated layers would release from the chip and float away into solution. The fabricated layers were not dissolving; instead they were

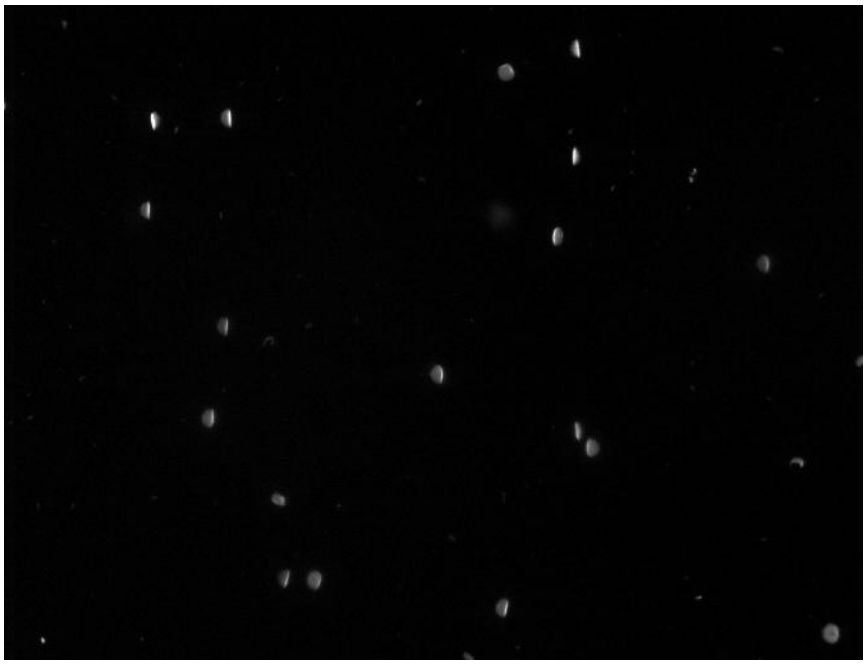

Figure 3.10: Layers lifted off into solution

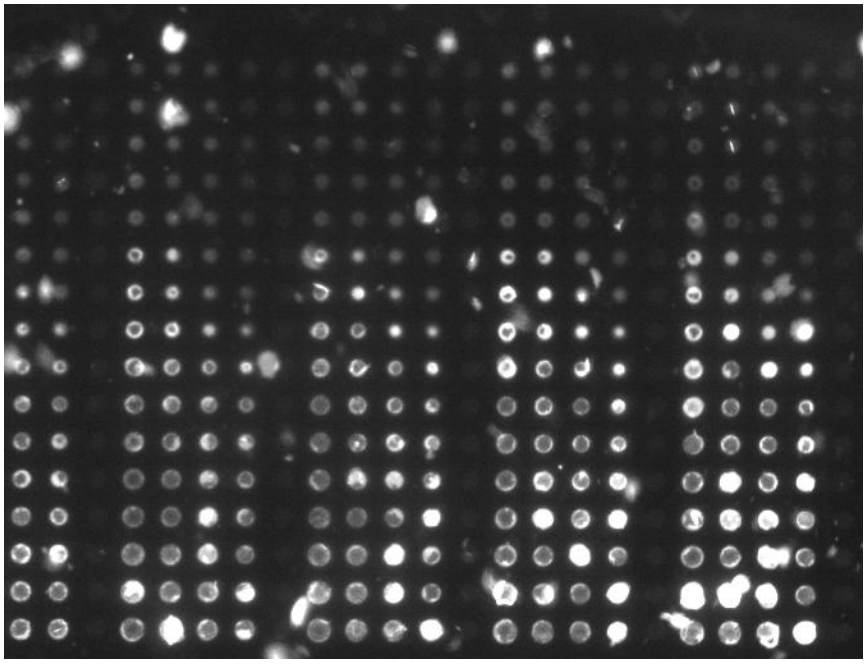

Figure 3.11: Lift off layers during the release process

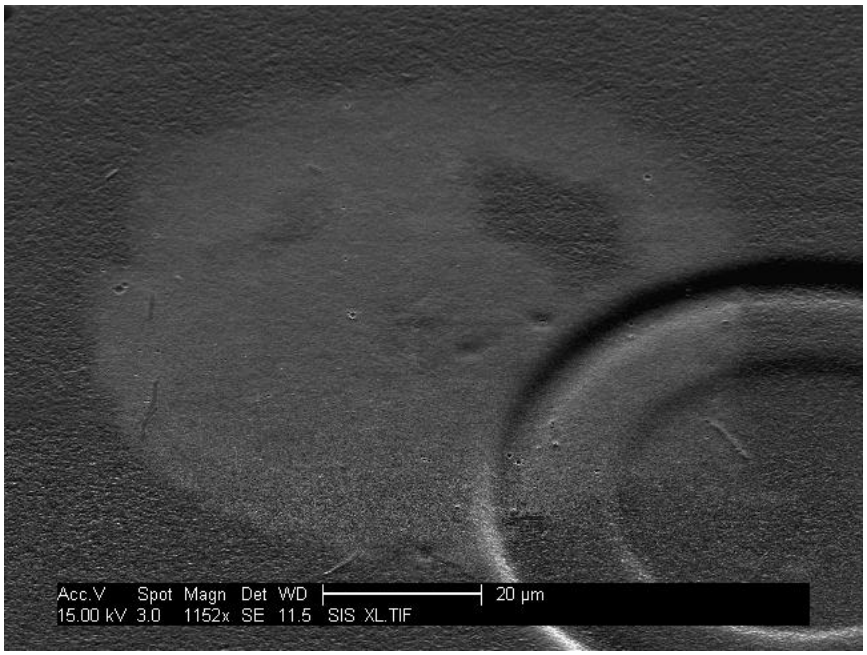

Figure 3.12: SEM of an individual layer that settled down to the surface

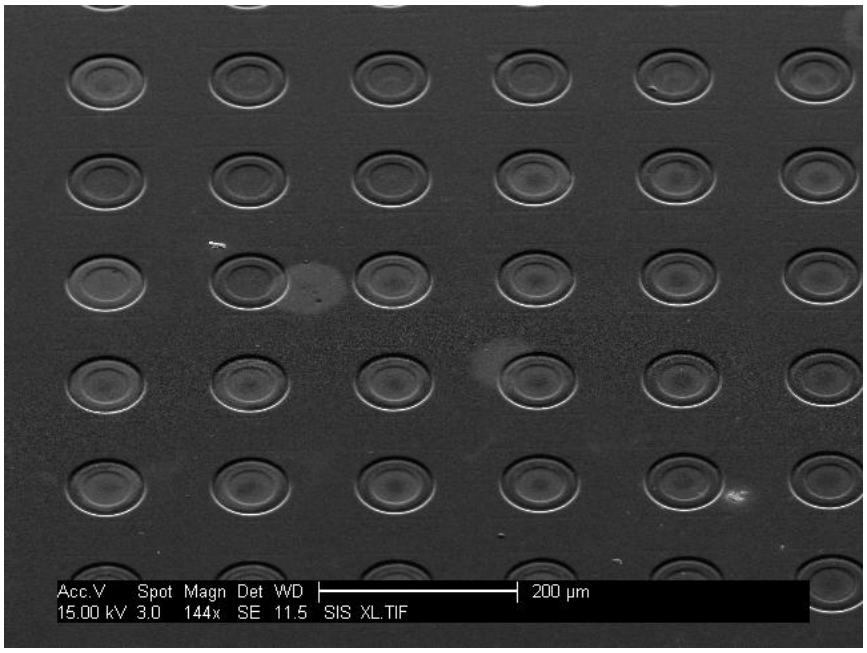

Figure 3.13: Several recaptured layers and the leftover beads on the electrodes after release.

actually growing in size and ripping off of the chip's surface. This effect was fully repeatable and would occur as soon as the water was introduced to the chip. The layers could be seen to physically grow in size during this process. (see figs 3.10-3.13). Once in solution the layers were physically cohesive, though their expansion in size caused them to fold in half in a taco like fashion. Since this process was relatively violent, often the liftoff process would leave a ring around the electrode of material that was unable to lift off along with the bulk of the material, and there was some residual nanoparticle left in the center of the main liftoff region. So while this was a repeatable effect, it was not entirely controlled.

We found this effect interesting because we had hopes that it would allow for some form of controlled release of fabricated structures. However because of the size change and rough release it is probably unsuitable for this purpose. However, it does tell us something about the layers themselves. The layers are composed of charged particles (by necessity, that's how they are pulled around in solution), and that charge is permanently fixed to the particle surface. As the particles are fabricated into a multiple layer structure, the particle surface charges remain fixed within the stack. Left by itself, all that charge would rip the structure apart due to electrical repulsion. As the negatively charged particles are pulled down to the electrode during the active deposition process, the positively charged ions in solution are repelled away at the same time. This likely means that the only positively charged ions left in the local area are hydrogen ions and hydrogenated histidine.

Since the chips are washed only with zwitterionic histidine buffer, it is unlikely that any additional positive ions are able to diffuse into the layer structure. Only during the brief period when a new bead solution is placed on the chip are other positive ions present, and those are rapidly pushed away once the next activation begins.

Therefore once this structure of tightly associated charges is exposed to a solution of pure water, it experiences a strong osmotic flow. Water rushes into the structure, causing it to rapidly expand. This expansion causes stresses stronger than the relatively weak surface bonds can handle, causing the structure to simply pop off into solution. This does not occur in the histidine solution because we are actually quite close to the saturation concentration of histidine itself (260mM at 25C), and therefore there isn't as much of an osmotic gradient. This effect needs to be accounted for in any case where the structure would possibly be exposed to a solution with low amounts of solute. There are likely many solutions to this issue, but that is beyond the scope of this work.

3.7. Gel compression

As has been discussed previously, the fabrication of nanoparticle layers is subject to various windows as current and deposition times are varied. At low currents/times not enough particles are deposited to the gel surface to create a sufficient monolayer for the next layer to bind to, so no real layers form. However at higher current and times, the reasons for the degradation of the deposited layers are

less clear. While the layers themselves form as we would expect, they are increasingly fragile and have a tendency to break up at the center of the electrode area, though subsequent layers deposit once again on the broken surface. There are two effects that we know occur that may influence layer stability. The first effect (which will not be discussed in depth here) is the increasing amount of acid that passes though the deposited layer as time and current increase. Simulations (discussed in the next chapter) show that current, of which the H^+ ion makes up a significant fraction) moves preferentially through the higher resistance particle layers as opposed to the larger charged nanoparticles which are stopped at the gel surface. Highly acidic conditions are known to break the biotin/streptavidin bond, which likely contributes to the layer degradation.

However, there is a second effect, mechanical in nature which we have also observed. As the current in increased, we see that the layer itself physically deforms. The deposited layer stack appears to compress radially towards the electrode center. This is not surprising, since the particles that make up the deposited layers retain their charge. This charge will experience a force towards the source of the electric field once the electrodes are turned on. This force is enough to deform the layers for the duration of the applied field. This deformation should be roughly proportional to the current and the thickness of the applied layers. However, the consequence of this is that layers fabricated under these conditions will be under stress at all times when the electric field is not applied, since the fabrication state is

the default state in which the particles formed into a layer, and are packed with respect to that configuration. As we have already established, the layers become dislodged from the surface when they expand (as discussed in the previous section), it is not surprising that this stress leads to the layers breaking. Between the layer stress and the possible action of acid weakening of the biotin bonding the layers break in the region where we would expect.

There are reasons though, why we would like to be able to mitigate this effect. The layers form more rapidly and cleaner at higher currents, so such conditions would be more favorable to use if possible. Also, as we saw with the difference between 40 nm beads and 200nm beads, different particles deposit optimally at different current ranges, so to be able to accommodate a system that involves many different types of particles, we need to be able to accommodate many different currents and times in a single structure. To do this, we would need to reduce the total magnitude of the physical deformation, and possibly reduce the effect acid has on the system. Acid can be dealt with by increasing the amount of histidine in solution. While for this work, we were near the saturation concentration of histidine, by increasing the temperature we would be able to increase this limit somewhat. This would depend on the temperature stability of the particles in use. However, to reduce the physical distortion of the layers, we would need to decrease the compression of the substrate upon which the particles sit. This could be done one of two ways. First we could make the layer itself thinner. Assuming that the gel layer

is roughly a spring like material, the compression it feels when exposed to a given force is proportional to its thickness. The thicker the gel, the more it will compress (just like a longer spring will stretch a greater distance with the same force than a shorter one). The second thing we could do is to make the material out of something harder that is unable to physically deform as much (or at all). Adjusting the thickness and hardness would need to be understood with respect to the current profiles discussed in chapter 4.

Chapter 3, in part is a reprint of the material as found in Nano Letters: Dehlinger, D.A., Sullivan, B.D., Esener, S. and Heller, M.J. (2008) Directed Hybridization of DNA Derivatized Nanoparticles into Higher Order Structures. *Nano Lett*. The dissertation author was the primary investigator and author of this paper.

Chapter 4: Layer uniformity

4.1. Introduction

The results as discussed in chapter two point to an interesting and important phenomenon. When fabricated, the layers of nanoparticles tend to form centered distributions across the electrode. When examining optical intensity cross-sections of the collected data, the layers are usually seen to go from background intensity at the electrode edge, to peak intensity towards the center of the electrode. Of course, there are variations on this effect, but they exist in some sense in the "failed" deposition conditions. Failed deposition conditions are roughly the regions where multiple layer deposition fails to occur due to insufficient particle pulldown, or where the deposition stresses are so great that the fabricated layer breaks and forms into a "donut" shape. This donut shape however, is formed due to the loss of fabricated layers preferentially from the center of the electrode, rather than an enhanced rate of deposition. In fact, all the evidence point towards the electrical force being the greatest at the center of the electrode. This is fine, because it allows us to build more uniform layers, however it **is the exact opposite to what we expect from a simple analysis**.

To understand this, we need to look at the nature of the electrophoretic force. When an electric field is applied various forces will be applied to objects in solution. All these forces will have different spatial profiles, and modes of effect. In

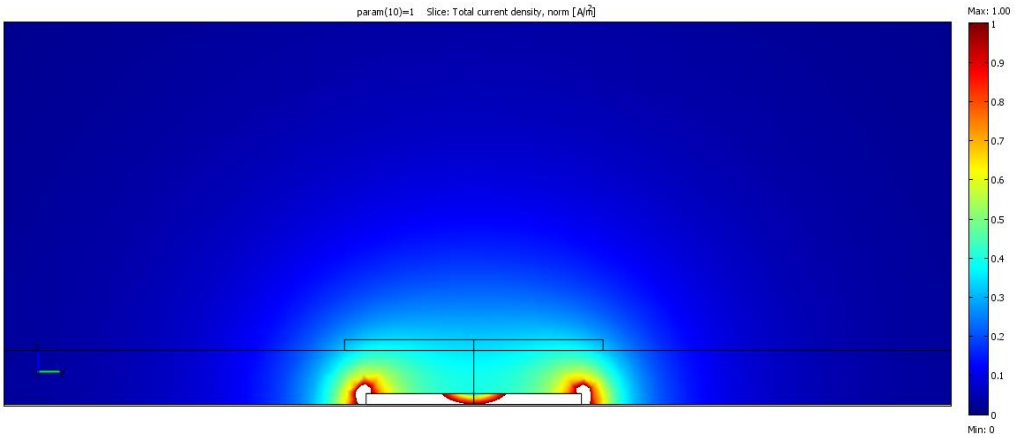

Figure 4.1: Predicted current distribution when the gel and deposited layer resistances are the same as the solution resistance. Image is in cross-section through the center of the electrode.

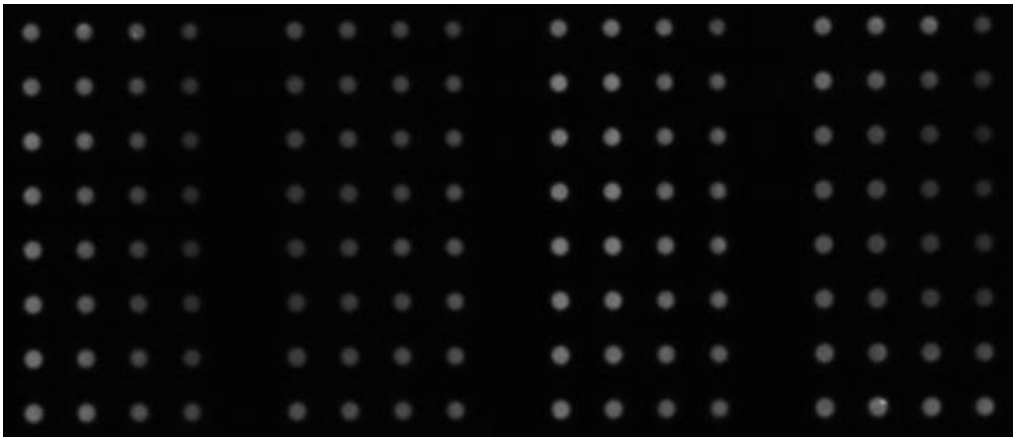

Figure 4.2 : Distribution of deposited particles over an electrode.

the case of electrophoresis, charged particles in solution become part of the total system current and move towards the appropriate positive or negative electrode, depending on their total charge. But more than moving towards the electrodes, the particles will move towards the source of current, the force the particles experience will be in the direction of the current for the simple reasons that the particles are one of its primary constituents. The electric force and current flow must be proportional to each other in simple systems. If we follow the flow of particles we are following the direction of the electric force, as long as we assume that there are no other significant forces along other directions.

Why then, is there a problem? The problem arises because the current should move towards the current source, not necessarily towards the electrode. While the electrode is technically the source of the current, that current is not uniform across the electrode surface. In fact, a simple analysis would indicate that the current originates entirely from the edge of the electrode, rather than from the center. However for the most part we see the bulk of the particle deposition, and thus the current take place in the center of the electrode. In fact, for most of the deposition process, the layer is observed to be brightest (and thus most densely populated by particles) in the center of the electrode, with a falloff towards the electrode edge. Only when the fabricated layer is physically deformed or broken is the edge of the electrode observed to be brighter than the center.

To better understand what is going on, let us go back to the geometry of the situation. The electrode is a 55 µm disk of exposed platinum. This disk extends a bit further, but this excess size is covered by a passivating layer of silicon dioxide which serves to prevent fluids from leaking underneath into the electronics beneath the electrode. Experiments with similar geometries have demonstrated that the current does not flow through the passivating outer layer, even though some amount of "active" electrode lies beneath. On top of the electrode lies a 10 µm thick layer of polyacrylamide gel, infused with streptavidin. When we say that particles are pulled to the electrode, we really mean that they are pulled to the gel surface atop the electrode. The electrode itself is not adhesive to the particles used. In fact the opposite problem arises; particles pulled directly to the electrode surface undergo a form of electrochemistry. Charge is stripped from their surface and they are transformed from a negative particle to a positive. At this point they are repelled from the electrode. The gel then provides a necessary component of the electrodepositing system. It provides an adhesive surface to build layers off of, and it protects the layers from the negative effects of direct electrochemistry.

What then, is the cause of the particle distribution we observe? There are several possible contributing factors. However I will demonstrate that most of these factors are unable to individually account for the behavior we observe. However, in this discussion these factors it will become clear why the distribution

effect we observe is a real and important feature of the electrophoretic layer by layer deposition process.

Possible contributing effects to the observed data include:

1) Optical measurement nonuniformities

2) Nonlinear deposition effects introduced in the layer by layer “passivation” process or nonspecific binding

3) Changes in the current distribution due to the gel standoff height

4) Electric field redistribution due to resistance difference between the gel and the bulk solution

These explanations run the gamut from experimental error to changes in the geometry of the system to a more complex model of particle deposition. They each will be addressed to understand why they are important questions, and how they contribute to the final deposition system.

Before I go on at great length about the possible causes of the particle distribution, I want to establish why this is an important topic. Why do we care what the deposition profile of particles across the electrode is? In fact, particle deposition uniformity is an important pursuit. The ultimate end goal of this work is not merely to study particle deposition on an array of widely spaced circular electrodes. The ultimate pursuit of this work would be to understand the parameters and geometries needed to create a rapid, maskless, full surface pattern of deposited particles. One requirement for such a system is that layers fabricated with it are deposited in a

uniform manner across the surface. Understanding the root causes of particle distribution will allow for fabrication of a next generation high density system in a rational manner.

4.2. Optical measurement nonuniformities

Could the differences in intensity from the center to the edge of the electrode be explainable purely by optical means? Our particle density is measured by fluorescent intensity. Within reasonable limits, measured fluorescent intensity is based on 3 parameters.

First there is the amount of fluorescent dye in the sample volume. As long as the absorbance of the particle isn't too high, the amount of fluorescent intensity will be directly proportional to the number of particles. Of course, if the particles each receive different amounts of excitation light, then the situation is more complicated. However, the particles by themselves are very small and basically transparent, and this radial effect is observed even when a single layer of particles has been deposited. Therefore the amount of light absorbed by other particles is taken to be negligible. Also, the intensity growth rate in the electrode center vs. number of deposited layers is seen to be linear for many layers, so this is not taken to be a serious problem.

The second reason why we might observe spatial variation in intensity would be that the illumination of the particles is spatially variant. While the light

from the microscope may have a slight variation, this variation is on the order of a few percent across the chip surface. However, the electrode itself is a flat metallic surface parallel to the fabricated bead layer, and strongly reflects any light that is incident upon it. Beads above the surface of the electrode will be exposed to up to twice the illumination intensity compared to beads binding to the area between the electrodes. Therefore, if a uniform layer of beads was large enough and extended from above the center of the electrode towards the region of the chip without metal underneath, we would expect there to be a point at which it would grow dimmer solely for reasons of illumination intensity.

The third reason why a particle might have a spatial variance in its measured fluorescent intensity is that less light is received from the particle of interest, even though it may be emitting as much or more than another particle. Once again the main reason for such an effect in this geometry would be due to the reflective nature of the electrode beneath the fabricated layer, as there are no nonuniformities in the microscope optical system.

Despite the possibility that either the emission or excitation light may be lower towards the edge of the electrode, we do not believe this to be a significant effect when all things are considered. Geometrically, the electrode is 55 μm in diameter. However, the electrode is defined not by the position of deposited platinum, but rather by a patterned layer of silicon dioxide on top of the metal. The actual metal (and thus the reflective layer) extends another 10um past the point

where the silicon dioxide ends. However, all the current from the electrode comes from the area of the exposed metal, therefore all the deposited particles are roughly found only over the activated electrode area, which is only about 75% of the total reflective diameter. The deposition of the particles primarily over the activated area is confirmed by SEM analysis (see figure 2.19). Furthermore, the data was collected using long distance low power objectives which source and collect light at very steep angles. Finally, this effect persists even when single layers of particles are deposited at lower currents. In such situations the deposited disk is smaller than normal, but is still formed over the center of the electrode, making a reflective optical explanation impossible. From this evidence, we conclude that the particles are well within the cone of sourced and emitted reflected light. Thus it is correct to say that the measured fluorescent intensity is directly proportional to deposited particles, at least at low numbers of layers.

4.3. Nonlinear deposition effects introduced in the layer by layer process

Theoretically, the layer by layer process should be self passivating. That is, as soon as a single layer has been attached to the surface no more particles can bind because all the binding sites have been used and the particles have a low level of self adhesion. Of course, with electrophoresis more particles will be pulled on top of the previously layered ones until the current has halted. However, if there was full particle stringency we would expect that all excess particles would wash away except

the bottom layer. Therefore we wouldn't expect the edge area to have a greater amount of particle deposition (even though there might be a greater amount of current), unless an insufficient number of particles would be deposited in the center region to form a complete layer there.

Would layer passivation be sufficient to explain the particle distribution we observe? If we posit that all the particles are being attracted to high current regions at the edge of the electrode and that the center regions are fully filled due to some form of spillover we would expect a few things to reveal this. Firstly, we would expect there to be a roughly similar amount of particle deposition radially out from the edge of the electrode due to spillover. While there is some size increase of the deposition disk with increased current, it is not on the order of the distance from the center to the edge of the electrode. However, more importantly, as we study electrodes with layers deposited at lower and lower currents, we would expect there to be a threshold in which the center of an electrode is no longer covered by a monolayer. This however, is not observed. As the current is lowered, the deposition of particles pulls from the edge of the electrode towards the center leaving a smaller spot. A donut shaped deposition pattern is not observed. The highest amount of current (or electrical force) is actually going through the center of the electrode, not the edge. Therefore, we are confident that the particle binding pattern across the electrode is not due to nonlinearities in the binding of particles above the electrode.

As was demonstrated, the particles do exhibit some level of nonspecific binding. There is no clear point where increasing the deposition time or current truly stops additional particles from binding. However, since we have SEM images of the surface we know for certain that the electrode has a full monolayer of particles deposited upon it within the range of time and currents we used in the experiments. Since more particles appear to deposit between electrodes with increasing currents, it is plausible that a similar effect might occur on a single electrode due to spatial variances in the current. Since the largest amount of particles is seen to deposit on the electrode center, this once again points to the fact that the point of the highest current density lies in the electrode center, rather than towards the edge.

We have established thus far that the current driving the particle deposition has a maximum at the electrode center, and is not explainable by secondary measurement or particle issues, which if anything, exists as evidence to the current emanating from the electrode center. To address this change of current distribution, we need to examine how the actual electrophoretic system differs from the ideal case of a steady state uniformly conductive system where particles bind directly to the electrode surface.

What are the assumptions we make, and where do they break down? Well, the simplest possible case to study is where an electrode at some normalized voltage discharges the current carrier into a region of uniform conductance (the medium conductance being many orders of magnitude less than that of the

electrode). The steady state current is then simulated from this situation. In a very real sense, such a model is entirely wrong.

The actual electrophoretic system has the following properties. It is not steady state, in that the current is applied only for a short period of time, and the current itself makes a large change in the system itself. There are multiple current carriers for the system, and those current carriers change their spatial density and relative proportion as time progresses. Initially the current is made up mostly of the negatively charged nanoparticles of interest and some residual ions from the buffering solution that they were initially stored in, previous to the experiment. The solution is heavily buffered by 100mM zwitterionic L-Histidine (more histidine would start to crystallize on the chip). As current is injected into solution from the electrode, H+ and OH- ions are necessarily created by the electrolysis of water to carry that current. Since these ions are small, they have a rapid mobility compared to the larger nanoparticles. Initially the effect these ions have on the solution are mitigated by the L-Histidine molecules. The L-Histidine forms a charged complex with the H+ and the OH- molecules, increasing their effective mass and drag as well as decreasing their effective mobility. However, this buffering has a limited local capacity. Looking at only the amount of histidine contained within the volume of gel above the electrode, we would expect the buffering capacity to last between ~10 to ~0.5 s depending on the current used at that particular electrode. Of course this association is subject to spatial variations as the histidine is carried away from the

electrode and as more ions are produced at the electrode and as the histidine disassociates with the H+ and OH-. The charged particles we care about are the nanoparticles we used for this work. However, due to their size they get stuck on the surface of the gel (which we want), 10 μm above the actual electrode, which further complicates current calculations. Finally, while current is continuous through the whole system, the current carriers in the electrode are fundamentally different than those in solution, and the transition process (electrolysis) between the two regimes is subject to current dependant energy losses. Therefore the simulations for DC electrophoresis presented in this work need to be understood as rough approximations taken for short times. They are presented in order to illustrate the concepts under discussion. Additional evidence supporting conclusions presented here will come from the form of work from AC dielectrophoresis, where many of the caveats listed above no longer apply, but where the overall system geometry is similar.

4.4. Changes in the current distribution due to the gel standoff height

As demonstrated above, the current distribution at the electrode surface is strongly biased towards edges and corners. Electric fields are strongest at these locations, and behave almost as a point source of current, despite the fact that the voltage across the electrode is identical. Now while we would expect that the current should most strongly emanate from the edge of the electrode, it is possible that the

electric current at the height of the gel would have diffused quite a bit. Taking into account that particles would feel a force emanating from the entirety of the edge of the circular electrode, we might expect to see an average electrical force that is actually strongest at the center of the electrode once we get to a sufficient height above the electrode. The question then becomes, is the fact that the fabrication surface is physically offset above the electrode sufficient to explain the data that demonstrates the current is highest towards the electrode center instead of the edge. To explore this possibility, a simulation was conducted to examine the current cross-section above a circular electrode at a variety of heights. The conductivity of the solution of the electrode was kept constant and parallel cross-sections at various heights above the electrode were examined.

As shown in figure 4.1, the current in the cross-section nearest the electrode is greatest towards the electrode edge. As the height of the cross-section is raised, the current as all points above the electrode lowers, but the extreme spikes of current at the edge of the electrode lowers much faster than that in the center. At some point sufficiently high above the electrode the current is actually highest in the center of the electrode, with the edge peaks disappearing completely. In some sense this is to be expected. If we go high enough above the electrode, the whole system will tend to appear as a point source, and current spikes attributed to the edge will be smoothed over. The system we worked with has a strong constraint, namely the height of the gel at which all the particles land. When we examine the current

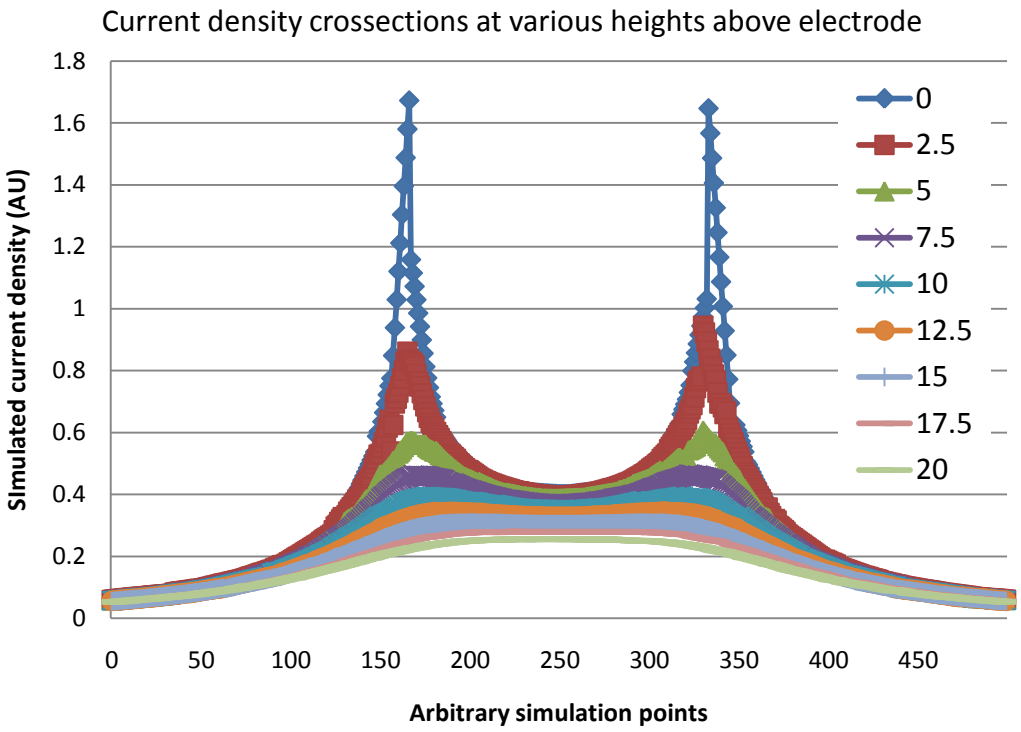

Figure 4.3: Simulated current density above electrode surface where the gel is assumed to have the same resistance as the solution. Gel/liquid boundary is at 10.

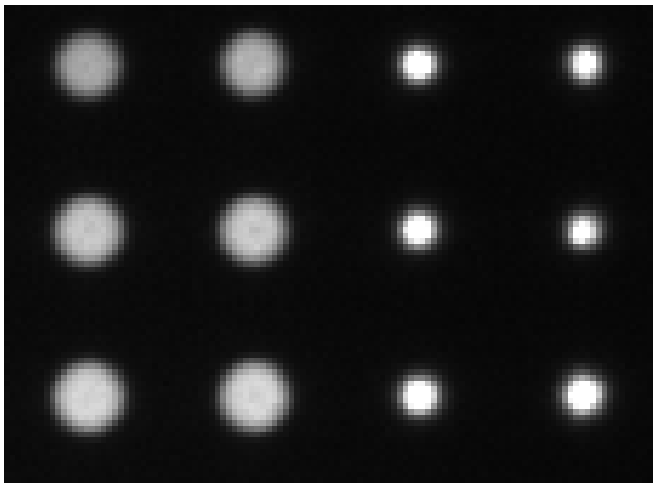

Figure 4.4: Blowup of biotin quantum dot deposition. Left 2 columns have both biotin and streptavidin deposited qdots, right 2 have only biotin

distribution at this particular height we see that the current at the edge is still slightly greater than that of the center. It should be noted however, that the gel thickness goes a long way towards explaining the uniformity of the particle distribution. If the gel were of negligible height above the electrode, the ratio of the current between the edge to the center would be around 4.2:1.0, whereas at the height of the gel used for this experiment, the ratio drops to 1.1:1.0 (figure 4.3). It is clear that the height of the gel can play a potentially large role in the current distribution at the gel surface. If we were limited to examining nanoparticles larger than the pore size of the gel, this discussion would be forced to end here. However, we have additional pieces of data which suggest that the current inside the gel itself is somehow maximized towards the center of the electrode. If the gel height effect were the sole contributor to the particle distribution then we would expect that as the gel grew thinner, or that as particles penetrated the gel itself, they would begin to concentrate on the supposed areas of greatest current, at the electrode edges.

An example of how this is not the case came from some of the earliest experiments on this subject. Initially we performed this technique on a variety of particles. One of those particle types were biotin and streptavidin quantum dots (figure 4.4). The quantum dots were much smaller than the 40 nm particles used for much of this research, on the order of 10 nm. When the streptavidinated quantum dots were pulled down to the activated gel surface, they formed a layer, much as the 40nm particles did. However, when the biotin quantum dots were pulled down to the

same surface, they formed a much smaller point. However if those same biotin quantum dots were pulled onto a layer of streptavidin quantum dots, they would form a smooth layer in the same manner (the two types of quantum dots could be viewed independently due to different spectral emission lines). This was initially confusing, but eventually made sense in the context of the gel itself. The streptavidin quantum dots have a larger size than the biotin coated quantum dots due to the addition of the outer layer of streptavidin. This size difference meant that the streptavidin quantum dots could not move into the gel, but the smaller biotin quantum dots could. When they moved into the gel, however, they concentrated at the electrode center, not the edge. This implies that the electrode current is actually highest at the center of the electrode near the electrode surface itself. This effect is observed for any small fluorescent particle or molecule that is small enough to move into the gel itself. Therefore it is clear that we cannot merely treat the gel as a simple structure that merely holds particles away from the electrode. It actually has a strong effect on the shape of the current moving through it.

We have further evidence that the gel itself is having a strong effect on the shape of the electric field. In AC dielectrophoresis experiments we have observed that electrodes without a gel coating will tend to accumulate particles towards the electrode edge. However, identical electrodes run under identical conditions except for the presence of a gel coating will accumulate the same particles in the electrode center. Dielectrophoresis is in some sense more of a pure electronics problem than

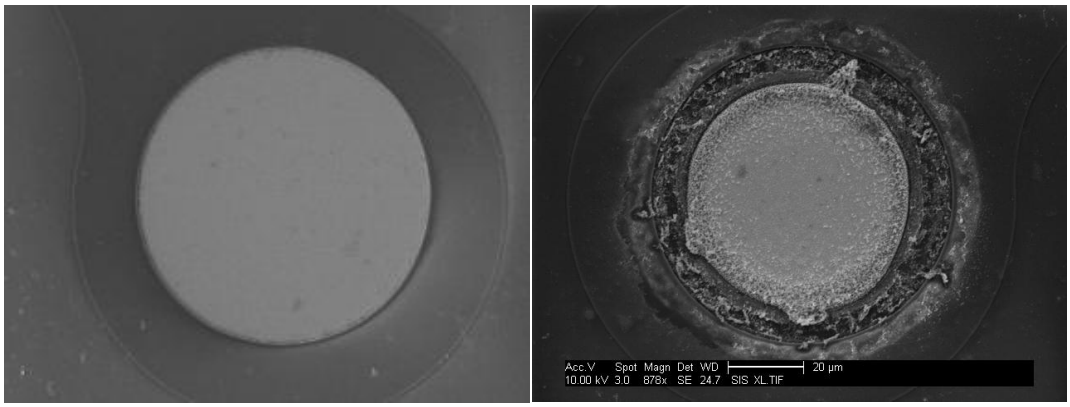

Figure 4.5: SEMs of DEP electrodes without an overcoating gel layer. Left is an unactivated control electrode and right is an electrodes used to pull down 200nm nanoparticles. Note the radial damage from the outside of the electrode inwards.

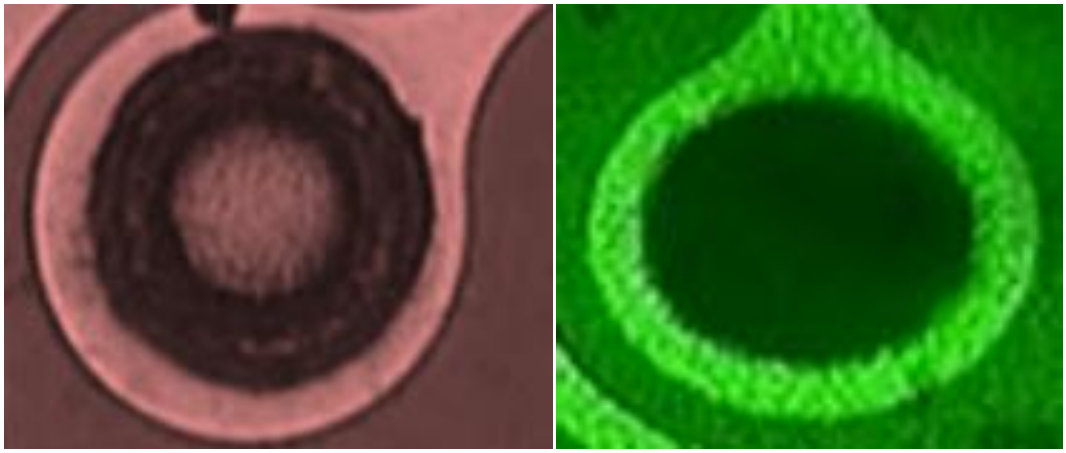

Figure 4.6: Optical images of activated electrodes used for DEP. Left has an electrode without an overcoating of gel, right has an electrode with gel.

electrophoresis, since the issues of electrolysis, buffering, carrier barriers, and current mobility are mostly unimportant. Even more compelling than the particle distribution are patterns of electrode degradation. We have observed that at higher voltages and conductivities the platinum electrodes tend to degrade (these voltages and conductivities are much higher than those used for the electrophoresis experiments reported here). Optically this degradation is observed as a darkening of the electrode surface under a microscope. SEM analysis correlates these dark electrode regions with regions of massive electrode destruction. Due to technical limitations, the SEMs could only be performed on the chips without gel, but the correlation between the dark regions and the electrode degradation was direct. The "darkness" was merely where the electrode had become so deformed that it was no longer a reflective surface. On the chips without gel, the dark region began at the electrode edge and moved radially inwards. With the chips with gel, the electrodes tend to darken uniformly across the entire surface. Since this effect is only observed at higher voltages, it is clear that it is driven by some electric field or current effect, since the edge of the electrode is where we would expect the bulk of the electric field to originate from for the chips without gel. This is clear evidence that the gel has the effect of smoothing out the current distribution across the electrode surface, increasing the current density in the middle at the expense of that on the edge. Therefore the effect is consistently observed across many situations and is clearly related to the presence of the gel coating the electrode itself.

4.5. Resistance differences between the gel and the bulk solution

The current density behaving differently with and without the gel present essentially implies one general fact; namely that resistance of the gel above the electrode is not the same as the bulk solution. The results of the simulations in section 4.3 suggest that the nanoparticle layering across the top of the gel might be partially attributable to current spreading effects alone. However the data presented in 4.4 shows that the current density at the electrode surface itself is modified strongly by the presence of gel. Given a physically real 3D current density pattern, there will always be some spatial distribution of conductivity that could create that pattern of current flow. Therefore, my effort here is not to calculate some arbitrary resistance pattern in the gel area, but rather to motivate which physical effects could contribute to the centering of the electrode current. In general I will discuss the increase in gel resistance due to ion and particle exclusion.

Let us examine the case where we have a gel of some conductivity less than the conductivity of the bulk solution above it. Why would we make this assumption? The conductivity of a solution is proportional to the sum of the product of the concentration of all the conductive particles multiplied by their electric mobility. That is the conductivity of a solution is higher when there are more charged particles in it, and when those particles can move faster under a given electric field. By locally reducing either of these parameters we can reduce the local conductivity. Reducing the conductivity due to charged particles is simple, you merely need to

have less of them in a given volume. While the gel is in direct physical contact with the bulk solution, and ions can diffuse equally in to both mediums, the gel itself physically excludes some portion of that volume. This exclusion means that there is effectively less free space left over for the ions to occupy, thus reducing their effective concentration over the volume of the gel. When dried, the gel shrinks to $1/10^{th}$ its original volume, so we would expect the exclusion of small ions to be at least that much. Furthermore, since a large fraction of the total system current is made up of 40 nm nanoparticles that are unable to penetrate the gel itself, we would expect the gel to have an even higher effective resistance since that fraction of the current is unable to carry its charge into the gel. Finally, the gel itself lowers the mobility of the ions passing through it since the ions collide with the physical structure of the gel, slowing them down and reducing their effective speed. All these effects taken together imply that the conductivity of the gel is less than that of the bulk solution. However, as shown in the diagram, as the conductivity of the gel is decreased, the current above the electrode both increases and becomes more uniform. Furthermore the width of the current distribution narrows (which accounts for the current increase at the center).

Physically, how do we account for this effect? If we examine the simulations of current flow where the gel is taken to have the same conductivity as the solution itself, then we can see that a large fraction of the current emanating from the electrode edge travels out radially from the electrode, rather than moving

straight up. The current is moving in a somewhat circular pattern in every direction away from the electrode. However, as we increase the effective resistance of the gel, current that was previously unconstrained will start to take the path of least resistance. Due to simple geometric factors, the path of least resistance increasingly becomes the path that minimizes the distance the current spends in the gel. This has the interesting effect that the gel can focus the electric current. Examine the current distribution at the lower gel conductivities compared to the case where the gel has the same conductivity of the bulk (figures 4.7-4.9). We can see at lower conductivities the current is confined within a rough cylinder, with the current only spreading out in all directions once it reaches the gel surface. The plots of the electric current at various heights above the electrode show this same effect. As the total gel resistance is increased, the fraction of current found towards the center of the electrode grows progressively higher, coming at the expense of current that would have moved sideways into solution but is prevent by the now higher resistance path. Furthermore, the current at the electrode surface increases in the center of the electrode as the gel resistance is raised. Since the gel must have a higher resistance than that of the bulk solution for the reasons discussed above, it is expected that this effect has some part in the overall current focusing, especially since it is not observed when the gel itself is not present.

If we further assume that the deposited layer of nanoparticles has a yet higher level of resistance (which is likely since it would consist of tightly packed

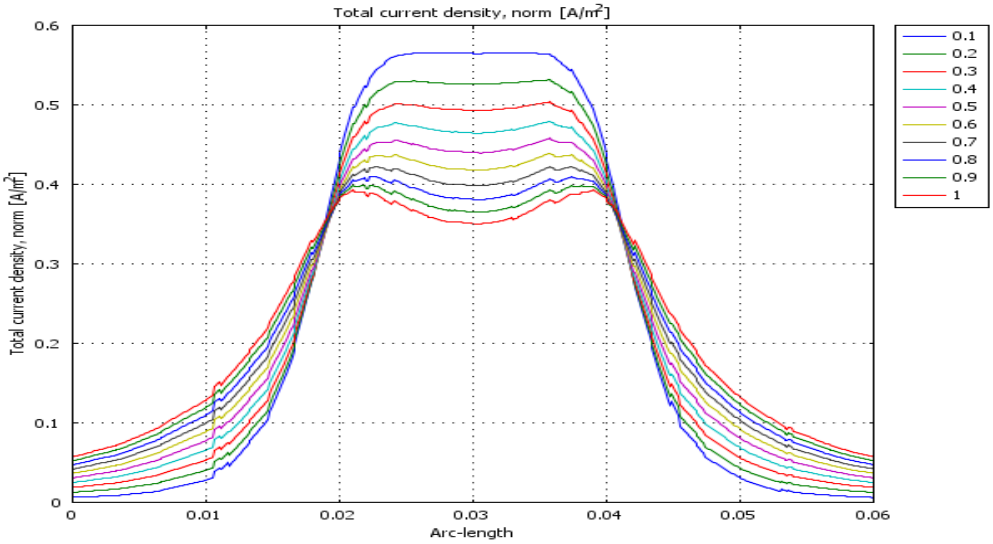

Figure 4.7: Simulated current density above at gel surface for various gel/solution conductivity ratios.

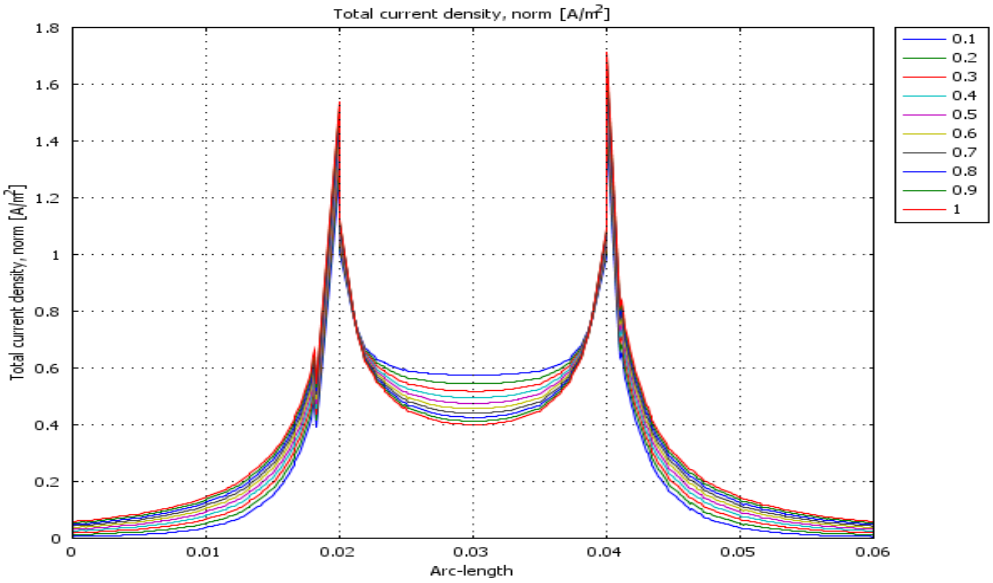

Figure 4.8: Simulated current density above at electrode surface for various gel/solution conductivity ratios.

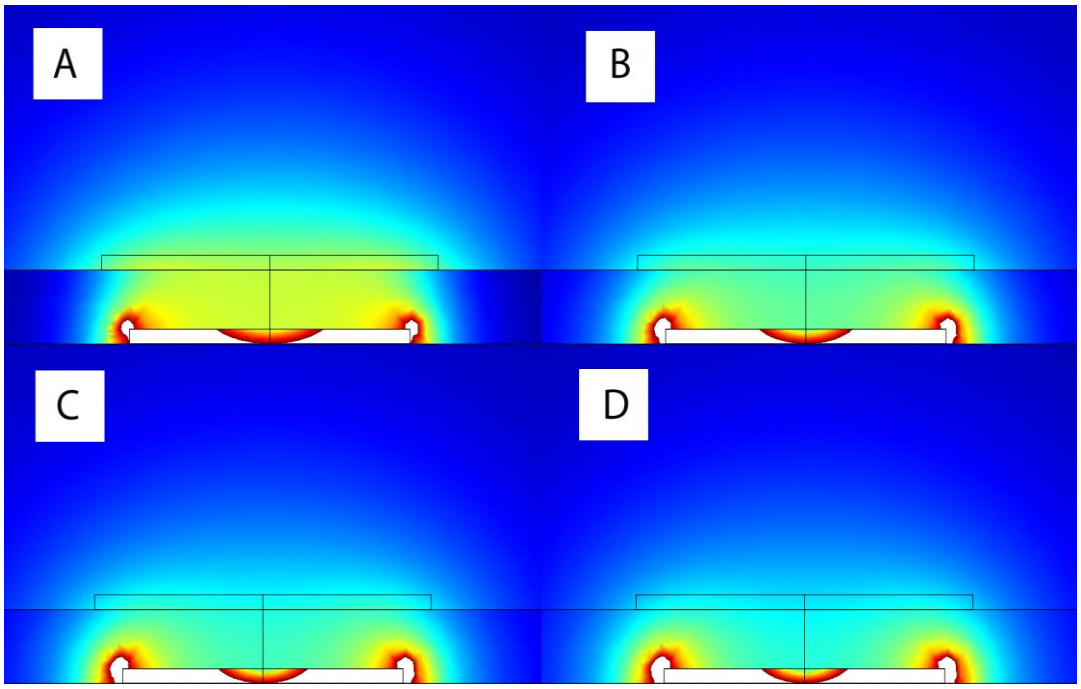

Figure 4.9: Simulated current density above gel in cross-section with the gel/solution conductivity being 0.1 (A), 0.5(B), 0.7 (C), and 0.9 (D).

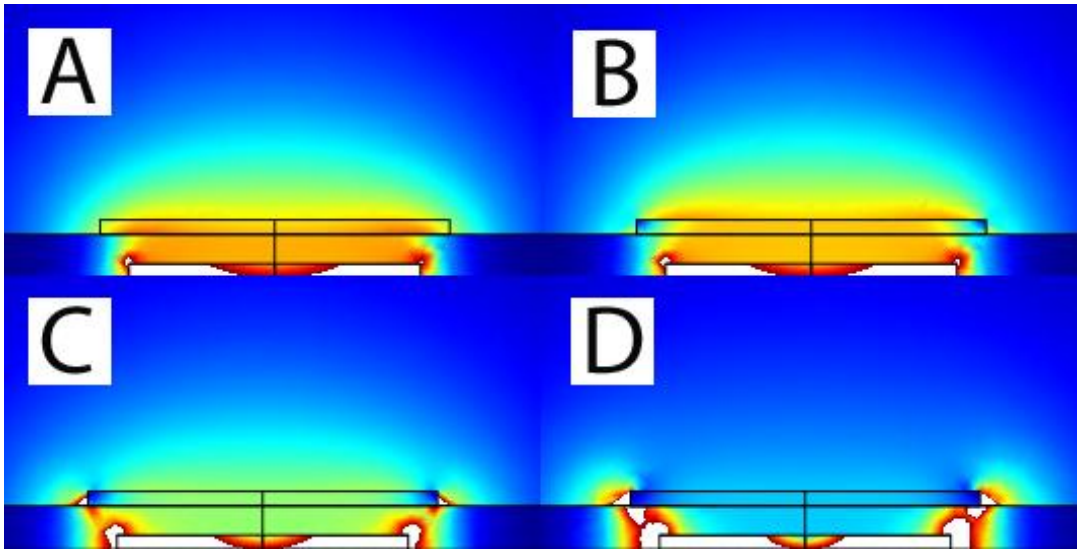

Figure 4.10: Simulated current density with gel resistance of 0.1 and a deposited layer resistance of 1(A), 0.1 (B), 0.01(C), and 0.005(D).

spheres with relatively little space), simulations point to there being an additional focusing of the electric current (figure 4.10). This occurs for the same reason that the initial current focusing occurred, it is simply easier to move straight up through the more resistive layer than out to the side. Moving at any angle other than straight up would mean moving through a proportionately greater amount of the higher resistance region. Only when the layer becomes very thick or very resistive will the current start to move out under it rather than straight through. Self focusing of the electric current is a feature of the gel that is absolutely essential to the electric field deposition process. Without it, layer formation would be decidedly nonuniform.

4.6. Conclusions

In this section I have discussed the causes behind the observed layer distribution. Experimentally we observed the deposited layers form with a brightness maximum originating on the gel above the electrode center, which grows larger as the current and time of deposition is increased. Simple models would expect the current to emanate from the edge of the electrode, and thus for the maximum deposition to be in those regions. The discrepancy between the edge current and the center deposition are explained as a combination of the offset of the gel surface from the electrode and an increase in the resistance of the gel due to ion and nanoparticle exclusion.

Chapter 5: Long range Dielectrophoresis

5.1. Introduction

The work described thus far is based on electrophoretic manipulation of particles. That is, charged particles move towards an electrode as part of the total current coming in or out of those electrodes. However, as discussed in the introduction, there are a number of electrically driven forces. These forces all vary from one another in terms of range, spatial profile, magnitude, and mode of effect. Besides the electrophoretic force, we are chiefly interested in the dielectrophoretic force. Where the electrophoretic force separates particles based on their net charge (positive or negative), dielectrophoresis separates particles based on their dielectric properties compared to that of the medium in which they reside. Particles with a dielectric constant greater than that of the solution will move towards a concentration of electric field, while particles with a dielectric constant less than that of the solution will move away from such concentrations. Because the dielectric constant is roughly unrelated to the charge of the particle it allows for another parameter of separation. Furthermore, the dielectric constant is typically a function of frequency, which varies differently for different particles (since it is based on geometrical and material factors), this allows for a wide range of possible separation parameters, merely by changing the frequency of the driving voltage.

It should be understood that in general there are two general ways of separating particles. One way is to observe some parameter (size, color, shape, material, density, surface chemistry, etc.) and to classify that particle based on that parameter into two or more groups. The particle can then be switched into a specific channel or location by some secondary method, such as pressure flow. While this method allows for the analysis of almost any measureable parameter, it often requires some secondary tag to allow that measurement (ie, a fluorescent antibody to measure a surface property of a cell). Such a labeling step can be counterproductive if the goal is to observe the particle in its native conditions or in a short period of time after it was generated. Furthermore, switching, while able to be performed relatively fast, can really only be done on a single particle at a time, or it is possible that a particle will be inadvertently switched into the wrong channel along with one that was meant to go there. This places an effective size, concentration, and throughput limit on such a sorting method.

A second way of sorting is to use the physical properties of the particle itself as the actual method of sorting, rather than as a way to categorize particles. This works in the situation where the particles that we would desire to sort have interestingly differentiable properties, and that those properties can be exploited in a physically viable way. Different methods of sorting may be physically relevant at different size scales. The number of various physical properties that can be exploited in this way are many. Particles are separable by size, mass, density, net charge, index

of refraction, dielectric constant, shape, and more. There are a variety of separation schemes that allow the sorting based on these parameters. What is important to note is that the separation of these particles is done in parallel, since a switching "decision" is being made by blind physics rather than an external algorithm based on some set of measurements and a controlled switching system. The measurement is the separation. Typically this form of separation is free of the need to perform a secondary labeling, since the parameter of interest is what is being separated for.

Of course, the utility of one method or class of sorting will vary situationally. In many cases the secondary labeling of a particle is not a primary issue, nor is the speed of sorting. Often the data analysis that the first class of sorting requires to do its sorting can provide invaluable data on populations of particles, data that is implicitly gathered and discarded in the second class of measurements. All methods have their own utility. That utility will depend on the class of particle one desires to examine.

Due to our group's past work in the field of electric field based manipulation of particles, we had become interested in using DEP to perform analysis on direct biological samples (such as blood, urine, etc) straight from their source. This is in contrast to using diluted or otherwise modified samples taken a relatively long period of time (hours or days) before analysis. It is our contention that performing assays rapidly, in physiological or near physiological conditions, will allow a more accurate detection of low concentration targets and reduce detection noise that

could arise from sample changes over time. We believe that traditional sample preparation and storage may damage or modify the sample in a manner sufficient to render analysis meaningless. The specific target of the work motivating this section is to detect large DNA fragments located in blood as a disease marker using DEP. We believe that sample preparation itself can muddy the waters enough to cover the presence of a sample of possible target DNA in whole blood, so that the blood itself should be analyzed directly if possible.

As mentioned previously, the dielectrophoretic force works by the difference on the dielectric constant of the material and the surrounding solution. More specifically, the complex dielectric constant, which at low frequencies is given as

$$\epsilon_x{}^* = \epsilon_x - \frac{I\sigma_x}{\omega}$$

With the dielectrophoretic force for solid spherical particles being given as

$$F_{dep} = 2\pi\epsilon_0\epsilon_m r^3 Re[K(\omega)]\nabla E^2$$

This force as a function of frequency is more complicated for more complex particle geometries (such as non spherical particles or layered structures), but for the most part, this serves to change the magnitude and sign of the force, not to change its spatial profile. For blood, the ionic concentration is very high, and thus the conductivity terms of the dielectric constant dominate. Traditionally, DEP is not performed at higher conductivities. We believe there are a few reasons for this. First, all particles would be expected to have a negative dielectrophoretic force since the

solution conductivity is greater than the dielectric constants of the material and solution, and greater than the conductivity of the particle. Thus particles would not be expected to be separable (since they would all go in the same direction). However work from our group has demonstrated that this is in fact not the case, speculatively because at higher conductivities the nanoparticles in question develop a charged conductive shell of tightly associated ions. That discussion however is beyond the scope of this work; the experimental evidence merely is a motivation for pursuing high conductivity DEP separation.

What we believe to be the practical reasons for the lack of high conductivity DEP is manyfold. First the DEP force grows weaker as higher conductivities are used, making separation significantly slower. Separations at low conductivities go from taking a few seconds to tens of minutes at higher conductivities (with the same voltage and electrode geometry). This slowing down can be counteracted by raising the voltage, since the DEP force is proportional to the square of the applied voltage for a given geometry. However, as voltages are raised many detrimental secondary effects occur. First, the electrodes begin to bubble due to brief but cumulative electrolysis effects. Voltages and frequencies that allow separation at low conductivities explode with gas as the ionic concentrations goes up. Along with this comes physical degradation of the electrode, it literally shreds on the nanoscale (see figure 4.5). We believe that these effects have limited the use of DEP on higher conductivity samples since they were basically unapproachable

situations. We were able to perform our confirmatory experiments with specially fabricated platinum electrodes coated in a gel layer. These electrodes were able to mitigate the degradation and bubbling somewhat (partially for reasons described in chapter 4) but in the long run, they too suffer bubbling and extreme degradation, just at a reduced rate.

We believe however, that these deleterious effects can be countered by a radical change of system geometries. In electrophoresis, high current systems are often used, systems that have extreme electrochemical and pH effects. These effects are mitigated by removing the electrodes from the sample area, and placing them in a region that contains the bubbling and electrochemical byproducts. In addition, the electrodes used are much more robust (a solid platinum wire is used instead of a sputtered electrode). We believe that a radical change of geometries will allow us to perform a similar move with dielectrophoresis. Once this is done, we can increase the voltage by one or two orders of magnitude, drastically increasing the applied force to particles, even in high conductance situations. Even if bubbling occurs near the electrodes, the separation between the electrode and sample would remove these effects from play.

5.2. Simulations and experiments

As noted in equation 5-2, the DEP force is proportional to the gradient of the square of the electric field (basically the electric energy density). Typically high

field regions are found near the electrodes, and the low field regions are found in the space between them. Particles will move towards or away from the electrodes based on their relative dielectric constants. Unlike electrophoresis, there is a relatively short range past which a particle will not experience a force. There is however, a powerful tool here to be used; the shape of electric field itself can be modified by changing the distribution of dielectric constants and conductivities in the system. For example, an unactivated metal electrode between two active electrodes will act as if it has voltage applied to it and attract or repel particles as a normal electrode would, even though it would be in the space traditionally thought of as a “low field” region. This is because it significantly distorts the electric fields in the nearby solution since it is lower conductance than the solution itself. Similarly, by placing a pillar in solution of low conductivity, the electric field will distribute itself to move around instead of through that volume of space. The shape of these electric fields can be easily determined through the use of computerized simulation packages, since AC fields in solution are not subject to the extreme effects visited upon DC current conduction (such as electrolysis byproducts and energy potentials for current flow).

By placing materials in between the electrodes, we can engineer high and low field regions anywhere we want, far from the actual electrodes themselves. The electrodes will still act as a high field region, but we can engineer additional high field regions that are not subject to the same degradation and electrochemical induced bubblings that the electrodes face, since they are not actual sources of voltage and

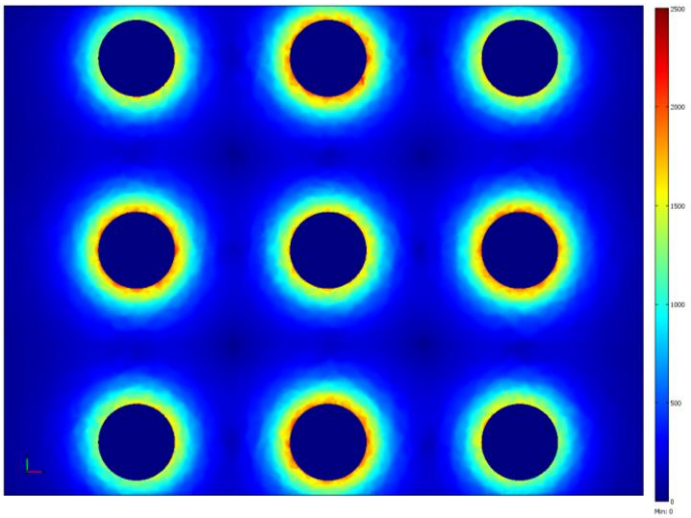

Figure 5.1: DEP Force simulation of a 3x3 array of electrodes. The dark circles are the location of the electrodes.

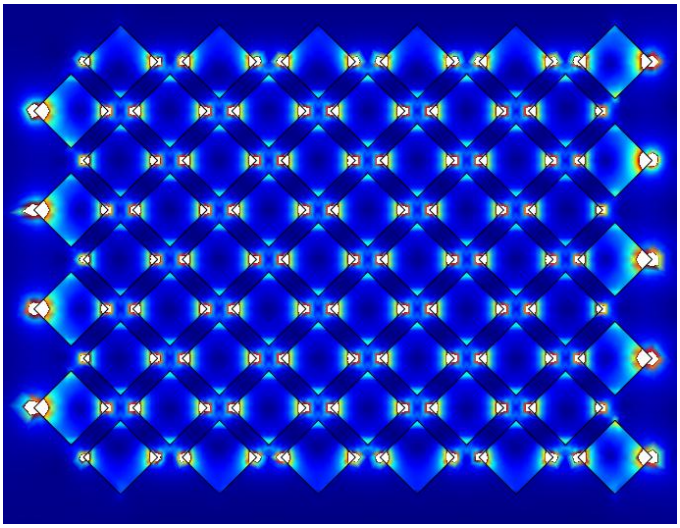

Figure 5.2: DEP force simulation of nonconductive pillars in a conductive solution. The source electrodes are above and below the simulation area.

current. By placing the electrodes at a removed distance from the actual region of interest, and behind a gel or membrane of some sort, we can entirely remove the effect the electrode has on the system; at the same time as allowing it to source the voltages we need to drive dielectrophoresis. Furthermore, we can fabricate it with a more robust method than those used to deposit the electrodes we normally use (we attribute the electrode decay more to physical damage to sputtered layers than to electrochemical action since platinum is nonpolarizable). By fabricating regions of high and low resistance, we can reduce the importance of the distance between the electrodes and the areas of interest, and drop a large fraction of the total voltage where we desire.

Our goal was to simulate, build, and test a DEP geometry that would allow us to focus the electric field by engineering the placement of high and low conductance regions. Using electrode arrays, we had previously determined that 10 μm particles experience a DEP force sufficient to be pushed away from an electrode at most around 400 μm from an electrode at 200 volts in a low conductivity solution. Using this dimension as a rough order of magnitude for construction, we designed a flow channel to focus the electric field from four separate electrodes spaced far apart. The device was fabricated using standard PDMS molding processes. A central flow channel (400 μm across, 40 μm high) was connected by small openings (200 μm wide) to four large chambers. Each chamber was electrically isolated from each other except by way of the central channel (see figure 5.4). The chambers were expanded

from the small mold by punching out the PDMS substrate to increase their volume and accessibility. Each chamber had an electrode running down in from the electrode opening, and the electrodes were powered such that two diagonally were connected to ground and the other two diagonally were set to 200 V at 10 kHz. The electrodes were formed from a 76 µm diameter piece of platinum wire laid into the chamber. This electrode configuration roughly mimics the checkerboard pattern we use for the electrode arrays we normally do our tests on. Due to geometric constraints of the designs we used, the electrodes could not physically get closer than ~5 mm (5000 µm), a far greater distance than we would expect DEP to act over. The limits on this distance were where the four punched holes could be placed in relation to the center channel. It should be noted that our goal was less “long range DEP” and more “DEP without the direct presence of electrode”. Had it been possible to move the electrodes closer in our initial designs we would have done so in order to maximize the useful voltage. As of this writing our group is working on optimizing the experimental system to allow this to occur. The central channel and four chambers were filled with 0.01x TBE, and particles suspended in that buffer were injected into the channel. Two sets of particles were used, 10 µm beads, which had been shown to move to low field regions on the electrode arrays, and fluorescent 200 nm particles which had been shown to move to high field regions. The results are shown in the following images.

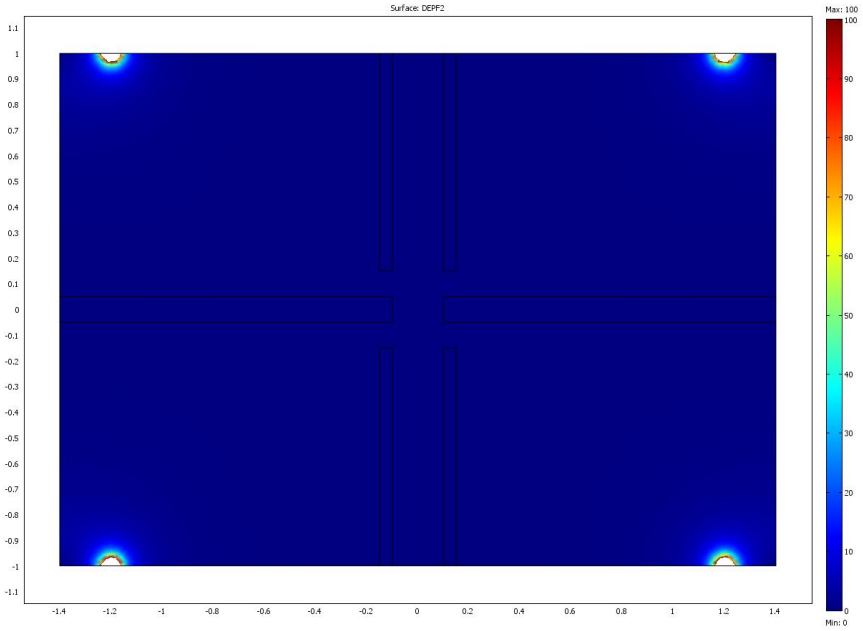

Figure 5.3: DEP force simulation for four small electrodes in a conductive medium

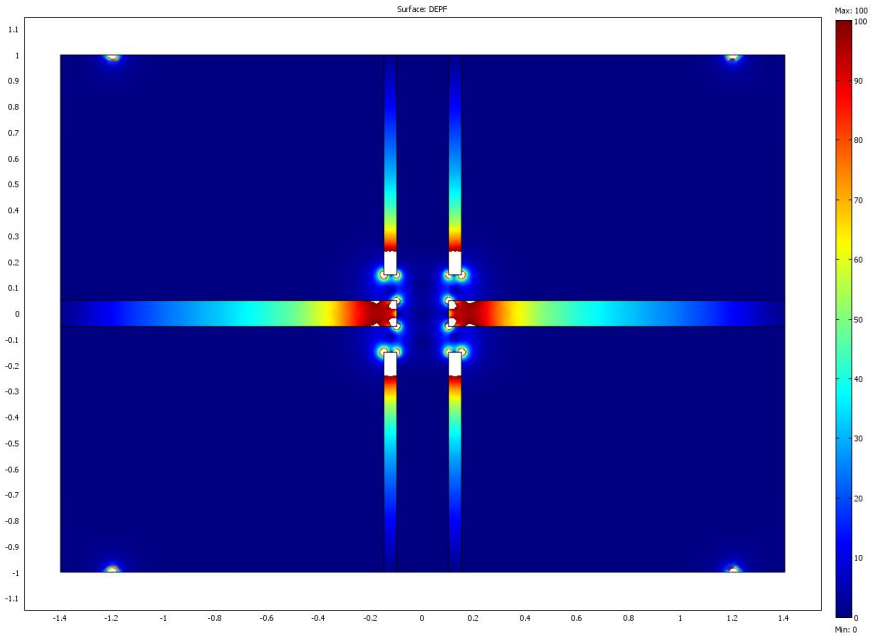

Figure: 5.4 DEP force simulation with nonconductive walls inserted into simulation in figure 5.3.

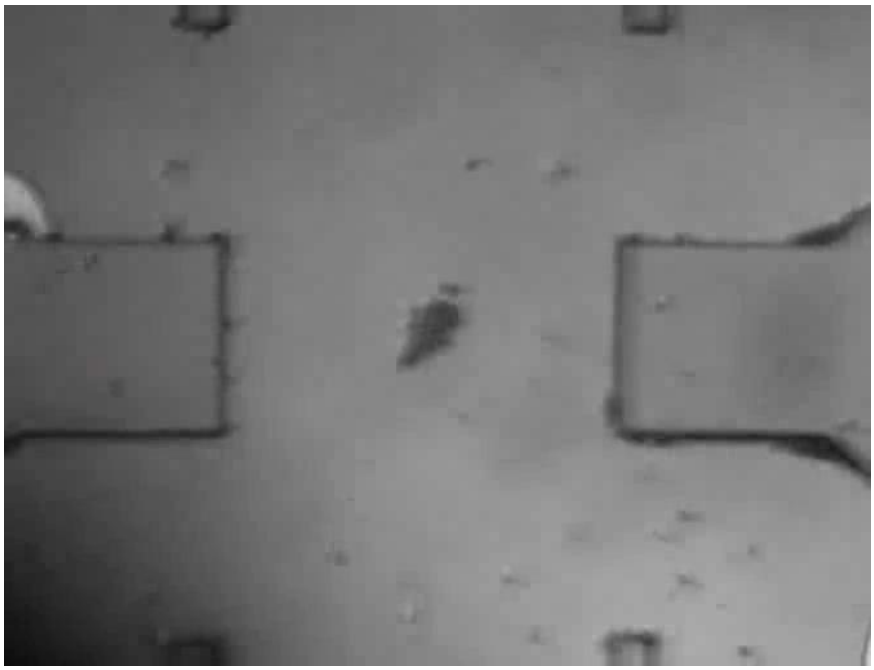

Figure 5.5: Optical image of 10 µm particles trapped in a structure similar to the one simulated in figure 5.4.

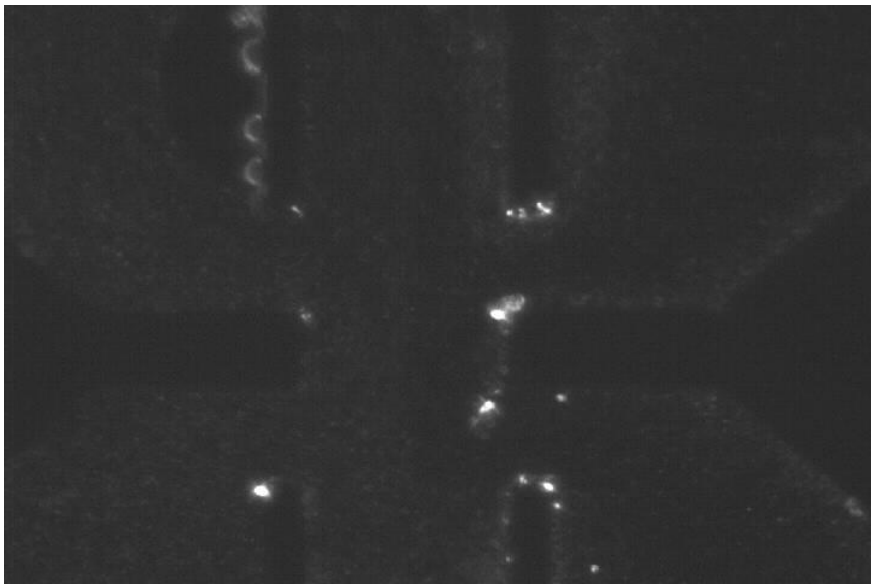

Figure 5.6: Fluorescent optical images of 200nm particles trapped in a structure similar to the one simulated in figure 5.4.

As can be seen in figure 5.5 and 5.6, the 10 μm particles gather in the region between the four openings, and the 200 nm particles gather at the channel corners. Both trappings occurred only when the voltage (200 V peak to peak ac) was applied, and instantly stopped when the voltage was turned off. The quality of the trapping potential depended on the relative position of the wire electrodes within their respective wells. Moving the electrodes around would change the strength of the trapping force. The trapping force was relatively weak for the 10 μm particles, and required all fluid flow between the chambers to reach equilibrium. The trapping force for the 200 nm particles was relatively strong and was resistant to fluid flow, though it appeared to have a short range of effect (which is similar to how particles accumulate on the electrodes).

Are these regions where we would expect the respective particles to accumulate? To answer this question I turned to simulation. Using COMSOL I simulated the relative DEP force of geometry similar to the system we used to determine the relative locations of high and low field regions. The walls were assumed to have no conductivity, and conductivity was assumed to dominate over material polarization (see figure 5.3). The simulation was also run in parallel with an identical geometry that assumes that the walls have the same material properties as the liquid (see figure 5.4). This was done in order to demonstrate the force differences between just the electrodes by themselves, and a situation with the wall in place to focus the electric fields. The simulation was performed in two dimensions

since the height dimension in the channels we used was much smaller than the other dimensions and did not vary across the system.

The results of the simulation are striking. The high field regions correspond exactly to where the small 200 nm particles were trapped, and the low field region is located in the middle region between all the chamber openings, exactly where the 10 µm particles became trapped. We had expected the 10 µm particles to accumulate in the channel center where they did because conceptually the focusing of the electric field through the channel/chamber hole was expected to be the source of a high field region. The four openings pushing away would create a low force region in the channel center. Conceptually however, I had expected the highest field regions to be in the narrowest part of the opening area between the channel and the electrode. However experimentally the small particles trapped around the corners of the PDMS, and the simulation bears out that the highest field lies in those locations. The openings do have relatively high field compared to the channel center, but not compared to the places where the electric field sharply bends. Since the particles are trapped exactly where we would expect them to be from simulations of high electric field gradients, this trapping is clearly the effect of DEP forces.

It should be noted that the forces in play here are relatively weak compared to using electrodes with a 400 µm spacing. Applying 200 volts at that distance will cause particles to instantly repel from the electrodes. That was not the case here, where the force was relatively anemic. It should be noted however, that a

large fraction of the voltage is dropped in the uninteresting regions between the electrodes and the edge of the buffer chamber. In the simulation geometry I used, around only 1/5 of the voltage was dropped in relevant regions. This could be mitigated by bringing the electrodes close to the channel and to decrease the resistance of the intervening space by varying the chamber height. By voltage loss alone, we would expect the force to be a factor of 25 less than if electrodes were used in the position of the channel openings. This is the subject of ongoing study.

It should also be noted that the specific geometry we chose for this experiment is somewhat arbitrary, and was chosen for its (very) loose similarity to our existing electrode architecture. We wanted the location of the estimated high field regions to be within a certain radial distance from the center to create a stable trap for larger particle there. However any geometry that incorporates a corner for which current can flow around will generate a high field region, and if these high field regions are placed in the correct manner, we can easily create a stable low field trap. Often however, we may not be even interested in simultaneous low and high field trapping of particles. It may be sufficient to trap a single type of particle in the high field region while all the other particles are allowed to flow past. In such a case we simply need to maximize the amount of corners available to maximize the number of high field regions. For example as in figure 5.2, by having a structure with a large corner to area ratio, we are able to ensure that the volume of liquid which contains the high field trappable particles is accessed completely, as opposed to with the

design in figure 5.4, which was only able to trap particles present near the channel edge. Such a design could act as a dielectrophoretic sieve, where one type of particle passes through, and another class of particle is trapped within the detection volume. To release the trapped particles, all that would need to be done is turn off the voltage.

5.3. Hot issues

The end result of this work would be to enable the use of long distance DEP separation systems in high conductance biological samples, such as blood or urine. The tests we performed showed that the concept is valid, but were performed at low conductances and high voltages (200 V peak to peak AC). To improve the trapping of the system we would have to move to even higher voltages and more refined geometries. However, in preliminary experiments conducted in 1x PBS solution, the system spontaneously boiled. While unfortunate, this was not unexpected (81,82). It should be noted that the boiling we observed is not the same as gaseous electrolysis products forming at the electrode, this boiling occurred in the high electric field regions where the 200nm particles were found to trap. Because we were generating high field regions at corners of the device, we were creating local spikes of joule heating, causing the water to boil.

What are the implications of this? Our initial goal was to run the system at even higher voltages than we are using now (we were equipment limited for this set

of experiments to 200 volts ptp signals). However, since the water boiled at 200 V, running a harder signal would only worsen the problem given the same system. The first question is to examine how heating and trapping scale with system changes. The local heating will be proportional to

$$Q \sim E(x,y,z)^2 \sigma$$

And the local DEP force will be proportional to

$$F \sim \nabla(E(x,y,z)^2)$$

The DEP force is also somewhat inversely proportional to the solution conductivity, but it is so in a nonobvious manner, likely because the Claussius-Mossatti factor becomes closer to zero at higher conductivities. To maximize the force, and minimize the heating, we can generally really only do three different things. First we can dilute the sample to lower conductivities, and second we can play around with the geometry to maximize the ratio of heating to trapping. Third, depending on the system geometry, we can also actively cool the sample to increase the amount of energy it can absorb before boiling. While the heating per unit volume will not be reduced significantly by making the system thinner (as long as the voltage drop across the device is kept constant), it would reduce the amount of energy dissipated per unit device area which may allow external cooling to function more effectively.

Reducing the solution conductivity may or may not be feasible, depending on the sample. Clearly, since the heating scales linearly with the conductivity of the

solution, any amount of reduction would allow us to further increase the system voltage. However, we would prefer to avoid any form of sample preparation if at all possible. It should be noted that for a given geometry, both the DEP force and the heating at any point will scale with the square of the applied voltage. However, while the DEP force is strongly geometry dependant, the heating is much less so. For example, it is entirely possible to have a situation with large amounts of heating but little to no DEP trapping (such as between two large parallel electrodes). New designs will focus on repeating trapping structures, so in such a situation each unit cell will be able to be examined on a heat/trapping basis. This work is ongoing.

5.4. Conclusions

What this work has demonstrated is that it is possible to exploit dielectrophoretic effects without the explicit need for an electrode present at the high field regions. By exploiting geometric effects and the physics of electric field propagation it is possible to build systems where the electrodes are far removed from the actual area of DEP separation. While this is a novel (but physically straightforward) effect, its power comes from the ability to run DEP in high conductance solutions. Just as gel electrophoresis removes the electrode to a buffered tank, this form of dielectrophoresis would allow the detrimental effects of high voltage, high conductivity situations to be mitigated. This will allow for the

previously unattainable ability to perform DEP separation on native biological samples without the need for any amount of sample preparation.

Chapter 6: Conclusions and Future Work

6.1. Conclusions

We have developed a method for both rapid and controllable deposition of nanoparticles into multilayer structures. The process of deposition was studied for various types and sizes of nanoparticles and was compared to simulations to examine the reasons behind particle uniformity. In addition, the beginnings of long range, high conductivity DEP were examined. More specifically we have shown that:

- Electric field directed self assembly of full nanoparticle monolayers from low concentration solutions can be rapidly and controllably conducted (with deposition times of around 10 seconds per layer). Multiple depositions have been performed up to 100 times. Under the correct deposition parameters, the process self terminates at a single layer of particles, due to the nature of the affinity binding reaction used to bind the particles together. This is different than previous methodologies where the process was either driven uncontrollably through bulk electric field deposition to an electrode (no affinity binding), or was done passively through high concentrations of affinity particles (no electric field deposition).
- The electric field assisted self assembly process was shown to work for a wide range of nanoparticles and binding mechanisms. This included quantum dots, alternating mixtures of 40nm/200nm polystyrene biotin and streptavidin particles,

and DNA derivatized particles were all shown to be deposited using the methodology described here. Additionally we have shown that the particle layers can be removed from the deposition surface relatively intact, and have enough internal binding that the structures do not disintegrate during or after the removal process. This demonstrates that this methodology has a potentially viable liftoff process for manufacturing purposes.

- Using simulations of electric current distributions, we have explained the reasons for the deposition pattern of the particles over the gel surface covering the microelectrodes. In the case of a very thin gel, the nanoparticles would tend to deposit around the electrode edge as that is the main source of the current. However, due to a combination of gel resistance and thickness, the particles tended to deposit relatively uniformly across the entire area above the electrode. This shows that the gel itself is necessary for the uniform deposition of particles. Without the gel, the particles would be in direct contact with the electrochemical reactions that drive the particle deposition, as well as seeing a highly nonuniform current. The utility of the gel layer needs to be considered for any future systems using the electric field assisted assmebly technique.

- We have demonstrated that long distance dielectrophoretic effects are possible by shaping AC electric fields using resistive structures (rather than by controlling their shape through electrode placement). Experimental trapping results are compared with simulations, and are shown to perform both positive and negative

dielectrophoresis on appropriate particles. Once fully developed, this methodology can possibly allow for the direct sampling of unmodified blood and other biological samples.

6.2. Future work

We believe that there are a number of possible directions for the directed electronic self assembly technique. Physically, the process could be taken to various size scales, going anywhere from the nanoscale to the macroscale. All that is required for this technique to work is a controlled current electrode and a bindable substrate. At the small end of the scale, we believe devices could be made to individually sense and analyze single particles before depositing it in a precise location. On the larger end of the scale, a device utilizing a fully packed electrode array could be built to rapidly fabricate a patterned full surface deposition of appropriate nanoparticles (this is in contrast to our current system that allows deposition only at electrodes separated by a relatively large distance). Furthermore we intend to combine dielectrophoresis and electrophoresis into single systems to make use of the advantages of both force regimes.

With the advent of arrays of electrodes that are directly adjacent to each other, the process would be able to build far more interesting structures than those demonstrated so far. Chiefly, we would be able to demonstrate the enclosure of various objects within a surrounding layer of other particles. This would allow for the full 3D encapsulation of materials within a surrounding coat, which is currently

something the system we used does not allow for because the electrodes are spaced so far apart that fabricated layers are necessarily independent of each other. Because of this, we cannot currently fabricate structured with walls; we are limited only to stacks that vary in the z dimension.

There are two main directions we would like to demonstrate with a full electrode array system. The first would be to lie down fields (lines, planes, vertical columns, or arbitrary shapes) of one particle type within (between and on top of) another type of particle. The particles for example could be conductors and insulators forming simple circuitry, enzyme based biosensors within a protective but porous system to sense various biomolecules, sacrificial particles to be dissolved later to create internal channels in a 3D dimensional structure (for the transport of fluid or gases) or possible drug delivery systems. All these applications are fairly straightforward applications of the technology and processes demonstrated in this dissertation, but would be the desired end goal.

The second direction we would like to examine is the integration of prefabricated electronic liftoff devices into a soft shell fabricated though this method. Nanogen at one point demonstrated the feasibility of using electric fields to place liftoff devices into specific locations. Here those locations would have layers of particles that would consist of one side of a total device. After the deposition of the liftoff device, the walls and ceiling would be fabricated over it to create the rest of the system. Lines of conductive particles could be laid down to electrically connect

many such liftoff systems. This would allow for the insertion of complex sensors into highly integrated systems that would be otherwise unfabricatable. The main requirement on the liftoff devices is that they be designed for use in this process such as being rotationally symmetric so that it doesn't matter which direction they face once they are deposited (various electrical connections could be made through the top or bottom at different radiuses).

To take the process a step further we would want to further the study of various liftoff methods. The method demonstrated in this work is the relatively uncontrolled result of osmotic expansion once pure, unbuffered water is introduced onto the chip. However, there are many possible ways to remove a fabricated device cleanly from the deposition substrate. Chiefly would be the use of a cleavable linker molecule binding the bottom layer of material to the deposition surface. By introducing the cleavage mechanism the entire fabricated system could be gently removed.

In addition, there are directions for various process integrations that we would like to pursue. Chiefly, we would like to integrate lithographic processes into the electronic layer by layer methodology. Many binding substrates (such as streptavidin and DNA) can be inactivated by a sufficient exposure to uv radiation. This allows for the introduction of photopatterning into the layer by layer assembly process. With the case of DNA, the photopatterning only degrades the thymine base, so with proper tailoring of the sequences used, some areas could be made inactive to

a given sequence, but still remain active to other sequences. The utility of this method is that it allows for the fabrication of structures smaller than the electrode size. The electronic assisted self assembly process is resolution limited to the depositing electrodes. If we want to make structures smaller than a given set of electrodes, we either need to fabricate smaller electrodes, or introduce a secondary patterning step.

Making electrodes smaller is usually possible, but after a while it would reach a level a level of diminishing returns of cost vs. performance. Making smaller electrodes might require more expensive processes. In addition, because the gel layer thickness is critical to the resolution properties of the process, a gel designed for one size of electrode might not function as well for a different size, meaning that a system with mixed electrode sizes would produce suboptimal results. Ideally, if most features on a desired system are of a given size, it is best to use electrodes appropriate for that size so as to avoid requiring costlier deposition systems. However, if a small fraction of the fabricated features are smaller in size than the rest, lithography would be able to provide the extra level of patterning. In such a case after pattering particles would still be pulled down to an electrode, but would only remain bound in the non patterned areas. Additional particles could be pulled down and bound to the patterned areas selectively through the appropriate use of DNA sequences, for example. In keeping with our desire to build “maskless” systems, a photopatterning step would ideally use something like a reconfigurable micromirror

array to change patterning arbitrarily. Such a system would allow for the occasional smaller scale patterning while maintaining the overall use of larger electrodes.

For the dielectrophoresis we plan to continue our development of the long range system, with an eye to use 3 dimensional structures to maximize the trapping forces, as well as adding active cooling to counteract the electrical heating observed during high voltage, high conductivity operation.

The DEP force at any one point is proportional to the square of the gradient in the electric field. The systems we have been molding out of PDMS have essentially been only 2 dimensional. By design, they consist of fluidic channels with some pillars that reach from the floor to the ceiling. Within the channel (where all the particles to be trapped are located), the electric field is for the most part uniform in the z dimension due to this geometry. However, by fabricating structures that also vary in the 3rd dimension will allow for stronger trapping forces, since the gradient will be stronger. This should allow for a greater trapping force to applied voltage ratio than the current devices which would help with heat dissipation issues.

Because heat appears to be the limiting factor at higher voltages, we plan to incorporate various heat mitigation methods. Besides increasing the trapping efficiency, we also plan to reduce the channel thickness (reduces the total amount of dissipated heat), cool the incoming sample, actively cool the system, and determine to what level we can dilute various samples to reduce their conductivity.

Bibliography

1. Gates, B.D., Xu, Q.B., Stewart, M., Ryan, D., Willson, C.G. and Whitesides, G.M. (2005) New approaches to nanofabrication: Molding, printing, and other techniques. *Chemical Reviews*, **105**, 1171-1196.

2. Zhang, H., Li, Z. and Mirkin, C.A. (2002) Dip-pen nanolithography-based methodology for preparing arrays of nanostructures functionalized with oligonucleotides. *Advanced Materials*, **14**, 1472-+.

3. Betancourt, T. and Brannon-Peppas, L. (2006) Micro- and nanofabrication methods in nanotechnological medical and pharmaceutical devices. *International Journal of Nanomedicine*, **1**, 483-495.

4. Sarikaya, M., Tamerler, C., Jen, A.K.Y., Schulten, K. and Baneyx, F. (2003) Molecular biomimetics: nanotechnology through biology. *Nature Materials*, **2**, 577-585.

5. Lu, W. and Sastry, A.M. (2007) Self-assembly for semiconductor industry. *Ieee Transactions on Semiconductor Manufacturing*, **20**, 421-431.

6. Lu, W. and Lieber, C.M. (2007) Nanoelectronics from the bottom up. *Nature Materials*, **6**, 841-850.

7. Roy, S. (2007) Fabrication of micro- and nano-structured materials using mask-less processes. *Journal of Physics D-Applied Physics*, **40**, R413-R426.

8. Cheng, J.Y., Ross, C.A., Smith, H.I. and Thomas, E.L. (2006) Templated self-assembly of block copolymers: Top-down helps bottom-up. *Advanced Materials*, **18**, 2505-2521.

9. Negrete, O.D. and Cerrina, F. (2008) Step-and-scan maskless lithography for ultra large scale DNA chips. *Microelectronic Engineering*, **85**, 834-837.

10. Bratton, D., Yang, D., Dai, J.Y. and Ober, C.K. (2006) Recent progress in high resolution lithography. *Polymers for Advanced Technologies*, **17**, 94-103.

11. Turchanin, A., Schnietz, M., El-Desawy, M., Solak, H.H., David, C. and Golzhauser, A. (2007) Fabrication of molecular nanotemplates in self-assembled monolayers by extreme-ultraviolet-induced chemical lithography. *Small*, **3**, 2114-2119.

12. Schift, H. (2008) Nanoimprint lithography: An old story in modern times? A review. *Journal of Vacuum Science & Technology B*, **26**, 458-480.

13. Guo, L.J. (2007) Nanoimprint lithography: Methods and material requirements. *Advanced Materials*, **19**, 495-513.

14. Menard, E., Meitl, M.A., Sun, Y.G., Park, J.U., Shir, D.J.L., Nam, Y.S., Jeon, S. and Rogers, J.A. (2007) Micro- and nanopatterning techniques for organic electronic and optoelectronic systems. *Chemical Reviews*, **107**, 1117-1160.

15. Shibata, T., Takahashi, Y., Kawashima, T., Kubota, T., Mita, M., Mineta, T. and Makino, E. (2008) Micromachining of electroformed nickel mold using thick photoresist microstructure for imprint technology. *Microsystem Technologies-Micro-and Nanosystems-Information Storage and Processing Systems*, **14**, 1359-1365.

16. Nie, Z.H. and Kumacheva, E. (2008) Patterning surfaces with functional polymers. *Nature Materials*, **7**, 277-290.

17. Cross, G.L.W. (2006) The production of nanostructures by mechanical forming. *Journal of Physics D-Applied Physics*, **39**, R363-R386.

18. Quist, A.P., Pavlovic, E. and Oscarsson, S. (2005) Recent advances in microcontact printing. *Analytical and Bioanalytical Chemistry*, **381**, 591-600.

19. Gates, B.D., Xu, Q.B., Love, J.C., Wolfe, D.B. and Whitesides, G.M. (2004) Unconventional nanofabrication. *Annual Review of Materials Research*, **34**, 339-372.

20. Salaita, K., Wang, Y.H. and Mirkin, C.A. (2007) Applications of dip-pen nanolithography. *Nature Nanotechnology*, **2**, 145-155.

21. Basabe-Desmonts, L., Wu, C.C., van der Werf, K.O., Peter, M., Bennink, M., Otto, C., Velders, A.H., Reinhoudt, D.N., Subramaniam, V. and Crego-Calama, M. (2008) Fabrication and visualization of metal-ion patterns on glass by dip-pen nanolithography. *Chemphyschem*, **9**, 1680-1687.

22. Xie, X.N., Chung, H.J., Sow, C.H. and Wee, A.T.S. (2006) Nanoscale materials patterning and engineering by atomic force microscopy nanolithography. *Materials Science & Engineering R-Reports*, **54**, 1-48.

23. Tseng, A.A., Jou, S., Notargiacomo, A. and Chen, T.P. (2008) Recent developments in tip-based nanofabrication and its roadmap. *Journal of Nanoscience and Nanotechnology*, **8**, 2167-2186.

24. Koh, S.J. (2007) Strategies for controlled placement of nanoscale building blocks. *Nanoscale Research Letters*, **2**, 519-545.

25. Storhoff, J.J. and Mirkin, C.A. (1999) Programmed Materials Synthesis with DNA. *Chem Rev*, **99**, 1849-1862.

26. Mann, S., Shenton, W., Li, M., Connolly, S. and Fitzmaurice, D. (2000) Biologically programmed nanoparticle assembly. *Advanced Materials*, **12**, 147-150.

27. Dujardin, E., Peet, C., Stubbs, G., Culver, J.N. and Mann, S. (2003) Organization of metallic nanoparticles using tobacco mosaic virus templates. *Nano Letters*, **3**, 413-417.

28. Feng, X.J. and Jiang, L. (2006) Design and creation of superwetting/antiwetting surfaces. *Advanced Materials*, **18**, 3063-3078.

29. Onclin, S., Ravoo, B.J. and Reinhoudt, D.N. (2005) Engineering silicon oxide surfaces using self-assembled monolayers. *Angewandte Chemie-International Edition*, **44**, 6282-6304.

30. De Feyter, S. and De Schryver, F.C. (2005) Self-assembly at the liquid/solid interface: STM reveals. *Journal of Physical Chemistry B*, **109**, 4290-4302.

31. Mendes, P.M., Yeung, C.L. and Preece, J.A. (2007) Bio-nanopatterning of surfaces. *Nanoscale Research Letters*, **2**, 373-384.

32. Sharma, J., Ke, Y.G., Lin, C.X., Chhabra, R., Wang, Q.B., Nangreave, J., Liu, Y. and Yan, H. (2008) DNA-tile-directed self-assembly of quantum dots into two-dimensional nanopatterns. *Angewandte Chemie-International Edition*, **47**, 5157-5159.

33. Pruneanu, S., Al-Said, S.A.F., Dong, L.Q., Hollis, T.A., Galindo, M.A., Wright, N.G., Houlton, A. and Horrocks, B.R. (2008) Self-assembly of DNA-templated polypyrrole nanowires: Spontaneous formation of conductive nanoropes. *Advanced Functional Materials*, **18**, 2444-2454.

34. Ariga, K., Hill, J.P. and Endo, H. (2007) Developments in molecular recognition and sensing at interfaces. *International Journal of Molecular Sciences*, **8**, 864-883.

35. Zhang, J.P., Liu, Y., Ke, Y.G. and Yan, H. (2006) Periodic square-like gold nanoparticle arrays templated by self-assembled 2D DNA nanogrids on a surface. *Nano Letters*, **6**, 248-251.

36. Xu, X.Y., Rosi, N.L., Wang, Y.H., Huo, F.W. and Mirkin, C.A. (2006) Asymmetric functionalization of gold nanoparticles with oligonucleotides. *Journal of the American Chemical Society*, **128**, 9286-9287.

37. Rothemund, P.W.K. (2006) Folding DNA to create nanoscale shapes and patterns. *Nature*, **440**, 297-302.

38. Sullivan, B.D. (2007), pp. xxiv, 230 p.

39. Sukhorukov, G.B. and Mohwald, H. (2007) Multifunctional cargo systems for biotechnology. *Trends in Biotechnology*, **25**, 93-98.

40. Johnston, A.P.R., Cortez, C., Angelatos, A.S. and Caruso, F. (2006) Layer-by-layer engineered capsules and their applications. *Current Opinion in Colloid & Interface Science*, **11**, 203-209.

41. Yuan, J.H., Wang, Z.J., Zhang, Y.J., Shen, Y.F., Han, D.X., Zhang, Q., Xu, X.Y. and Niu, L. (2008) Electrostatic layer-by-layer a of platinum-loaded multiwall carbon nanotube multilayer: A tunable catalyst film for anodic methanol oxidation. *Thin Solid Films*, **516**, 6531-6535.

42. Haga, M., Kobayashi, K. and Terada, K. (2007) Fabrication and functions of surface nanomaterials based on multilayered or nanoarrayed assembly of metal complexes. *Coordination Chemistry Reviews*, **251**, 2688-2701.

43. Zhao, W., Xu, J.J. and Chen, H.Y. (2006) Electrochemical biosensors based on layer-by-layer assemblies. *Electroanalysis*, **18**, 1737-1748.

44. Lutkenhaus, J.L. and Hammond, P.T. (2007) Electrochemically enabled polyelectrolyte multilayer devices: from fuel cells to sensors. *Soft Matter*, **3**, 804-816.

45. Tang, Z.Y., Wang, Y., Podsiadlo, P. and Kotov, N.A. (2007) Biomedical applications of layer-by-layer assembly: From biomimetics to tissue engineering (vol 18, pg 3203, 2006). *Advanced Materials*, **19**, 906-906.

46. Cassier, T., Lowack, K. and Decher, G. (1998) Layer-by-layer assembled protein/polymer hybrid films: nanoconstruction via specific recognition. *Supramolecular Science*, **5**, 309-315.

47. Quinn, J.F., Johnston, A.P.R., Such, G.K., Zelikin, A.N. and Caruso, F. (2007) Next generation, sequentially assembled ultrathin films: beyond electrostatics. *Chemical Society Reviews*, **36**, 707-718.

48. Wang, Y., Angelatos, A.S. and Caruso, F. (2008) Template synthesis of nanostructured materials via layer-by-layer assembly. *Chemistry of Materials*, **20**, 848-858.

49. Hah, J.H., Mayya, S., Hata, M., Jang, Y.K., Kim, H.W., Ryoo, M., Woo, S.G., Cho, H.K. and Moon, J.T. (2006) Converging lithography by combination of electrostatic layer-by-layer self-assembly and 193 nm photolithography: Top-down meets bottom-up. *Journal of Vacuum Science & Technology B*, **24**, 2209-2213.

50. Velev, O.D. and Bhatt, K.H. (2006) On-chip micromanipulation and assembly of colloidal particles by electric fields. *Soft Matter*, **2**, 738-750.

51. Liz-Marzan, L.M. and Mulvaney, P. (2003) The assembly of coated nanocrystal. *Journal of Physical Chemistry B*, **107**, 7312-7326.

52. Cao, G.Z. and Liu, D.W. (2008) Template-based synthesis of nanorod, nanowire, and nanotube arrays. *Advances in Colloid and Interface Science*, **136**, 45-64.

53. Cho, J., Schaab, S., Roether, J.A. and Boccaccini, A.R. (2008) Nanostructured carbon nanotube/TiO2 composite coatings using electrophoretic deposition (EPD). *Journal of Nanoparticle Research*, **10**, 99-105.

54. Boccaccini, A.R., Cho, J., Roether, J.A., Thomas, B.J.C., Minay, E.J. and Shaffer, M.S.P. (2006) Electrophoretic deposition of carbon nanotubes. *Carbon*, **44**, 3149-3160.

55. Besra, L. and Liu, M. (2007) A review on fundamentals and applications of electrophoretic deposition (EPD). *Progress in Materials Science*, **52**, 1-61.

56. Smith, N.J., Emmett, K.J. and Rosenthal, S.J. (2008) Photovoltaic cells fabricated by electrophoretic deposition of CdSe nanocrystals. *Applied Physics Letters*, **93**, -.

57. Imahori, H. (2007) Electrophoretic deposition of donor-acceptor nanostructures on electrodes for molecular photovoltaics. *Journal of Materials Chemistry*, **17**, 31-41.

58. De Jonghe, L.C., Jacobson, C.P. and Visco, S.J. (2003) Supported electrolyte thin film synthesis of solid oxide fuel cells. *Annual Review of Materials Research*, **33**, 169-182.

59. Corni, I., Ryan, M.P. and Boccaccini, A.R. (2008) Electrophoretic deposition: From traditional ceramics to nanotechnology. *Journal of the European Ceramic Society*, **28**, 1353-1367.

60. Hayashi, K. and Furuya, N. (2004) Preparation of gas diffusion electrodes by electrophoretic deposition. *Journal of the Electrochemical Society*, **151**, A354-A357.

61. Wei, M., Ruys, A.J., Milthorpe, B.K., Sorrell, C.C. and Evans, J.H. (2001) Electrophoretic deposition of hydroxyapatite coatings on metal substrates: A nanoparticulate dual-coating approach. *Journal of Sol-Gel Science and Technology*, **21**, 39-48.

62. Hagiwara, R. and Lee, J.S. (2007) Ionic liquids for electrochemical devices. *Electrochemistry*, **75**, 23-34.

63. Li, S.F.Y. (1992) *Capillary electrophoresis : principles, practice, and applications*. Elsevier, Amsterdam ; New York.

64. Hughes, M.P. (2003) *Nanoelectromechanics in engineering and biology*. CRC Press, Boca Raton.

65. Krishnan, R., Sullivan, B.D., Mifflin, R.L., Esener, S.C. and Heller, M.J. (2008) Alternating current electrokinetic separation and detection of DNA nanoparticles in high-conductance solutions. *Electrophoresis*, **29**, 1765-1774.

66. An, L. and Friedrich, C.R. (2008) Real-time gap impedance monitoring of dielectrophoretic assembly of multiwalled carbon nanotubes. *Applied Physics Letters*, **92**, -.

67. Vijayaraghavan, A., Blatt, S., Weissenberger, D., Oron-Carl, M., Hennrich, F., Gerthsen, D., Hahn, H. and Krupke, R. (2007) Ultra-large-scale directed assembly of single-walled carbon nanotube devices. *Nano Letters*, **7**, 1556-1560.

68. Kuzyk, A., Yurke, B., Toppari, J.J., Linko, V. and Torma, P. (2008) Dielectrophoretic trapping of DNA origami. *Small*, **4**, 447-450.

69. Marcus, M.S., Shang, L., Li, B., Streifer, J.A., Beck, J.D., Perkins, E., Eriksson, M.A. and Hamers, R.J. (2007) Dielectrophoretic manipulation and real-time electrical detection of single-nanowire bridges in aqueous saline solutions. *Small*, **3**, 1610-1617.

70. Xiong, X.G. and Busnaina, A. (2008) Direct assembly of nanoparticles for large-scale fabrication of nanodevices and structures. *Journal of Nanoparticle Research*, **10**, 947-954.

71. Xiong, X., Busnaina, A., Selvarasah, S., Somu, S., Wei, M., Mead, J., Chen, C.L., Aceros, J., Makaram, P. and Dokmeci, M.R. (2007) Directed assembly of gold nanoparticle nanowires and networks for nanodevices. *Applied Physics Letters*, **91**, -.

72. Oh, K., Chung, J.H., Riley, J.J., Liu, Y.L. and Liu, W.K. (2007) Fluid flow-assisted dielectrophoretic assembly of nanowires. *Langmuir*, **23**, 11932-11940.

73. Aubry, N., Singh, P., Janjua, M. and Nudurupati, S. (2008) Micro- and nanoparticles self-assembly for virtually defect-free, adjustable monolayers. *Proceedings of the National Academy of Sciences of the United States of America*, **105**, 3711-3714.

74. Monica, A.H., Papadakis, S.J., Osiander, R. and Paranjape, M. (2008) Wafer-level assembly of carbon nanotube networks using dielectrophoresis. *Nanotechnology*, **19**, -.

75. Dehlinger, D.A., Sullivan, B.D., Esener, S. and Heller, M.J. (2007) Electric-field-directed assembly of biomolecular-derivatized nanoparticles into higher-order structures. *Small*, **3**, 1237-1244.

76. Heller, M.J., Forster, A.H. and Tu, E. (2000) Active microelectronic chip devices which utilize controlled electrophoretic fields for multiplex DNA hybridization and other genomic applications. *Electrophoresis*, **21**, 157-164.

77. Edman, C.F., Raymond, D.E., Wu, D.J., Tu, E.G., Sosnowski, R.G., Butler, W.F., Nerenberg, M. and Heller, M.J. (1997) Electric field directed nucleic acid hybridization on microchips. *Nucleic Acids Research*, **25**, 4907-4914.

78. Gurtner, C., Tu, E., Jamshidi, N., Haigis, R.W., Onofrey, T.J., Edman, C.F., Sosnowski, R., Wallace, B. and Heller, M.J. (2002) Microelectronic array devices and techniques for electric field enhanced DNA hybridization in low-conductance buffers. *Electrophoresis*, **23**, 1543-1550.

79. Edman, C.F., Swint, R.B., Gurtner, C., Formosa, R.E., Roh, S.D., Lee, K.E., Swanson, P.D., Ackley, D.E., Coleman, J.J. and Heller, M.J. (2000) Electric field directed assembly of an InGaAs LED onto silicon circuitry. *Ieee Photonics Technology Letters*, **12**, 1198-1200.

80. Dehlinger, D.A., Sullivan, B.D., Esener, S. and Heller, M.J. (2008) Directed Hybridization of DNA Derivatized Nanoparticles into Higher Order Structures. *Nano Lett*, **8**, 4053-4060.

81. Chou, C.F., Tegenfeldt, J.O., Bakajin, O., Chan, S.S., Cox, E.C., Darnton, N., Duke, T. and Austin, R.H. (2002) Electrodeless dielectrophoresis of single- and double-stranded DNA. *Biophys J*, **83**, 2170-2179.

82. Ozuna-Chacon, S., Lapizco-Encinas, B.H., Rito-Palomares, M., Martinez-Chapa, S.O. and Reyes-Betanzo, C. (2008) Performance characterization of an insulator-based dielectrophoretic microdevice. *Electrophoresis*, **29**, 3115-3122.